A THEORETICAL STUDY OF EARDRUM VIBRATIONS USING THE FINITE-ELEMENT METHOD

W.R.J. Funnell

Ph.D. thesis March 1975

BMEU 1975-3

A Theoretical Study of Eardrum Vibrations Using the Finite-Element Method

A Theoretical Study of Eardrum Vibrations Using the Finite-Element Method

W.R.J. Funnell

A thesis submitted to the Faculty of Graduate Studies and Research in partial fulfillment of the requirements for the degree of Doctor of Philosophy

Department of Electrical Engineering
&
BioMedical Engineering Unit
McGill University
Montréal, Québec, Canada

March 1975

Résumé

L'ETUDE THEORIQUE DES VIBRATIONS DU TYMPAN
AU MOYEN DE LA METHODE DES ELEMENTS FINIS

On analyse la structure et les propriétés structurales du tympan des mammifères, et adopte des descriptions précises dans le but de modeler les tympans de l'homme, du chat et du cobaye. On discute les observations expérimentales des vibrations du tympan, et les raisons possibles pour la contradiction entre les résultats de Békésy et ceux des autres. La méthode des éléments finis est présentée comme outil de grande valeur pour l'analyse mécanique du tympan. On décrit des méthodes pour la simulation du manche du marteau, des osselets, et des cavités de l'oreille moyenne. En employant la méthode des éléments finis, on démontre qu'un modèle très simple du tympan, comme membrane plane tendue, possède plusieurs des caractéristiques du tympan. On étudie aussi un modèle plus réaliste, comme planche courbe, mince et isotrope, et le suggère comme une description nouvelle de la fonction du tympan.

. . . . . .

Abstract

A THEORETICAL STUDY OF EARDRUM VIBRATIONS
USING THE FINITE-ELEMENT METHOD

The structure and structural properties of the mammalian eardrum are reviewed, and specific descriptions and parameter values are adopted for the purposes of modelling the human, cat and guinea-pig eardrums. Experimental observations of eardrum vibrations are re-examined; possible reasons for the discrepancy between Békésy's results and others are discussed. The finite-element method is presented as a useful tool for analyzing the mechanical behaviour of the eardrum. Methods are described for simulating the manubrium embedded in the drum, and the effects of the ossicular chain and middle-ear air cavities. Using the finite-element method, it is shown that a very simple model of the eardrum as a plane membrane under tension is able to duplicate many of the eardrum's characteristics qualitatively. A more realistic model of the eardrum as a thin isotropic curved plate (shell) is also investigated, and is proposed as a new description of eardrum behaviour.

Acknowledgements

I should like to thank Dr. C.A. Laszlo, not only for his invaluable supervision of the work reported here, but also for all that I have learned from him about biomedical engineering in general.

I am also indebted to Drs. S.M. Khanna and J. Tonndorf for their encouragement and assistance, and specifically for discussions of various unpublished data. Similar thanks are sincerely extended to Dr. G.A. Manley. For the provision of and assistance with computer programmes, I am grateful to Drs. P. Silvester and P.J. Harris, and to Dr. Z. Csendes, A. Konrad and Y. Fabien.

I should also like to thank Drs. D.H. Moscovitch and J.S. Outerbridge for their guidance, and the other members of the BioMedical Engineering Unit for their contributions to its atmosphere. In particular, I appreciate the heroic efforts of J.E. Cooper and D. Kernaghan, the one for (among many other things) the typing of this thesis, the other for the maintenance of a sometimes temperamental computer. I have also benefited from the helpful assistance of J. Charlebois of the Medical Library, and from the photographic skills of K. Holeczek of the Department of Physiology.

This work has been supported by the Medical Research Council of Canada, le Ministère de l'Education du Québec, and the McConnell Foundation, for which I am very grateful.

Finally, I wish to acknowledge my debt for the moral support of family and friends. This applies especially to C.A. Funnell, whose tremendous patience has made everything possible.

Table of Contents

Chapter 6. THEORIES OF EARDRUM FUNCTION

Chapter 7. SIMULATION METHODS

Chapter 8. IMPLEMENTATION OF FINITE-ELEMENT METHOD

Chapter 9. DESCRIPTION OF MEMBRANE MODELS

Chapter 10. RESULTS OF MEMBRANE MODELS

Chapter 11. DESCRIPTION OF SHELL MODELS

Chapter 12. RESULTS OF SHELL MODELS

Chapter 13. CONCLUSIONS AND FUTURE DEVELOPMENTS

Notation

Particular symbols will be defined where appropriate throughout the text. In general, however, bold-face majuscules will be used to denote matrices, and bold-face minuscules will denote column vectors. Light-face symbols will indicate scalars. Transposition of matrices and vectors will be denoted by primes ($\mathbf{A}'$, $\mathbf{v}'$, *etc.*).

CHAPTER 1

INTRODUCTION

1.1 Objectives

Presently available models of the eardrum are inadequate either to provide insight into the principles of the mechanical operation of the drum, or to permit quantitative analysis of pathological conditions as an aid to planning and evaluation of corrective techniques. The over-all objective of the work reported here is therefore the study of the mechanical behaviour of the mammalian eardrum.

More specifically, one objective of this work is a review of the experimental data available concerning eardrum structure and behaviour, in order to provide a firm basis for quantitative modelling and to identify areas where further information is required. A second objective is the introduction of the finite-element method as a powerful tool for the study of eardrum models. This method will be used to investigate a new hypothesis concerning the essential nature of the eardrum as a mechanical system.

1.2 Outline

Chapters 2 to 4 are a review of structure and mechanical properties of the eardrum and its surroundings. In particular, Chapter 2 reviews the anatomical structure of the eardrum, Chapter 3 covers its properties, and Chapter 4 discusses the surrounding structures and their coupling to the eardrum.

Chapter 5 reviews the experimental data available concerning the vibrations of the eardrum under acoustical stimuli. Chapter 6 then considers the various theories that have been proposed to describe the function of the eardrum.

Chapters 7 and 8 introduce the finite-element method. Chapter 7 discusses the concepts involved, while Chapter 8 gives more details on the methods actually

used in this work.

Chapters 9 to 12 concern the actual use of the finite-element method on two models of the eardrum. Chapters 9 and 11 describe the models themselves while Chapters 10 and 12 present the eardrum behaviour calculated from the models. One of the models represents the eardrum as a curved shell. This is a new way of looking at the eardrum; it is basically simple and yet is consistent with what is known about the drum. The other model presented here assumes the eardrum to be a plane membrane under tension. This is not to be taken as a realistic model, but is included because it shows how much of the eardrum's behaviour can be explained in terms of extremely simple models, and because it permits the qualitative study of dynamic effects that are much more difficult with the shell model.

Finally, the conclusions are presented in Chapter 13, together with a discussion of possible future developments.

CHAPTER 2

STRUCTURE OF THE EARDRUM

2.1 Introduction

This chapter presents a brief description of mammalian eardrum structure. Sections 2.2 and 2.3 present the gross anatomy and microscopic structure, respectively, of the mature drum, and then Section 2.4 discusses the drum's ontogenesis. Section 2.5 is a short review of eardrum evolution, to put the structure of the mammalian drum in perspective.

2.2 Gross Anatomy

2.2.1 Introduction. The following paragraphs will present the shape and thickness of the eardrum. The discussion will compare the situations in various mammals. Section 2.2.2 will describe the outline of the base of the eardrum, that is, the shape of the tympanic ring, and the position of the manubrium within that outline. The next section will then discuss the conical shape of the drum, and Section 2.2.4 will discuss the curvature of the sides of the cone. Finally, Section 2.2.5 will discuss the thickness of the eardrum.

2.2.2 Tympanic ring and manubrium. Fig. 2.1 shows a schematic outline of the human eardrum. There are three main anatomical areas demarcated: the pars tensa, the pars flaccida and the manubrium. The pars tensa forms the main surface of the drum, with the manubrium (handle) of the malleus embedded in it. The pars flaccida is a less important (and more elastic) part of the drum surface. The pars tensa is entirely surrounded by the annular ligament, a thickened fibrous structure which

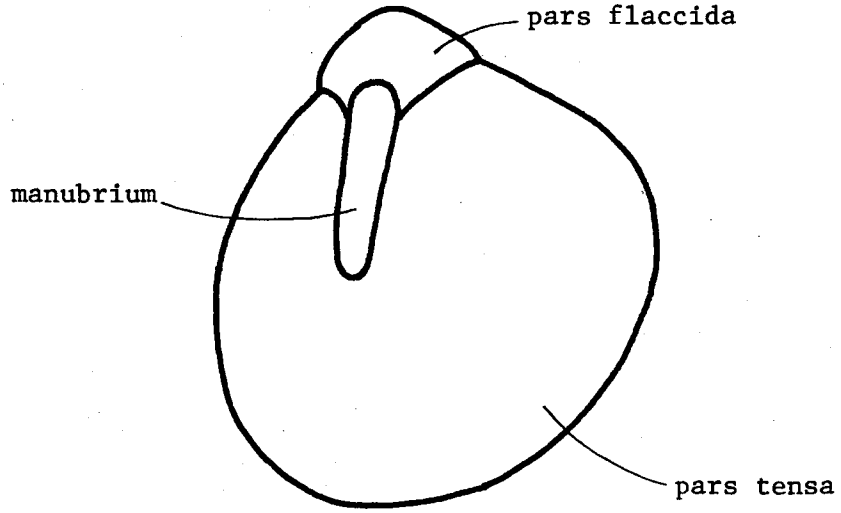

Fig. 2.1. Schematic outline of the human eardrum. (After Kojo, 1954)

joins the pars tensa to the surrounding tympanic bone and, superiorly, separates it from the pars flaccida.

Fig. 2.2 shows outlines of the eardrums of a number of mammalian species, all drawn to approximately the same scale. (The human drum is shown again for comparison.) In each case the outline is oriented so that the rotational axis of the malleus and incus is approximately horizontal. Two features may immediately be noted as being very variable: the size of the pars flaccida, and the angle between the manubrium and the axis of rotation. The pars flaccida is very large in the sheep and mouse, and absent in the guinea pig. In man and cat it is moderately small.

In some species, including man and guinea pig, the manubrium is almost perpendicular to the ossicular axis of rotation. In these cases the drum tends to be almost circular, and the manubrium is located nearly centrally. In other species, the angle between the manubrium and axis becomes quite small; here the drum tends to be elongated, and the manubrium is closer to the anterosuperior edge.

Note that the drums shown are all of similar size in spite of the great body-size differences among the species.

A parameter which is of considerable interest in discussions of middle-ear function is the ratio of the area of the eardrum to that of the oval window, since this is the largest single factor contributing to the middle-ear transformer ratio. Fig. 2.3 displays these areas separately (a), and also their ratio (b), for a number of mammalian species for comparison. Note that the figures indicate the area enclosed by the tympanic annulus, rather than the actual surface area of the conical drum.

The number of species shown is small, but some trends are visible. The semi-aquatic and fossorial (burrowing) species all have a similar area ratio in spite of the range in body size and the phylogenetic diversity. The ratio is small, presumably reflecting the relative unimportance of air-borne sound to these species.

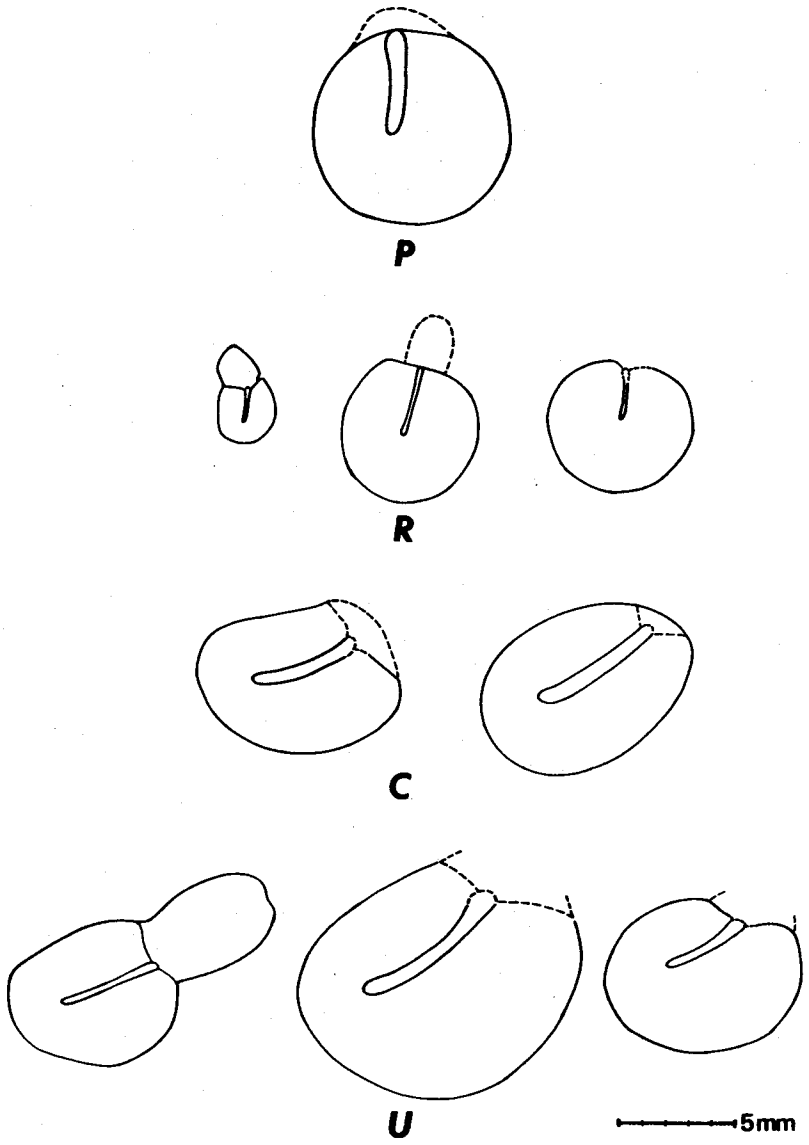

Fig. 2.2. Outlines of several mammalian eardrums. *P* = primate (human); *R* = rodents (mouse, rabbit and guinea pig, from left to right); *C* = carnivores (dog, cat); *U* = ungulates (sheep, ox, pig). The dashed lines were not present in the original drawings, and have been filled in based on my own observations or on various drawings and descriptions in the literature. They are meant to be suggestive only. (Mouse after Reijnen & Kuijpers, 1971; cat after Khanna, 1970; sheep after Lim, 1968b; all others after Fumagalli, 1949)

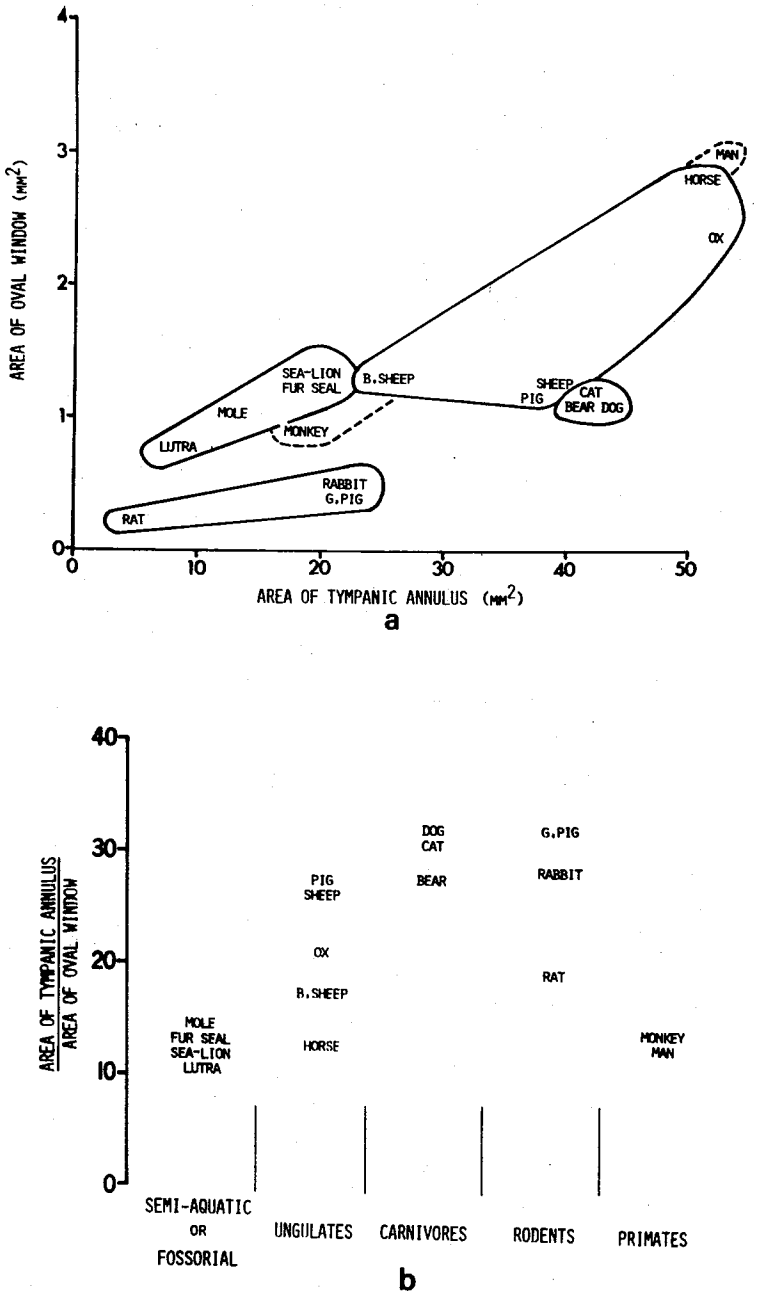

Fig. 2.3. Areas of tympanic annulus and of oval window, for various mammalian species. Part *a* shows the areas separately, while part *b* shows the ratio of the areas. Note that 'B.sheep' = Barbary sheep, and 'G.pig' = guinea pig. (Based on data of Kirikae, 1960)

The ungulates and rodents are both large, diverse families, and this diversity shows in the spreads in both the area and ratio data.

The three species of carnivore shown are remarkably uniform in both areas and ratio. The latter is quite high, which might represent a great dependence on hearing in this Order.

The two primate species shown have very similar area ratios in spite of a change in actual area by a factor of about three. The area ratio is small, which might indicate a reduced importance of hearing sensitivity in these species.

In some specialized rodents (among the Dipodidae and Gerbillinae) an accessory tympanic membrane (Hyrtl's) is found. Its position is similar to that of the pars flaccida, but structurally it is the same as the pars tensa. Lay (1972, p. 57) feels that it contributes significantly to the middle-ear transformer. I shall not consider it further in this work, although it deserves further study.

2.2.3 Conical shape. The mammalian eardrum is approximately conical, with the apex pointing medially. Fig. 2.4 illustrates this for a number of species, based on data of Fumagalli (1949). For these diagrams the sides of the cone have been taken to be straight. For each species, the triangle on the right represents a section along the long axis of the manubrium, perpendicular to the plane of the tympanic ring. The triangle at the bottom represents a plane of section perpendicular to the manubrial axis and to the plane of the tympanic ring.

Fumagalli found that the eardrum shapes of all of the species he observed could be represented approximately by a cone with an apex angle of 120^{o}, cut at various angles by the plane of the tympanic ring. The guinea-pig drum is a right cone, but the others all show some degree of obliquity, correlated with the angle of the manubrium commented on in the previous section.

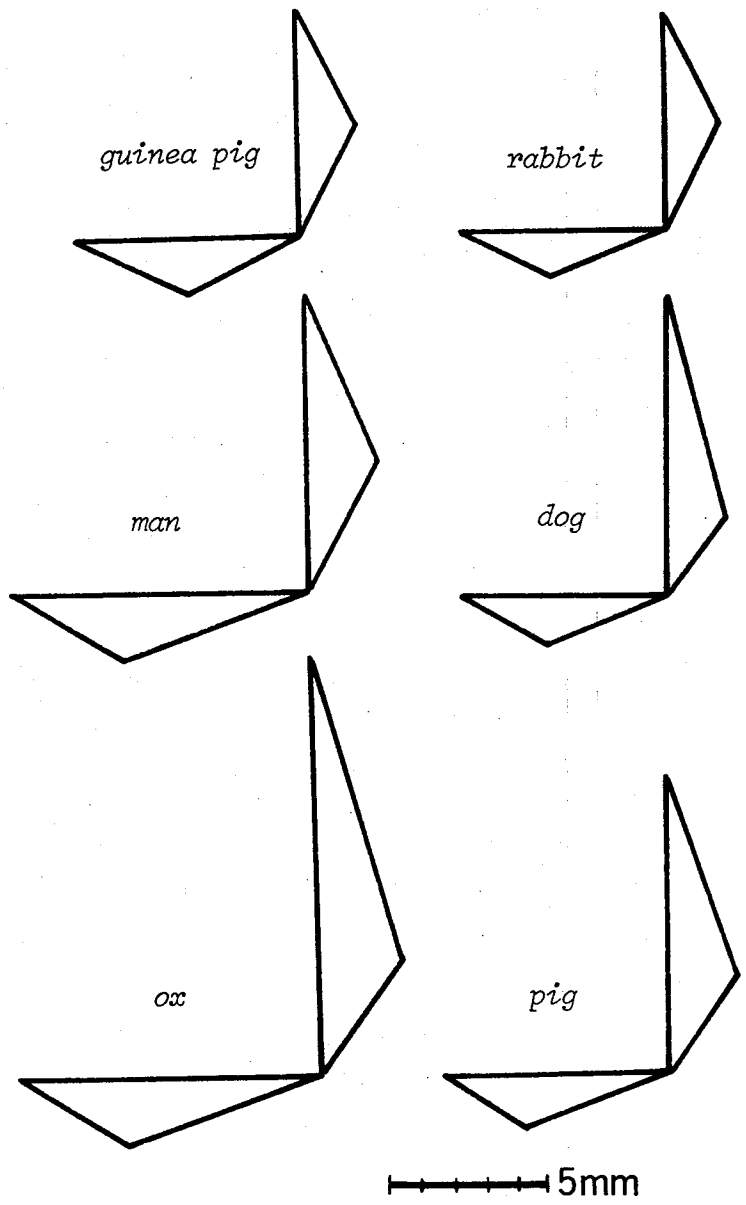

Fig. 2.4. Schematic representations of the conical shape of the eardrum for several mammalian species. The horizontal triangles represent sections through the drum perpendicular to the manubrium; the vertical triangles represent sections through the manubrium. The sides of the drum are shown by straight lines. (After Fumagalli, 1949)

2.2.4 Curvature. The sides of the cone formed by the eardrum are not actually straight but are convex outward, as shown in Fig. 2.5. There are no reliable and precise data in the literature concerning the actual curvature of the drum. Kojo (1954) published six contour plots representing the three-dimensional shape of the human drum, but they were published on quite a small scale and are rather irregular. They were obtained from castings made by pouring paraffin into the external ear canal, and this process probably introduced considerable distortion. Kirikae (1960), in addition to using paraffin moulds, also reported a single pair of curves taken by photographing "the shape of the impressed tympanic membrane" from directions corresponding to the two views in Fig. 2.5. I do not know what he meant by "impressed". The data are shown in Fig. 2.6; they are significantly different from the results he reported for the paraffin moulds.

More recently, Khanna & Tonndorf (1975) have used moiré topography (an optical technique) to study the three-dimensional shape of the guinea-pig eardrum. They apply a very thin layer of casting material to the drum, and then remove it when it has set. The measurements are taken from this casting. An example of the sort of contour patterns obtained is shown in Fig. 2.7. The effect of the procedure on the curvature is presumably less than that of the earlier paraffin moulds, and can be checked by means of a few point-by-point measurements of the shape of the drum before and after the casting.

Kirikae (1960) measured the angle included in the apex of the curved cone formed by the eardrum in each of several species, but reported only that it "ranged from 97^{o} for Barbary sheep to 135^{o} for the mole and squirrel in mammals". He noted that the ungulates and carnivora had "acute" apex angles and generally had long manubria (compared to the diameter of the drum) while other animals, with "obtuse" apex angles, have short manubria with the umbo located near the centre of the drum. (His usage of "acute" and "obtuse", if intended to mean "less than" and "greater than" 90^{o}, is inconsistent with the reported range of apex angles.)

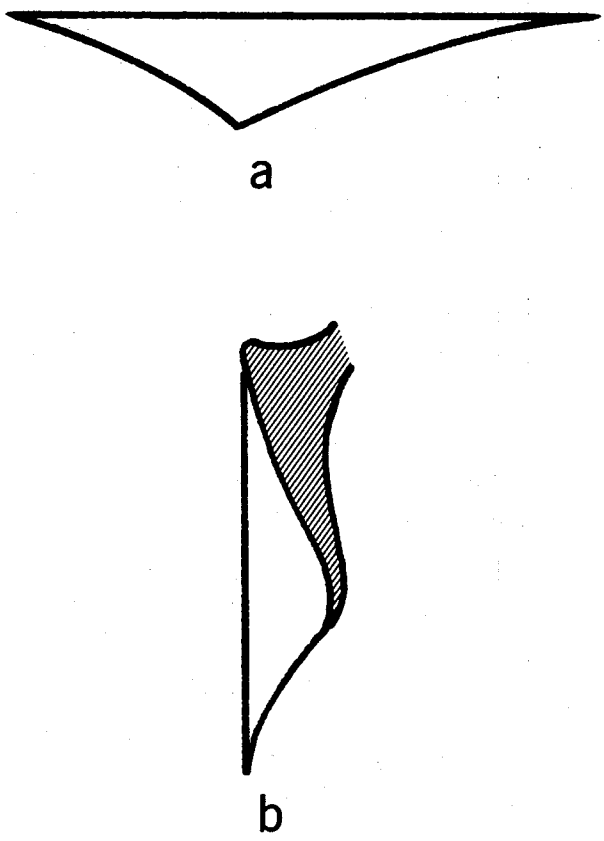

Fig. 2.5. Schematic representations of the curvature of the mammalian eardrum. Part *a* is a section through the human eardrum perpendicular to the manubrium; part *b* is a section through the manubrium of the pig eardrum. (After Fumagalli, 1949)

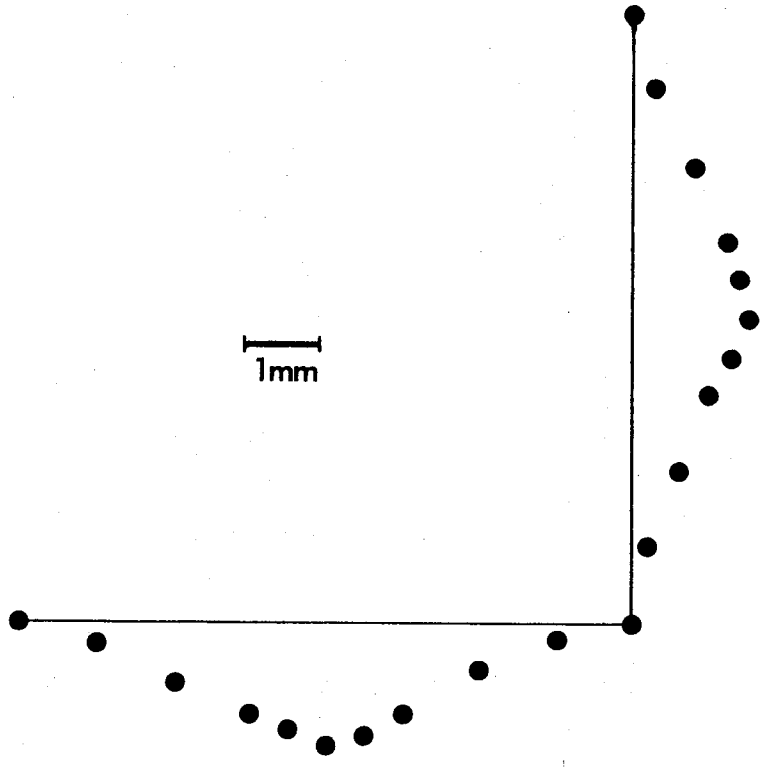

Fig. 2.6. Point-by-point measurements of the shape of the human eardrum. The bottom set of points represents a section through the eardrum perpendicular to the manubrium, while the points at the right represent a section through the manubrium. (Based on data of Kirikae, 1960)

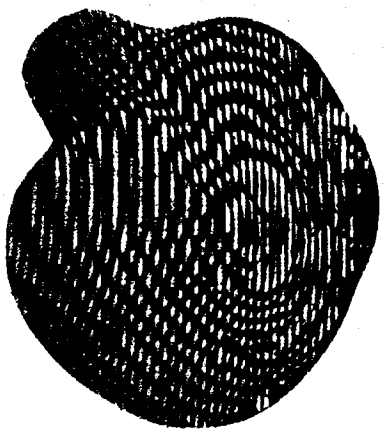

Fig. 2.7. An example of a contour pattern defining the shape of the guinea-pig eardrum, obtained using moiré topography. The vertical straight lines indicate the moiré grating. The curved contours, produced by interference between the shadow of the grating on the eardrum and the grating itself, represent lines of constant depth. This Figure is a retouched version of a photograph from a preliminary series of experiments (Khanna, personal communication).

The curvature of the eardrum described above is apparently universal among mammalian eardrums. Even in the Monotreme platypus, which in many ways is a very primitive mammal, and in which the middle and inner ear shows many differences in detail from the mammalian norm, the eardrum has the normal curvature (judging from Fig. 2.8, which is adapted from Gates *et al.*, 1974). The echidna, the only other living Monotreme, does not appear to have a typically curved drum, but here the gross mechanical behaviour of the entire middle ear is unusual (Aitkin & Johnstone, 1972).

2.2.5 Thickness. There are not many detailed data available concerning eardrum thickness. Kojo (1954) measured the thickness at seven locations on each of seven human eardrums: the total range was from 30 to 120 μm, with the average values for the seven locations ranging from 55 to 90 μm. By comparison, Lim (1970) reported that the human eardrum varies in thickness from 30 to 90 μm. The cat drum is 30 to 50 μm thick, and the guinea-pig drum is about 10 μm thick (Lim, 1968a).

Kojo found the drum to be thinnest part-way between the periphery and the manubrium, as shown in Fig. 2.9.

In my subsequent discussion of the density of the eardrum (Section 3.8) I shall need a value for its volume. I am not aware of any previous measurement or estimate of this. I have estimated it from Kojo's thickness data by averaging the thickness found in the inner, middle and outer regions, weighted by the surface areas of these regions. (From Kojo's Fig. 6, I have estimated the regional areas to be 4, 15 and 45 mm^2, respectively.) I arrive at an estimated drum volume of 5 mm^3. As indicated in Section 3.8, however, this estimate appears to be too low. More detailed measurements are required.

In the models presented in subsequent chapters, I have used eardrum thicknesses of 40 μm for the cat and 10 μm for the guinea pig. For the human drum I have assumed 50 μm, which is the value used by Békésy (1949) in his calculation of the stiffness of the eardrum (see Section 3.4).

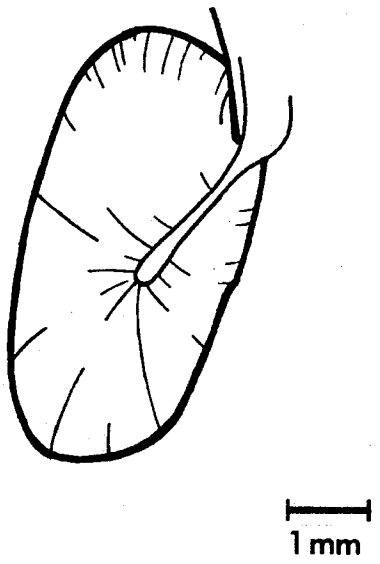

Fig. 2.8. Eardrum and manubrium of a platypus. The eardrum is conical pointing inwards, with the sides being convex outwards. (After Gates *et al.*, 1974)

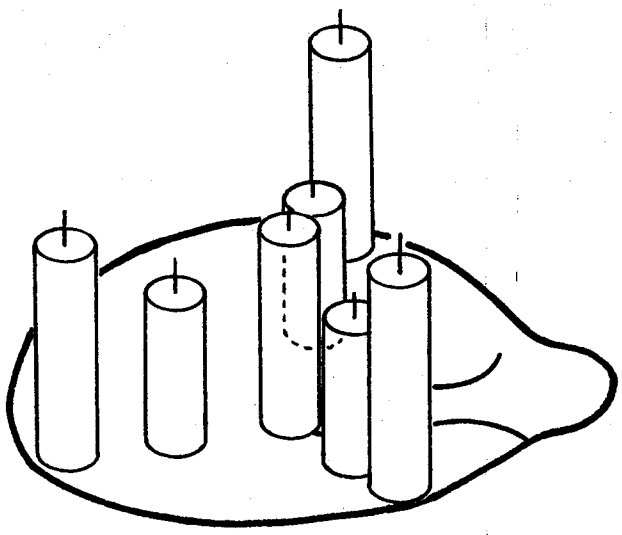

Fig. 2.9. Diagrammatic representation of the human eardrum-thickness data of Kojo (1954). The height of each cylinder is proportional to the average measured thickness of the eardrum at that point. The length of the small vertical line atop each cylinder indicates half of the range of the measurements in seven eardrums; the lower half is omitted for clarity. The tallest cylinder represents a thickness of 90 μm.

2.3 Microscopic Structure

2.3.1 Introduction. The pars tensa is composed of three layers: an outer epidermal layer; the lamina propria; and an inner mucosal layer. The first and last of these will be discussed in Sections 2.3.2 and 2.3.3, respectively. The lamina propria will be discussed in Sections 2.3.4 and 2.3.5, covering the subepidermal and submucosal connective tissue layers in 2.3.4, and the two highly organized fibre layers in Section 2.3.5.

The pars flaccida is much the same as the pars tensa except that it lacks the highly organized layers of the lamina propria, and contains a higher proportion of elastic fibres compared to inelastic (collagen) ones. It is usually small, and because of its greater elasticity has little effect on the vibration of the eardrum. I shall not consider it further; for a detailed study see Lim (1968b).

2.3.2 Epidermal layer. This layer is continuous with the epidermis of the external ear canal, and is quite similar to epidermis found elsewhere on the body. Thus, I shall first describe briefly the structure of typical epidermis and then discuss the characteristics peculiar to eardrum epidermis.

Epidermis is cellular tissue composed of five layers. The deepest layer (stratum basale, or germinativum) is a single layer of reproducing epithelial cells, which gradually migrate toward the higher layers. By the time they reach the third layer (stratum granulosum) considerable degeneration of nuclei and of intercellular bridges has occurred, and keratohyalin granules have started to appear. By the fourth layer most of the cells are dead, and by the fifth and outermost layer (the stratum corneum) all of them are metabolically inactive: they are dehydrated, flattened and stacked in regular layers, and the nuclei and cytoplasm have been replaced by the fibrous protein keratin. This progression from stratum basale to stratum corneum takes a cell about two weeks typically; the cell then spends another two weeks in the stratum corneum and finally is sloughed off (desquamated). (For further details, see

Wilkes *et al.*, 1973, among others.)

The epidermis of the eardrum and of the deepest (bony) part of the external ear canal is basically as described above, but it is somewhat specialized — it does not contain any glands or hair follicles (Johnson *et al.*, 1968; Reijnen & Kuijpers, 1971, for example) as does other skin, and also it shows powers of lateral migration not encountered in epidermis elsewhere (Magnoni, 1938; Alberti, 1963, 1964; Litton, 1968). The drum epithelium constantly migrates outward from the centre of the drum as new cells are formed, desquamating only when it reaches the cartilaginous portion of the ear canal. The process accounts for the self-cleaning ability of the ear canal.

The stratum corneum, although very thin, is very dense. It is possible that it has some effect on the mechanical properties of the eardrum.

2.3.3 Mucosal layer. The mucosal layer of the eardrum is a continuation of the mucosal lining of the middle-ear cavity. It is a very thin layer of cells and presumably has no mechanical function.

2.3.4 Loose connective-tissue layers. The subepidermal and submucosal connective-tissue layers contain abundant collagen fibrils held in a considerable volume of ground substance. There are a few elastic fibres near the pars flaccida.

The collagen fibres are described as "irregularly arranged" (Lim, 1970) and "loose" (Lim, 1968a), but in some photomicrographs (Lim, 1970, Fig. 3a; Lim, 1968a, Fig. 4a) there does seem to be a dominant direction. This organization is presumably only local. These connective-tissue layers probably have little effect on the behaviour of the eardrum.

2.3.5 Fibre layers. The main structural components of the eardrum are the highly organized radial (outer) and circular (inner) fibre layers. They consist of parallel arrays of fibres in a relatively scanty matrix of ground substance. Between the two layers is a thin layer of oblique fibres.

The detailed descriptions of this layer differ between authors and between species, and the fibres have at various times been called parabolic, crescentic and transverse. Although Fumagalli (1949) ascribes a functional significance to these fibres, at least in some species, it would seem that they are too few to be of major importance. There are also a few radial fibres on the medial surface of the circular-fibre layer, which presumably are not very important. Shimada & Lim (1971) have recently reviewed the status of these miscellaneous fibre systems.

The radial fibres generally run more or less straight from the manubrium to the annular ligament, although some curve before reaching the latter (Shimada & Lim, 1971, for example). The fibres become more closely packed as they converge on the manubrium.

Relatively little attention has been paid to the precise way in which the fibres insert into the manubrium and annular ligament. Fumagalli (1949) reported that in the upper third of the manubrium the radial fibres cross the lateral face of the manubrium and wrap part-way around before inserting, while lower down the anterior radial fibres change patterns and wrap around the medial face of the manubrium. More recent authors have neither confirmed nor denied this pattern. Tonndorf & Khanna (1972) noted a difference between the fibre insertions in the cat and those in man: in the cat the fibres insert directly into the manubrium, whereas in man the fibres are connected to the middle portion of the manubrium by a short ligament (Politzer, 1889, Fig. 138-141, for example).

The circular fibres start from the manubrium, curve around below the umbo, and insert again on the opposite side of the manubrium. Most of them are attached to the manubrium fairly close to the upper end, near the short process. The circular-fibre layer is less well developed than the radial-fibre layer, and near the centre of the drum is very thin or even absent. It grows thicker toward the periphery. Helmholtz quoted two earlier authors (Gerlach, Gruber) as stating that it is absent or

very thin at the extreme periphery, but Gruber (1867) at least was apparently just alluding to the fact that few circular fibres actually enter the tympanic annulus.

The fibres of both the radial and circular layers are composed of some typical collagen fibrils (diameters on the order of 50 nm) mixed with large numbers of finer fibrils (about 5 nm square, apparently composed of four sub-units). In the guinea pig, none of the larger fibrils are found at all (Lim, 1968a). In man, the proportion of the finer fibrils compared to the larger ones is greater in the radial fibres than in the circular fibres (Lim, 1970).

The nature of the finer fibrils is not known. They do not show the 65-nm banding typical of collagen (caused by a very regular alignment as the 1.5-nm-diameter, 300-nm-long molecules combine to form filaments and fibrils). On the basis of an amino-acid analysis, Johnson *et al.* (1968) suggested that they are neither collagen nor elastin: their amino-acid composition shows some of the features of both. Other authors have suggested that they are keratin or reticulin, two other fibrous proteins (see Lim, 1970, for discussion). They could also be a form of collagen whose supramolecular structure is not sufficiently regular to display banding. The composition of collagen can vary considerably from tissue to tissue, and between species (see, for example, Dayhoff, 1972; Stenzel *et al.*, 1974).

2.4 Ontogenesis of the Eardrum

According to Pearson *et al.* (1967) the human eardrum starts to develop early in foetal life and is "well formed" by the fourth month, but Keith (1923) wrote that the outer aspect of the drum is formed during the seventh month by the breakdown of the older cells of a solid ingrowth of epithelium from the outside of the skull; the inner aspect is formed "during the later months of foetal life" by absorption of the gelatinous tissue in the tympanum. At birth the human drum is of nearly adult size

but is almost horizontal; during childhood the external auditory meatus lengthens and the drum becomes more vertical (Pearson *et al.*). At birth the tympanic space is still partially filled by a residue of connective tissue which is gradually absorbed within the first few months of life (Patten, 1953); whether any of this unresorbed tissue touches the eardrum is not clear.

Concerning the microscopic structure of the drum, Zanzucchi (1938) reported that in man the system of elastic fibres around the periphery, and at the insertion of the malleus, does not form until after the first year of life, and that it continues to develop thereafter. The only post-natal modification found by Filogamo (1943) was a very slight increase in fibre diameter.

I am not aware of any data concerning eardrum thickness before and after birth, nor of any ultrastructural studies of eardrum development.

2.5 Evolutionary Trends

2.5.1 Introduction. The following discussion is presented in order of phylogenetic development, followed by a discussion. Except for the paragraph on insects, much of the material is based on work by Filogamo (1949) and Owada (1959).

2.5.2 Invertebrates. An eardrum, in the sense of a thin structure with air on both sides acting as an acoustic receptor, evolved once among the vertebrates (as the amphibians moved from water onto land). Such structures, functionally but not anatomically related, also developed several times among the invertebrates. The insect "eardrum" is a simple plane structure, and its principles of operation are very different from those of the vertebrate ear (Michelsen, 1971, 1973; Adams, 1972).

2.5.3 Amphibians. The earliest vertebrates were aquatic and did not have an eardrum vibrating in air. The typical amphibian eardrum is plane, and consists mainly of a set of radial fibres which converge on a thick fibrous disk in the centre. The fibres are apparently composed of elastin or a similar protein, as opposed to a collagen-like protein. The drum transmits vibrations to the extracolumella whose tip is set in the centre of the fibrous disk. There are radial bundles of muscle cells distributed among the fibres.

2.5.4 Reptiles. Evolved from the earliest amphibians, the reptiles have an eardrum which typically is flat except for a small lateral protrusion at the centre. There are non-radial fibres in addition to the radial ones, and there are both elastic and collagenous fibres intermingled. The non-radial fibres are grouped into three or four bundles. The attachment of the extracolumella is by processes embedded in the drum, rather than by a simple attachment of the tip. Only the radial fibres are inserted into these processes. The bundles of muscle cells are now found around the inferior border of the drum, rather than in the interior.

Note that some reptiles, such as turtles and snakes, do not rely on air-conducted sound and do not have the typical thin air-suspended eardrum.

2.5.5 Birds. The avian eardrum is evolved from the reptilian. It is markedly conical, pointing outward. Again there are radial and non-radial fibres, elastic and collagenous, all intermingled, and again the non-radial fibres are grouped into a few bundles. There are also some bundles of radial fibres. The extracolumella is again attached by processes embedded in the drum, mainly by radial fibres. There are no longer muscle cells within the drum but there are some tendon fibres from the tensor muscle.

2.5.6 Mammals. The mammals have evolved from the reptiles independently of the birds. As described in previous sections, the drum is conical as in birds, but pointing inward instead of outward. There are few or no elastic fibres except near the periphery, and the radial and non-radial fibres are separated into two distinct layers. A process of the malleus is embedded in the eardrum, analogous to a process of the extracolumella, and the main attachments to it are again by radial fibres. There are neither muscle cells nor tendon fibres in the drum, the tensor muscle inserting directly into the malleus.

Note that some groups of mammals, such as the whales, no longer use the typical arrangement described above.

2.5.7 Discussion. There are some trends in the evolution of the eardrum which are of uncertain significance but which are suggestive. After the amphibians, collagenous and non-radial fibres were mixed in with the radial elastic ones, the type of coupling to the middle ear was changed, and the muscle cells and tendons were gradually removed from the surface of the drum. After the reptiles, the drum became strongly conical. The mammals are peculiar in having lost all of the elastic fibres, and in having the radial and circular fibres completely separated into two different layers.

With respect to the fact that both birds and mammals have conical drums, albeit pointing in opposite directions, it is interesting to note that Gaudin (1968) has suggested that birds also have an effective ossicular lever, implemented differently than the mammalian one is. From an illustration in Gaudin (1968), it would appear that the avian drum as well as the mammalian has sides that are curved and convex towards the interior of the cone.

CHAPTER 3

STRUCTURAL PROPERTIES OF THE EARDRUM

3.1 Introduction

The first two sections below will deal with the general questions of isotropy and uniformity, respectively, of the mechanical properties of the eardrum. The following sections will then deal in turn with the eardrum's stiffness, Poisson's ratio, tension, internal damping, and mass. In each section, after a review of the experimental results available and a discussion of their significance, I shall conclude by stating what characteristics have been adopted for each of the two models (membrane and shell) presented in later chapters.

3.2 Isotropy

A material is mechanically isotropic if its mechanical properties are the same in all directions. In the cases of membranes and thin plates one is not concerned about the properties in directions normal to the surface, and the question of isotropy becomes two-dimensional. This is the situation with the eardrum since its thickness is very small compared to its diameter.

Békésy (1941) said that, in studies "in which small portions of the eardrum were cut out", he found that there was a difference in strength in different directions but that elasticity was "of the same order of magnitude". He also said that, if one touches a fresh eardrum with a fine hair, the resultant depression will "nearly always" be circular, indicating isotropy. In a later paper (1949) he said that eardrum elasticity shows "no change with direction"in either guinea pig or man, in spite of a definite tendency of the guinea-pig drum to split in the

radial direction. Unfortunately, no further details were published concerning any of these observations.

Kirikae (1960), in his studies of adult human eardrums, found that the intact drum responds in the same way to small slits cut in different directions. However, when he removed the epidermal layer the slits pulled open when cut perpendicular to the radial fibres, but not when they were parallel.

In evaluating the above observations, three factors must be taken into account. First, there is always the possibility of post-mortem changes when working with cadaver material. Second, the displacements involved in observing either depressions in the drum or the behaviour of slits are much larger than those due to acoustical vibrations in the normally operating eardrum. Third, tests involving slits may produce local fibre damage and distortion that affect the observed behaviour, as remarked on by Wilkes *et al.* (1973) in connection with puncture tests in skin.

Anatomical evidence would appear to indicate some degree of anisotropy in the eardrum. Each of the two layers of fibres, radial and circular, is geometrically highly anisotropic, being composed of regular arrays of unbranching fibrils and fibres. Such an arrangement should be much stiffer along the axis of the fibres than across it, unless the transverse bonding (presumably due to the ground substance) is very strong. In addition, the circular layer is thinner than the radial layer, which suggests that the drum should be stiffer in one direction than in the other. This assumes, of course, that the drum's properties are determined by the fibrous layers. Kirikae's observations of the effect of removing the epidermal layer, mentioned above, indicate that this layer has some effect on the mechanical behaviour of the overall eardrum.

Although further work is required to resolve the question, at present there is no experimental evidence of eardrum anisotropy under normal operating conditions. Therefore, in both the membrane and the shell models presented later, I assume that the eardrum's mechanical properties are isotropic, except in Section 12.10 where one case is

presented illustrating the effect of reducing the stiffness of the circular fibres.

3.3 Uniformity

Békésy (1941, 1949) did not mention having measured eardrum stiffness at different locations. His only remarks concerning eardrum uniformity concerned the "lower fold". He said that at the lower edge of the human drum there is a "pronounced fold ... that permits free movement of the cone", and by implication he referred to it as a "special elastic structure". It is not clear, however, if he was referring to a structural non-uniformity. In the guinea pig he said there is no lower fold, but that the same purpose is served just by the geometry of the cone. Kirikae (1960) reported that the behaviour of small slits cut in the human eardrum is independent of location.

Békésy (1949), in his observations on calf and sheep eardrums, found that the behaviour of cut-out flaps was independent of place. This is of little relevance for the human and guinea-pig drums, however, because of the apparently great difference in construction.

Anatomically one expects some degree of non-uniformity in the drum. The circular fibres become fewer toward the centre of the eardrum and the radial ones become less closely packed toward the periphery. Kojo (1954) found the drum to be thinner part-way between the periphery and the centre (see Section 2.2.5 above). In addition, the radial fibres are absent in a small area near the pars flaccida. However, there are no experimental measurements to support the assumption of non-uniformity of mechanical properties, except perhaps for mass density (see Section 3.8 below).

In this thesis I have assumed complete uniformity of the pars tensa in both the membrane and shell models.

3.4 Stiffness

3.4.1 Introduction. Békésy (1949) and Kirikae (1960) reported measurements of the elasticity of the eardrum. The two sets of experiments are discussed in Sections 3.4.2 and 3.4.3, respectively. Section 3.4.4 is a discussion of the differences between the two. Section 3.4.5 compares their results with measurements on collagen, and Section 3.4.6 concludes with a statement of the stiffness values used in the models.

3.4.2 Békésy (1949) measured the bending stiffness of the human cadaver eardrum by cutting out a rectangular flap along three sides. The flap formed a cantilever beam 2 mm long and 0.5 mm wide. He applied a pre-calibrated force of 0.2 mg to the free end and measured the displacement to be 50 μm. Assuming the flap to be a 50-μm-thick, uniform, isotropic beam clamped at one end, he used a standard formula from mechanics to calculate an elastic modulus of 2×10^8 dyn cm^{-2}. He stated that the elastic coefficient is about the same in the guinea pig, presumably on the basis of similar measurements.

The displacement measured by Békésy was about equal to the thickness of the eardrum. It was about 60 times (35 dB) larger than the largest low-frequency (525 Hz) drum displacement of the human drum measured by Tonndorf and Khanna (1972) at 121 dB SPL. This would be beyond the linear range in the intact middle ear. However, the classical beam-bending theory used in calculating the elastic modulus predicts a maximal fibre stress of only about 2×10^5 dyn cm^{-2}, compared to the breaking stress of more than 15×10^8 dyn cm^{-2} reported by Wilkes *et al.* (1973) for collagen tendon. On this basis it would appear that Békésy's measurement was not forcing the eardrum fibres into nonlinear operation.

Békésy (1949) also measured the stiffness of the calf eardrum, using a somewhat different technique. From his description the arrangement would seem to have been as shown in Fig. 3.1. A flap was cut out, rolled into a rod, and supported against the tympanic ring. He used the formulae from mechanics appropriate for a uniform, isotropic cylindrical beam clamped

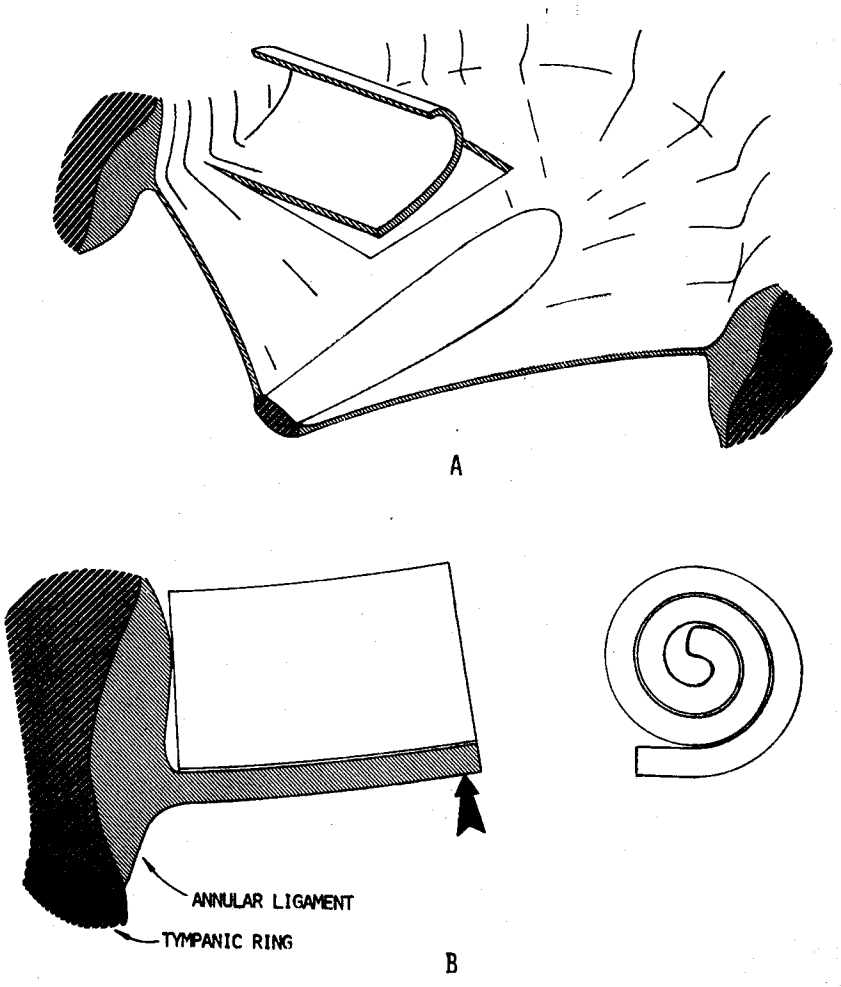

Fig. 3.1. Arrangement of Békésy's calf-eardrum measurement, based on his description. Part *a* shows the way in which a flap was cut in the eardrum; the actual position and size of this flap are conjectural. Part *b* shows longitudinal and transverse sections through the flap after it has been rolled. The arrow indicates where the force was applied.

at one end, and arrived at an elastic modulus of 2×10^4 dyn cm^{-2}, very much smaller than the value found for the human and guinea-pig drums. He might have underestimated the stiffness somewhat by modelling the rolled-up flap as a solid cylinder when in fact it was a laminar structure with the laminae not bonded together. However, the drum he was examining was definitely unusual, being described by him as "a kind of gelatinous film", very viscous, about 100 μm thick. Filogamo (1949) did not make note of any unusual characteristics of the bovine eardrum in his comparative anatomical study of 20 mammalian species. The peculiarity of Békésy's specimen might be attributable to immaturity.

3.4.3 Kirikae (1960) measured the stiffness of a 10-mm-long, 1.5-mm-wide strip of human eardrum, vibrating longitudinally at 890 Hz. He calculated a Young's modulus of 4×10^8 dyn cm^{-2}, based on a drum thickness of 75 μm. Taking the thickness as 50 μm, as Békésy did, would have given a modulus of 6×10^8 dyn cm^{-2}. These values are two and three times stiffer than Békésy's, respectively.

From the details published by Kirikae (1960) it is not possible to calculate either the forces or the displacements imposed on his specimen, in order to decide whether or not it was operating linearly. However, he reported that he obtained the same results when the weight hanging from the eardrum strip was varied from 300 mg to 1000 mg, indicating linearity.

3.4.4 Differences. There are four chief differences between the experiments of Békésy and Kirikae that may explain the difference between their elastic moduli (apart from the question of whether the sample was acting linearly in each case). First, the sizes, positions and orientations of their samples were different. Kirikae's strip was almost as long as the drum diameter, and was located across the drum below the umbo. Thus, the radial fibres were approximately normal to its length in some places, the circular fibres were approximately normal to its length in

others, and in the part nearest the umbo there were very few circular fibres at all. By contrast, Békésy's flap was only a fifth as long and a third as wide, so the fibre distribution within it would have been more uniform. Unfortunately Békésy did not describe the position or orientation of his flap.

A second difference between their experiments was that Békésy measured a transverse displacement while Kirikae measured a longitudinal one. This would not matter if the strips were truly isotropic and uniform.

Third, Békésy's measurement was static while Kirikae's was dynamic (890 Hz). There are no data available to indicate whether a frequency dependence of the elastic modulus is to be expected. A number of common polymers, such as natural rubber, thermoplastics and crystalline polymers, have more-or-less constant elasticities within and below the audio-frequency range, while in high-damping rubbers the stiffness increases rapidly over this range (Snowdon, 1968). Witnauer & Palm (1961) found the modulus of elasticity of leather to be practically the same at 15 to 20 Hz as at 0 Hz.

A fourth difference between the two sets of experiments involves the handling of the specimens and the environmental conditions during testing. The length of time the specimen has been without an intact blood supply may be significant. In addition, the temperature and humidity of the air in which the testing takes place are important. Kirikae used a temperature of 18 C and a relative humidity of 75%. Békésy (1949) said only that his measurements were done in a chamber with "controlled humidity". In an earlier (1941) paper he mentioned the use of "low temperature" and 100% relative humidity in investigations of the eardrum. The effect of temperature is probably small: Viidik (1973) concluded from the literature that the mechanical properties of collagen tissues do not change much between room temperature and body-core temperature although there may well be some small, possibly significant, effects; he did not mention the effects of low temperatures. Humidity probably is

more important, but Galante (1967) found that 65% relative humidity at 21 C is sufficient to prevent significant changes in certain mechanical properties of collagen tissue for about 10 minutes. Kirikae (1960) reported that after 10 minutes of drying (at an unspecified relative humidity) the stiffness of the eardrum more than doubled.

In this connection one should note that the eardrum normally functions near body-core temperature, with eardrum temperature displaying a sensitivity of about 5% to ambient temperature (Baker *et al.*, 1972). The relative humidity, at least on the medial face of the eardrum, is normally 100%.

3.4.5 Comparison to collagen. If one uses an effective thickness equal to that of the combined radial and circular layers (33 μm in Lim, 1970, Fig. 4), instead of the total drum thickness, one should obtain a value for Young's modulus corresponding to the fibres themselves (assuming that they dominate the eardrum's mechanical properties). On this basis I have calculated a modulus of 7×10^8 dyn cm^{-2} from Békésy's data. Using the thickness of either the radial or circular layer alone would raise the value further, as would the use of Kirikae's data. It is interesting to compare this elasticity to values measured for other collagenous tissues. Haut & Little (1969) found a stiffness of 10 to 20×10^8 dyn cm^{-2} for an "almost entirely collagenous" ligament when the strain was high enough that the fibres were being stretched rather than just re-oriented. Under similar conditions, Grahame (1970) found a stiffness of 10^8 to 10^9 dyn cm^{-2} for human skin *in vivo* (with considerable individual variation as well as dependence on age and sex). These figures are quite similar to the values measured for the eardrum. Even though the fibres of the eardrum may not be collagen, or at least not ordinary collagen (as discussed in Section 2.3.5 above), their mechanical properties appear to be similar to those of collagen.

(For the purposes of comparison, I should like to mention the Young's moduli of the following materials:

6×10^6 dyn cm^{-2} for elastic fibres (Carton *et al.*, 1962);

10^7 " " smoked rubber (Kirikae, 1960);

5×10^8 " " vulcanized rubber (Kirikae, 1960);

8×10^{10} " " pine wood (Békésy, 1949);

and 2×10^{12} " " steel.)

3.4.6 Conclusion. For the shell model presented below I have chosen Békésy's value of 2×10^8 dyn cm^{-2} for the Young's modulus of the pars tensa. I have used the same value for the cat and guinea pig since there are no experimental data available to indicate whether they are different in this respect from the human.

The pars flaccida has been described as very yielding, composed of elastic fibres and irregularly arranged collagen fibres. Consequently I have assigned it a Young's modulus of 10^6 dyn cm^{-2}, which is typical of elastic fibres (Carton *et al.*, 1962, for example). This value is so low that this part of the model has little effect on the over-all behaviour.

For the manubrium in the shell models I have used an elastic modulus of 10^{11} dyn cm^{-2}, which is typical of compact bone (Vayo, 1971, for example). It is so high that the manubrium behaves essentially as a rigid body.

The Young's modulus is not a relevant parameter for the membrane model.

3.5 Poisson's Ratio

Poisson's ratio is the ratio of transverse to axial strain when a material is submitted to uni-axial stress. It has never been measured for the eardrum. For common materials it ranges from about 0.3 for isotropic crystalline solids, to 0.5 for rubberlike materials (Snowdon,

1968). For a material composed of parallel fibres with no lateral interaction among the fibres, Poisson's ratio would be zero for a stress applied in the direction of the fibres.

Wilkes *et al.* (1973) reported that the passive transverse strain in human skin is essentially constant once the skin is stretched far enough that the collagen fibres are all aligned, which corresponds to the condition in the eardrum. Taken at face value, this would imply a Poisson's ratio of zero. However, once the skin is stretched that far even the axial strain increases only slowly with increasing stress. Thus, even if the Poisson's ratio were non-zero the transverse strain would be small and difficult to measure.

Since there are no experimental data to decide the issue, I have adopted a value of 0.3 for the Poisson's ratio in the shell model, as a compromise. It will be shown below (Section 12.6) that the behaviour of the model is not very sensitive to the value of Poisson's ratio in the range of 0 to 0.5.

3.6 Tension

The only attempts that have been made to evaluate the degree of tension in the eardrum are those of Békésy (1949) and Kirikae (1960). Békésy cut out U-shaped flaps in the eardrum. In the calf and sheep the flaps shrank and the cut-out hole expanded, which he interpreted as evidence of tension. The shrinkage and expansion occurred very slowly (over about 10 seconds), which Békésy thought was due to a large viscosity in the drum; it might also indicate that the dimensional changes were a result of tissue distortion along the cut edges, rather than tension release. In any case, the flaps apparently did not shrink in the human and guinea-pig drums, since he stated that they were not under tension.

Kirikae investigated the tension by cutting slits about 0.5 mm long at various positions and orientations on human cadaver eardrums, both with and without removing the epidermal layer. The only slits that became

enlarged (to about 0.1 mm wide), suggesting tension, were those cut perpendicular to the radial fibres with the epidermis removed. Kirikae interpreted these results as merely confirming Békésy's finding that the eardrum's properties are uniform and isotropic. If the spreading of the slit really indicates tension, however, then Kirikae's observations indicate that the radial fibres are under more tension than the circular ones, and that the epidermis is able to prevent the radial fibres from shrinking when their tension is released.

It is uncertain that tests such as the above are sensitive enough to detect tension in the eardrum. If one assumes that the resting tension in the eardrum is comparable to the tension that can be developed by the tensor tympani, then one can calculate that the amount of radial-fibre stretch to be released by a slit is on the order of 25 μm (see Appendix 1). For a short slit the release would be less because of the restraints imposed by neighbouring fibres. An enlargement of a slit or flap by 25 μm would be difficult to detect, and might indeed be caused by local structural damage in the act of cutting.

The fact that Békésy's and Kirikae's experiments were done on cadaver ears obviously means that they could not detect any component of eardrum tension due to tonus in the tensor tympani. Also, any tension maintained passively by the ossicular ligaments might be sensitive to post-mortem tissue changes.

Helmholtz (1869) believed that the curvature of the eardrum was maintained by a tension working against the circular fibres. That the curvature cannot all be explained as due to resting tension is indicated by the observation that a completely detached human eardrum, after being "rolled up, ... unfolds itself rapidly under water, and displays its exact contours" (Politzer, 1889, p. 76).

In the shell model below I have assumed that there is no resting tension in the eardrum. In the plane-membrane model, of course, it is the tension that supplies the effective stiffness of the membrane, but this tension is not necessarily correlated to any real physical property of the

eardrum. The values of tension used will be chosen by comparing the model's behaviour with experimental data.

3.7 Internal Damping

No-one has ever attempted to measure the internal resistance of the eardrum. In fact, very little attention has been paid to vibration damping in any collagenous tissue. Witnauer & Palm (1961) estimated the internal resistance of leather from the width of the resonance in their measurement of the dynamic modulus of elasticity. The ratio of the modulus of elasticity to the internal resistance was found to be about 10^3 sec^{-1} at their observed resonance frequency of 15 to 20 Hz. (Note that they report the "dynamic bulk modulus" in "dyn/cm^{-2}", and the "internal bulk resistance" in "$dyn/sec/cm^{-2}$". They use the slash, "/", simply as a separator, and not to indicate division.)

The shell model presented below is applicable only for static displacements, so damping is not relevant. In the membrane model I shall choose values of damping that best fit the experimental data available. For convenience I assume that the ratio of elasticity (represented by the tension, in units of dyn cm^{-1}) to resistance (dyn sec cm^{-1}) is constant over the frequency range of interest. It will be seen (Chapter 10) that a resistance is chosen which is considerably less than would be indicated by the low-frequency ratio of 10^3 sec^{-1} indicated above; this is consistent with some very indirect evidence that the ground substance in collagenous tissue may be thixotropic, that is, its viscosity may decrease with increasing shear rate or frequency (Wilkes *et al.*, 1973).

3.8 Density

Kojo (1954) reported an average total weight of 14 mg for the human eardrum. From his area measurements he derived an overall area density of 25 mg cm^{-2}. There do not appear to be any more detailed data in his paper (which is in Japanese), but Kirikae (1960, p. 53) said that Kojo had found that "the central and peripheral parts of the drum are larger in their thickness and surface density" than the intermediate part. This implies a more-or-less constant volume density. Using my estimate of drum volume (Section 2.2.5), one can estimate the volume density to be about 3 g cm^{-3}. (From this one can work back to calculate area densities for the various parts of the drum; the area density, rather than the volume density and thickness separately, is required for the membrane model described below.)

This density of 3 g cm^{-3} may be compared with the density of light, cellular tissue which is mostly water, namely 1 g cm^{-3}; with that for dry collagen tissue, namely 1.4 g cm^{-3} (Harkness, 1961); and with that for compact bone, namely 2 g cm^{-3} (used by Vayo, 1971, for example). Harkness (1961) gave a typical value of 1.2 g cm^{-3} for undehydrated collagen. My estimate would appear to be too high, indicating either that Kojo's thickness measurements were too small, or that my estimate of drum volume from these measurements was inaccurate. (It seems unlikely that his weight measurement could have been so excessively large as to explain the discrepancy, unless he included the weight of the manubrium without so stating.) Although it is possible that the eardrum contains unusually dense collagenous tissue, it seems unlikely that its density, especially combined with the non-fibrous layers, could be as high as 3 g cm^{-3}.

One can suggest that the epidermal and mucosal layers are probably less dense than the lamina propria, and that within the latter the subepidermal and submucosal connective-tissue layers may be less dense than the fibrous layers. However, even if one could estimate the volume densities of the different types of tissue, there are no quantitative data available concerning thickness variations of the individual layers,

so it would be difficult to estimate variations of area densities.

Assuming, for lack of anything better, that the volume density is the same in other species as it is in man, then the area densities for use in the cat and guinea-pig membrane models would be smaller than for the human one because the drums are thinner (30-50 μm for cat, about 10μm for guinea pig, according to Lim, 68a).

Because the shell model considers only static conditions, the ear-drum mass is irrelevant there. For the cat membrane model I have used a surface density of 5 mg cm^{-2}, which corresponds to a volume density of something over 1 gm cm^{-3}, with a thickness of about 40 μm. For the guinea pig, with a thickness of 10 μm, I have used a surface density of 1 mg cm^{-2}.

CHAPTER 4

PROPERTIES OF STRUCTURES SURROUNDING THE EARDRUM

4.1 Introduction

This chapter will discuss the mechanical properties of structures around the eardrum, and the nature of the eardrum's coupling to them. Sections 4.2 and 4.3 concern the annular ligament and the manubrium, respectively. The main interest there is how the eardrum is attached to them. Sections 4.4 and 4.5 discuss the ossicular chain, which in the models exerts its effect on the eardrum through reactive and resistive forces acting on the manubrium. Finally, Section 4.6 discusses the middle-ear cavities.

As in the previous chapter, each section concludes with a statement of the parameter values adopted for the membrane and shell eardrum models.

4.2 Annular Ligament

The radial fibres of the eardrum, and some of the non-radial ones, extend into the annular ligament around the periphery of the pars tensa. This ligament is a fibrous thickening firmly attached to the bony tympanic ring, except superiorly where it separates the pars tensa from the pars flaccida. Even there it is stiff enough that one may consider it to be a rigid support for the eardrum.

The coupling between the eardrum and the annular ligament defines the peripheral boundary conditions for the system of partial differential equations describing the eardrum. For the purposes of the membrane model, all that one need specify is that the displacements of the eardrum are zero at the boundary. For the shell model, however, one needs to know not

only if the displacements are zero, but also whether the first derivatives of the displacements (slopes, or rotations) are zero at the boundary. If the derivatives are forced to be zero, the boundary is said to be "fully clamped". If they are unconstrained, the boundary is "simply supported". The two conditions are illustrated schematically in Fig. 4.1.

From drawings showing the insertion of the eardrum into the annular ligament (see, for example, Politzer, 1889, Fig. 135; Ruttin, 1921; and Filogamo, 1943, Fig. 16) one gets the impression that the boundary of the eardrum is fully clamped to the annular ligament and thence to the bony ring. The fact that there are elastic fibres in the ligament, and in the drum itself near the ligament, might however provide enough flexibility that the boundary should be considered to be simply supported.

In the shell model below I have chosen to treat the boundary as fully clamped. In Section 12.11 I show that making the boundary simply supported instead does not change the drum's overall behaviour very much.

(Gran (1968) said that Békésy had taken the boundary of the eardrum to be fully clamped, based on the fact that Békésy used the formulae for clamped beams when calculating eardrum stiffness (as discussed in Section 3.4.2 above). In fact, however, that assumption of fully clamped beams was independent of the nature of the drum's boundary conditions. In the case of the human experiment, the flap concerned was not supported at the periphery of the drum (or, at least, Békésy did not say it was). In the calf experiment, the rod was effectively fully clamped only because of the particular geometry of Békésy's test, as illustrated in Fig. 3.1.

4.3 Manubrium

The manubrium behaves as a rigid rod, at least by comparison with the eardrum. It is much stiffer than the latter both because it is bone and because it is much thicker. Khanna (1970) demonstrated that it does not bend significantly when the eardrum vibrates. In the membrane model below I assume that it is perfectly rigid, whereas in the shell model I

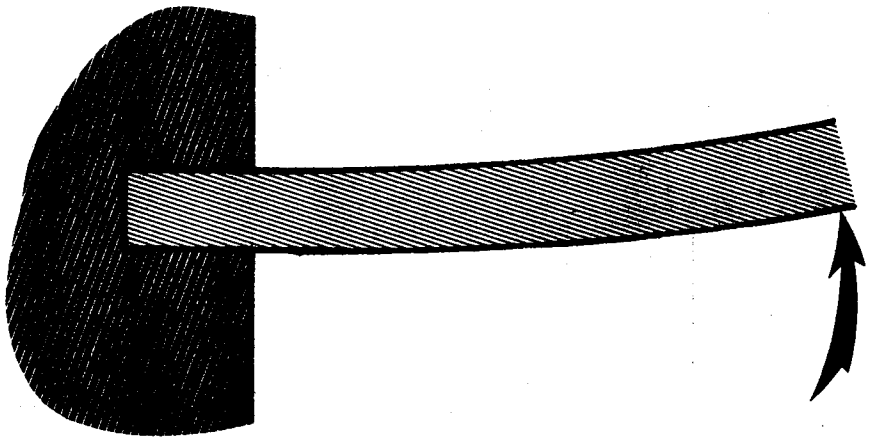

Fully Clamped

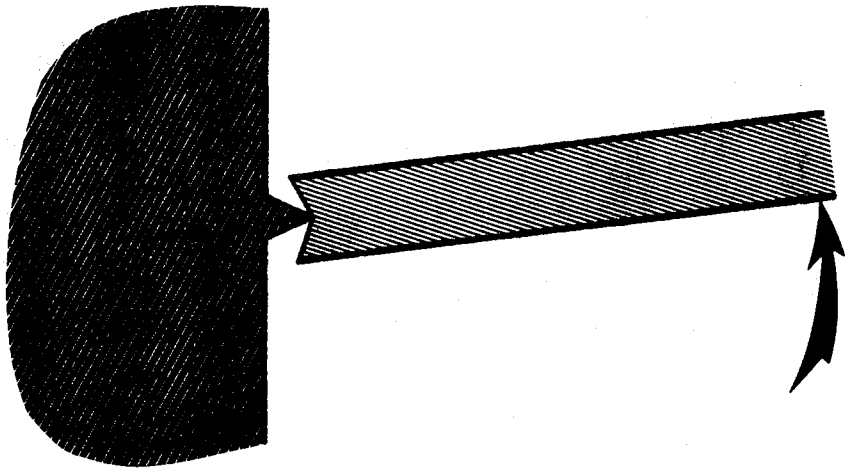

Simply Supported

Fig. 4.1. Schematic representation of two types of boundary conditions for plates. For a fully clamped plate, all of the displacements and slopes are constrained at the boundary. For a simply supported plate, on the other hand, only the displacements are constrained.

just assume it to be very stiff. The reasons for this slightly different treatment, and its implications, are discussed in Section 8.7.

As for the question of whether the eardrum is simply supported on or fully clamped to the manubrium, much the same considerations apply as in the preceding section. In the shell model I have assumed it to be fully clamped.

As noted in Section 2.3.5 above, the fibres of the eardrum are not directly inserted into the middle third of the manubrium, at least in the human. Tonndorf & Khanna (1972) noted that the drum and manubrium did not seem to be so tightly coupled in this region, although the effect was quite small. This condition has not been included in either of the models presented here.

4.4 Ossicular-Chain Stiffness and Damping

4.4.1 Introduction. As has been the practice in earlier models of the guinea-pig middle ear (Zwislocki, 1963; Funnell, 1972; Nuttall, 1972), I have lumped the mechanical properties of the ossicular chain (including the cochlear load) into three lumped elements: a spring, a dashpot (damper) and a mass. (This procedure was also followed by Peake & Guinan (1967) for the cat middle ear except that they also took into account a small compliance for the incudo-malleolar joint.) In this section I shall discuss the values to be given to the spring and dashpot elements for the guinea-pig, cat and human models. Note that the spring constant is used in both the membrane and shell models. The dashpot enters into only the membrane model, since the shell model does not consider dynamic effects.

4.4.2 Stiffness. There are no data available which provide an estimate for the stiffness of the ossicular chain separate from that of the eardrum. The middle-ear circuit models mentioned above do use parameter values for this quantity, but they are based strictly on empirical curve-fitting with models whose eardrum representations are very crude.

Consequently I have made an order-of-magnitude estimate of the ossicular stiffness by considering the suspensory ligament of the guinea-pig incus. For the purposes of the estimate I have modelled the ligament as a cylinder clamped to the incus at one end and to the cavity wall at the other end (see Fig. 4.2). If the central axis of the cylinder is taken to be in line with the axis of rotation of the ossicles, then the angular stiffness of the ligament is given (Seely & Smith, 1956, equation 62) by

$$\text{angular stiffness} = \frac{T}{\theta} = \frac{G\,J}{\ell} = \frac{G\,\pi\,d^4}{32\,\ell}\ ,$$

where T = torque (dyn cm),
θ = angle of twist (rad),
G = shear modulus (dyn cm^{-2}),
ℓ = length (cm),
J = polar moment of inertia of area (cm^4),
and d = diameter (cm).

Using values of 0.1 cm for d and ℓ, and 0.77×10^8 dyn cm^{-2} for G (corresponding to a Young's modulus of 2×10^8 dyn cm^{-2}, as used for the eardrum, and a Poisson's ratio of 0.3) gives an angular stiffness of 7500 dyn cm. Taking a lever arm of 0.3 cm (for a point about half way down the manubrium) gives a linear stiffness of 8×10^4 dyn cm^{-1}. With a cosine correction term for the inward-pointing angle of the manubrium, this becomes about 10^5 dyn cm^{-1}. It might be argued that this estimate will be too high since the ligament would not be able to use its fibres' stiffness fully when operating in torsion, but Fumagalli (1949) has reported a spiral fibre arrangement in the incudal ligament (see Fig. 4.3) that would tend to increase the effective stiffness. In addition, this stiffness estimate must be increased to account for any departure of the axis of rotation from the centre of the cylinder, as well as for the other suspensory structures of the ossicular chain (especially the annular ligament of the stapes).

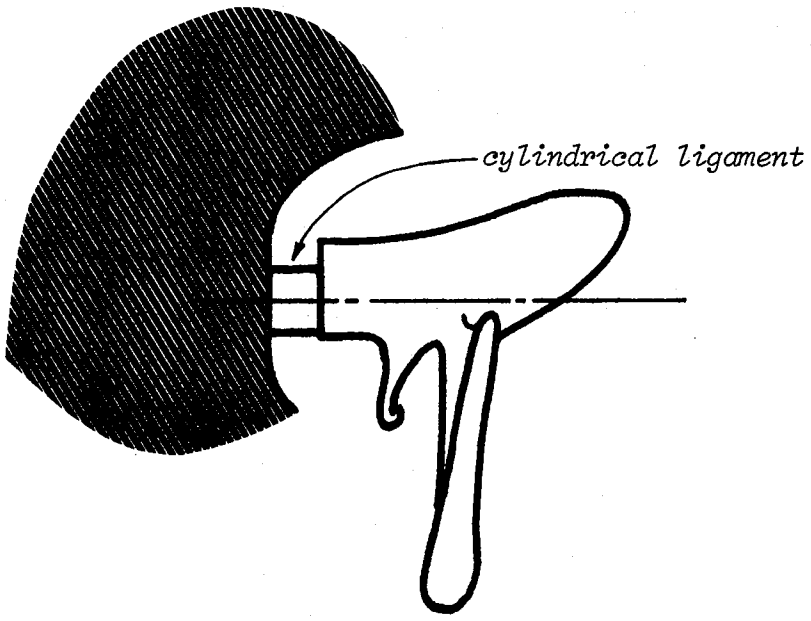

Fig. 4.2. A simplified model of the guinea-pig posterior incudal ligament. The malleus and incus are considered to be fixed to the wall of the tympanic cavity by a right-cylindrical ligament.

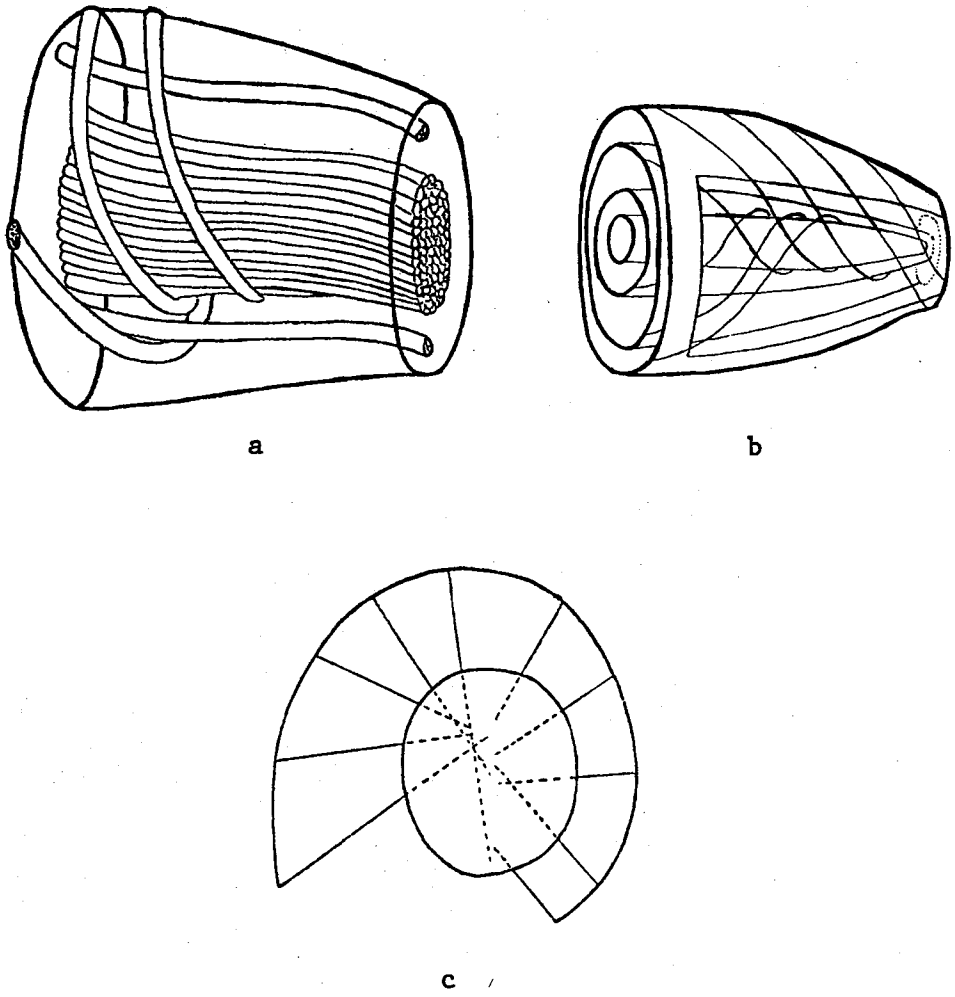

Fig. 4.3. Fibre structure of the incudal ligament. Parts *a* and *b* represent the lateral incudal ligaments of man and dog, respectively. (The ligament in the cat is very similar to that of the dog.) In each case the wall of the tympanic cavity is on the left and the incus is on the right, as in Fig. 4.2. The spiral arrangement of the collagenous fibres is obvious. Part *c* shows a cross-section through the guinea-pig tympanic wall, ligament and incus. Although a regular spiral arrangement is not evident, neither is the arrangement of fibres strictly radial. (After Fumagalli, 1949)

For the eardrum models presented below, I have adopted 10^5 dyn cm^{-1} as the value of the ossicular stiffness for the guinea pig. For the cat and human models I have used a value three times as large, since the ossicles and ligaments are larger in these species.

These values are very crude estimates, but they do provide orders of magnitude for physiologically reasonable parameter values. It will be seen that these estimates do in fact come reasonably close to matching observed eardrum behaviour. It is not within the scope of this work to search for better estimates.

4.4.3 Resistance. As was the case for the stiffness discussed above, previous estimates for ossicular-chain damping, or resistance, have been based on curve-fitting with models which incorporate rough empirical approximations of the eardrum. Similarly, attempts to measure the degree of damping of the middle ear (Frank, 1923; Békésy, 1933) have included the effects of the air cavities and of the eardrum as well as of the ossicular chain.

As a first approximation, I have adopted the same ratio of stiffness to resistance as mentioned in Section 3.7 above for collagenous tissue, namely, 10^3 sec^{-1}. In fact, the total resistance is likely to be higher than this, in part because of viscous losses in the cochlea. For the purposes of studying the vibration of the eardrum, however, this parameter is not of primary importance.

4.5 Ossicular Moment of Inertia

4.5.1 Introduction. I have estimated moments of inertia for the ossicles of the cat, guinea pig and human by modelling them as assemblages of cylinders based on morphological data. For example, Fig. 4.4 shows the model used for the human. The bodies of the malleus and incus are represented by two cylinders fixed end-to-end, and the long processes are

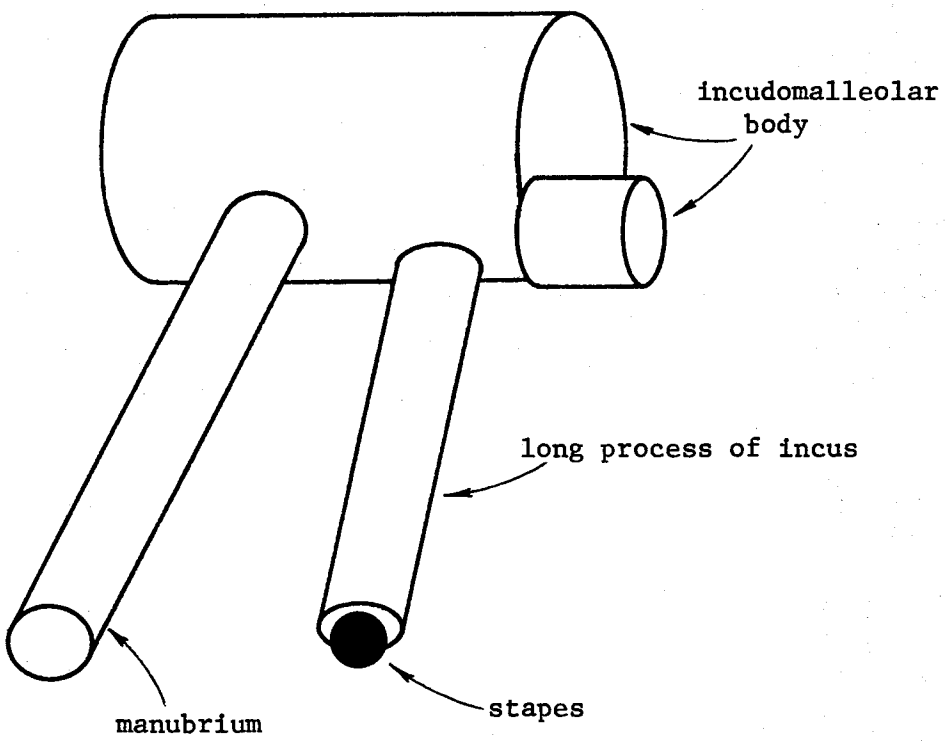

Fig. 4.4. Geometrically simplified model of the ossicular chain. The malleus and incus are modelled by a combination of four right cylinders. The stapes is represented by a point mass.

represented by two long, narrow cylinders perpendicular to the body cylinders. The densities are assumed to be uniform for convenience, in spite of evidence to the contrary (Kirikae, 1960). The stapes is represented by a point mass at the end of the long process of the incus; its shape does not matter since it is assumed to move in a straight line (that is, piston-like motion) parallel to the direction of the force applied to the eardrum. Its effect is small compared to the inertia of the malleus and incus.

4.5.2 Human. Fig. 4.5a shows the dimensions of the model used for the human ossicles. The dimensions are based on measurements by Fumagalli (1949); I have estimated equivalent lengths for the cylinders by eye. The total volume of the malleus-and-incus model is about 0.04 cm^3. (Note that Wever & Lawrence (1954, p. 417) quoted an ossicular volume of 0.5 to 0.8 cm^3 from Békésy (1936). In fact, Békésy was reporting the volume of that part of the middle-ear cavities where the ossicles are located. Stuhlman (1943, p. 262) reported that the ossicular volume was about 7% of the cavity volume, or 0.035 to 0.056 cm^3.)

The combined mass of the malleus and incus has been taken as 55 mg, which is approximately the value given in Wever & Lawrence (1954); it corresponds to a density of about 1.4 gm cm^{-3}. The stapedial mass is taken as 3 mg, based on the same source.

Fig. 4.5b shows the calculated ossicular moment of inertia as a function of the assumed position of the axis of rotation. The minimum moment of inertia is 2.1 mg cm^2, and it ranges up to about 3 mg cm^2 for likely positions of the axis of rotation. By comparison, Frank (1923, p. 63) measured (rather indirectly) a value of 2.5 mg cm^2. (Wever & Lawrence (1954, p. 391) incorrectly quoted the units as gm cm^{-2} instead of gm cm^2.) Frank's value is equivalent to the inductance of 40 mH used by Zwislocki (1962) in his circuit model, based on a lever arm of about 0.5 cm and an 'effective' eardrum area of 0.55 cm^2.

The dotted curve in part *b* of the Figure is the moment of inertia recalculated with zero stapedial mass. The difference is not great.

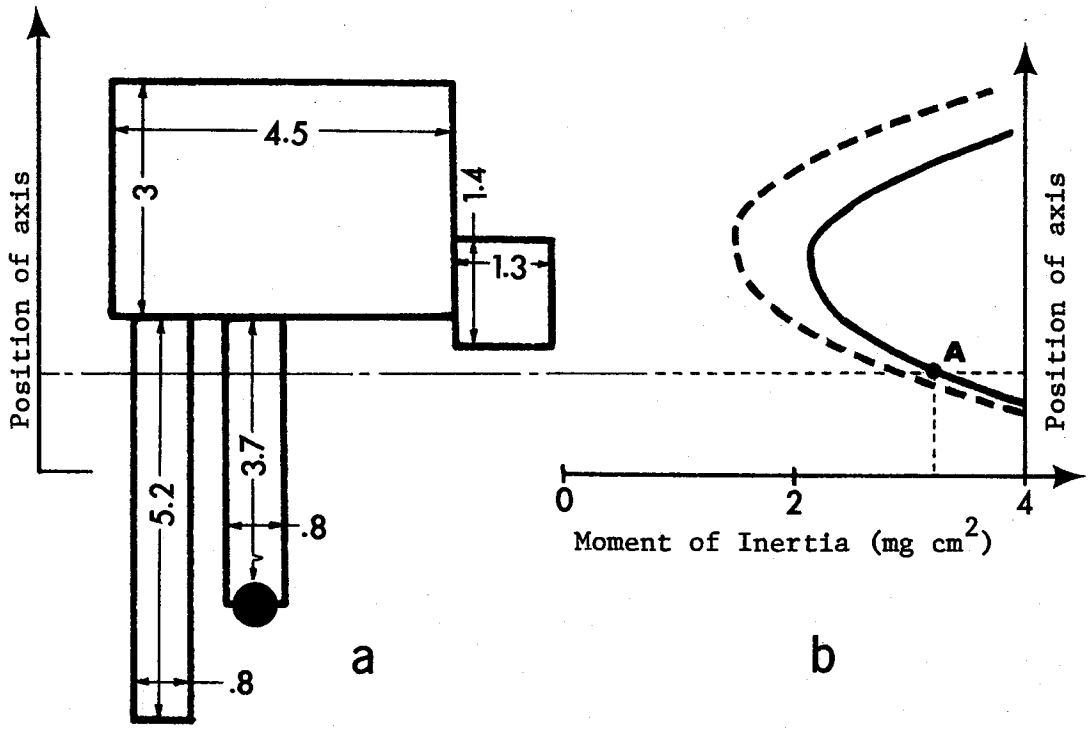

Fig. 4.5. Moment of inertia of human ossicles. Part *a* shows the dimensions (in mm) of the model used. Part *b* shows the calculated ossicular moment of inertia as a function of the position of the axis of rotation, which is taken to be parallel to the axes of the cylinders representing the incudo-malleolar bodies. A given point on the vertical axis in *b* corresponds to an axis position at the same level in *a*. For example, point *A* gives the moment of inertia for the particular axis position indicated. The solid curve was calculated with the stapedial mass included, the dashed curve without it.

4.5.3 Cat. Fig. 4.6a shows the model dimensions used for the cat. Since I could not find a published figure for the mass of the ossicles, I estimated their volumes (6.3 mm^3) and calculated a mass based on a density of 1.8 gm cm^{-3}: the result was a combined incudo-malleolar mass of 11 mg. I adopted a mass of 1 mg for the stapes (scaled down from the human value).

Part *b* of the Figure shows the calculated moment of inertia in the same format as Figure 4.5b. The minimum is 0.12 mg cm^2, and it does not become much larger for reasonable axis locations. To allow for the added masses of ligaments and muscles, and for cochlear loading, I have used a value of 0.2 mg cm^2, or 2 x 10^{-4} dyn cm sec^2, in the membrane model. The shell model applies only to static displacements and thus does not use this parameter.

4.5.4 Guinea Pig. Fig. 4.7a shows the dimensions of the model for the guinea pig. The masses used were 8 mg for the malleus and incus, and 0.5 mg for the stapes (Mundie, 1971). This results in a density of 1.8 gm cm^{-3}.

Again, part *b* of the Figure shows the calculated moment of inertia. The minimum is at 0.06 mg cm^2. As for the cat, I have added to this somewhat, using a value of 0.1 mg cm^2 in the membrane model.

Note that if one assumes a lever arm of 0.5 cm, corresponding approximately to the length of the manubrium, and an eardrum area of 0.4 cm^2, then the augmented estimate of 0.1 mg cm^2 corresponds to an acoustical inertance of $\frac{I}{\ell^2 A^2} = 2.5$ mg cm^{-4}. This is equivalent to an inductance of 2.5 mH in terms of the circuit model of Zwislocki (1963). By comparison, Zwislocki used values of 30 to 40 mH in the model. The much smaller value used here is consistent with the demonstration by Johnstone & Taylor (1971) that ossicular mass appears to have little effect on middle-ear transmission within the audio-frequency range.

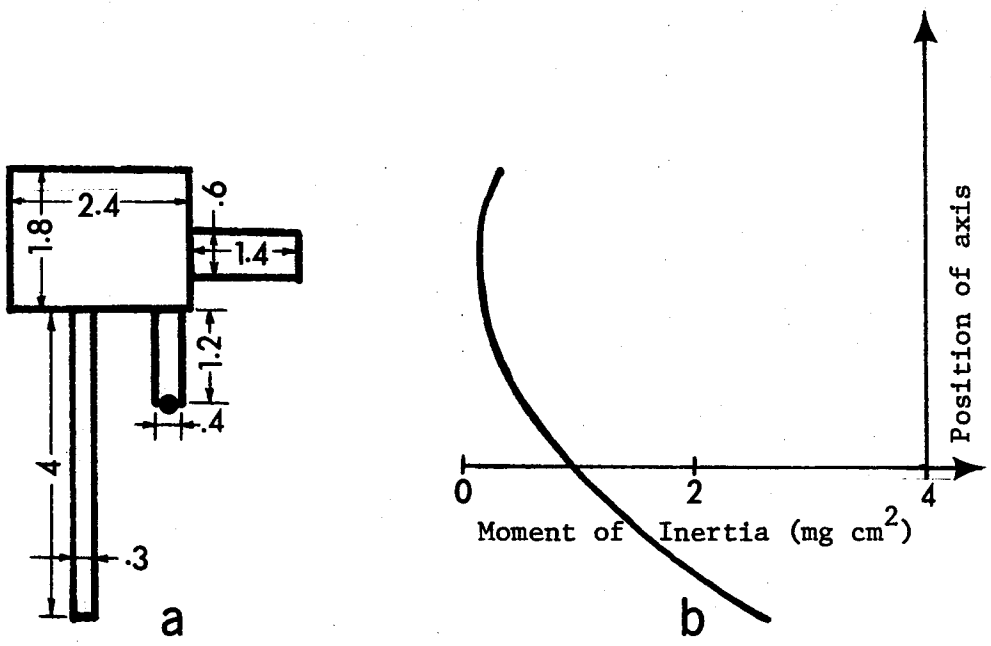

Fig. 4.6. Moment of inertia of cat ossicles. The format is the same as that of Fig. 4.5.

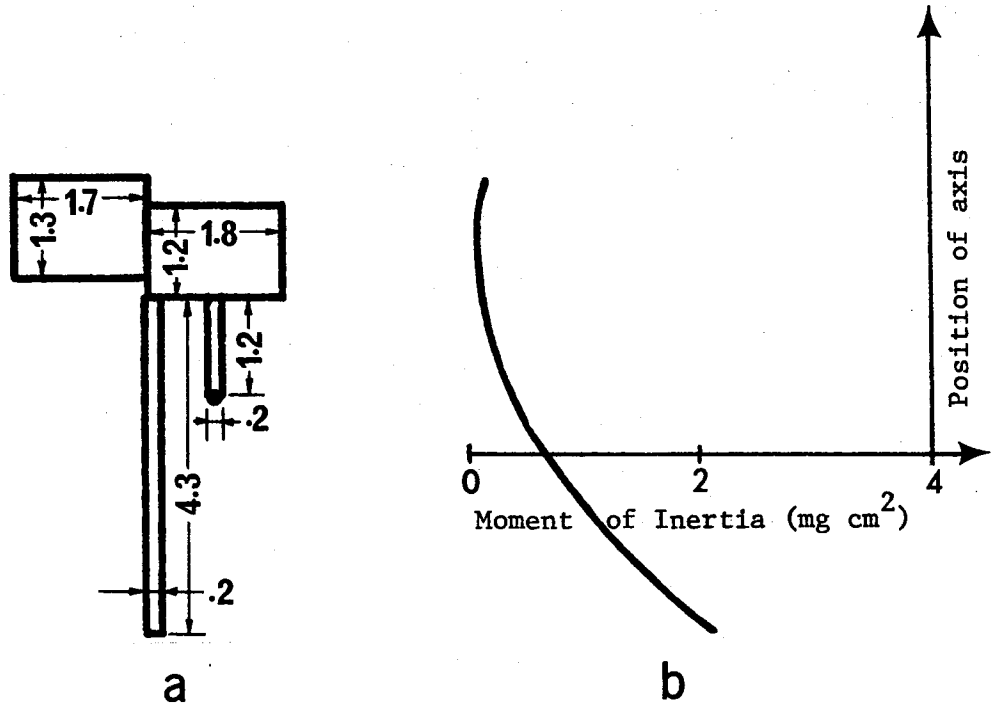

Fig. 4.7. Moment of inertia of guinea-pig ossicles. The format is the same as that of Fig. 4.5.

4.6 Middle-Ear Air Cavities

The relationships of the middle-ear and external-ear cavities to the eardrum and ossicular chain are shown schematically in Fig. 4.8a. The effects of these cavities are included in the model as shown by the equivalent electrical circuit in Fig. 4.8b. The large block represents the eardrum model itself, with associated boundary conditions and ossicular forces. The main middle-ear cavity is represented by the capacitor C_{b1}, which effectively applies a uniform pressure to the medial face of the eardrum. This pressure combines with the applied sound pressure to form the net force acting on the drum. The capacitor C_{b2} represents a secondary cavity, the epitympanic in the guinea pig and the entotympanic in the cat. This secondary cavity is connected with the primary one by a narrow opening whose acoustical resistance and inertance are given by R and L , respectively. This arrangement is the one first used by Zwislocki (1963) in his guinea-pig middle-ear model, based on observations by Mundie (1962).

The capacitor C_e represents part of the volume of the external ear canal. This is immaterial in calculating eardrum displacements but has some effect on the calculations of acoustical input impedance of the middle ear (see Section 8.10). It is included for the purposes of comparing the eardrum model to my earlier guinea-pig impedance data (Funnell, 1972).

For the shell models, both guinea-pig and cat, I have not included the effects of the air cavities. It is not necessary since for the guinea pig the experimental data to which it is compared (Manley & Johnstone, 1974) were measured with the bulla open; and for the cat the middle-ear cavities are large enough that they have a negligible effect at the low frequencies to which the model is applied (Peake & Guinan, 1967).

For the cat membrane model I have taken both R and L to be zero, and have assumed the total cavity volume to be 2 cm^3; this is equivalent to a total capacitance $(C_{b1}+C_{b2})$ of 1.4 μF.

However, these values are unimportant since, except at low frequencies, I only compare the shapes of the vibration patterns with the experimental

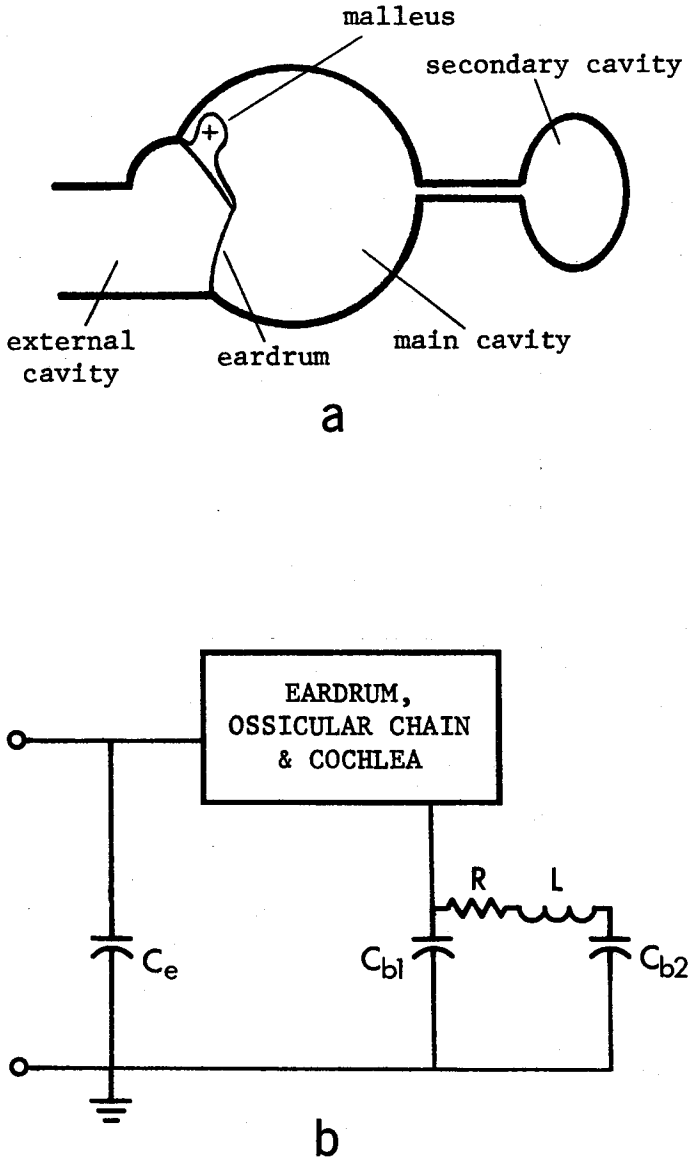

Fig. 4.8. Schematic representations of the effects of the air cavities on the eardrum. Part *a* is a simplified diagram of the acoustical system. (The incus, stapes and cochlea have been omitted for clarity. See Fig. 5.12 for a more accurate representation of the guinea-pig middle ear.) Part *b* is an equivalent electrical circuit, as explained in the text.

results of Khanna and Tonndorf, not the actual displacements. The low-frequency displacements are little affected by the air cavities, as mentioned above, and the shapes of the vibration patterns are completely independent of the air cavities (since the back pressure on the drum is assumed to be uniform). In any case, Khanna & Tonndorf (1972a) did not measure the cavity volumes in their cats.

The volume represented by C_e in the cat membrane model has been taken to be very small, so that it would have an insignificant effect on the calculated impedance. It is immaterial since I do not compare the impedance of the cat model with experimental data.

The cavity parameters are more important for the guinea-pig membrane model, since for it I calculate the input impedance as a function of frequency for comparison with some experimental results. I have used the same parameter values used in Funnell (1972) for a typical guinea pig. These values were based on anatomical measurements and on measurements of the impedance of the cavities themselves. The values are 0.12 μF, 0.02 μF, 200 ohm, 76 mH, and 0.03 μF for C_{b1}, C_{b2}, R, L and C_e respectively.

Note that the radiation impedance of the air surrounding the eardrum has not been taken into account in the membrane model. This has generally been neglected in middle-ear models, although Michelsen (1971) did attempt to account for it in his analysis of the locust ear.

CHAPTER 5

EXPERIMENTAL OBSERVATIONS OF EARDRUM VIBRATIONS

5.1 Introduction

This chapter is a review of previously published observations of eardrum vibration patterns. Most of these observations have been at low frequencies, that is, zero to 1 or 2 kHz: the eardrum's mode and amplitude of vibration are essentially constant over this frequency range. Section 5.2 presents an approximately chronological discussion of such low-frequency observations. Section 5.3 discusses higher-frequency observations, which essentially consist of the recent work of Khanna & Tonndorf.

There are many ways of monitoring middle-ear function which do not provide explicit information about the vibration pattern of the eardrum. In particular, a great many measurements have been made of such things as ossicular displacements, cochlear potentials and middle-ear acoustical input impedance. The last, although it does not give a direct description of the drum's vibration pattern, does depend more on the behaviour of the drum and less on the rest of the middle ear than do ossicular displacements and cochlear potentials. For this reason it will be discussed in Section 5.4.

This chapter will be concerned only with the normal behaviour of the eardrum. Many reports have been published on the effects of changes in the ossicular chain (Elpern *et al.*, 1965), in the tympanic cavities (Onchi, 1961; Mundie, 1962; Webster, 1962), in the static pressure on the drum (Mundie, 1962; Hoeft, 1964), and in the middle-ear muscles (Borg, 1972); and on the effects of eardrum excisions and perforations, whether covered, healed or left open (Payne & Githler, 1951; McArdle & Tonndorf, 1968; Tonndorf *et al.*, 1971, 1972). However, only the holographic experiments of Tonndorf *et al.* produced measurements of actual vibration

patterns, and even these experiments do not yet provide enough information to permit quantitative modelling. I shall therefore not consider pathological behaviour of the eardrum in this thesis.

5.2 Low-Frequency Vibration Pattern

5.2.1 Introduction. The earliest observations of eardrum vibrations were direct visual ones, generally under stroboscopic illumination. These experiments are discussed in Section 5.2.2. In 1900, the use of a mechanical probe was reported; this is discussed in Section 5.2.3. Later, in an attempt to magnify the small motions of the eardrum, the reflection of light from small mirrors attached to the drum was observed, as described in Section 5.2.4.

Section 5.2.5 deals with the famous measurements of Békésy (1941) using a capacitive probe. The next section then discusses some further visual (or photographic) observations.

The first technique which produced detailed vibration patterns was reported by Khanna (1970). Section 5.2.7 treats those observations and subsequent ones by Khanna and Tonndorf. Section 5.2.8 discusses the measurements by Manley & Johnstone (1974) using the Mössbauer technique.

Section 5.2.9 consists of a discussion of this body of experimental results, and in particular considers some possible reasons for the discrepancy between Békésy's data and the rest. Finally, Section 5.2.10 concludes with a statement of the eardrum vibration characteristics used for comparison with the models in Chapters 10 and 12.

5.2.2 Visual observations I. Kessel (1874) reported direct visual observations of eardrum displacements due to static pressures in human cadaver ears, using a simple magnifying lens. With respect to the pars tensa, he found that under a positive pressure in the ear canal the eardrum moved inwards and the curvature of the radial fibres flattened; under a negative pressure the curvature increased. The greatest displacements were

seen in the posterior segment of the drum.

Kessel also used a stroboscope to observe vibrations at 256 Hz and 512 Hz, again using a magnifying lens. Again the displacements were larger posteriorly, although in this case he said that the greatest displacements occurred in the central region of the drum where there are no circular fibres.

The pressure used in these experiments was 3 to 4 inches of water. (Note that these were not English inches: there were a number of different definitions of the unit "Zoll" in use in Germany at the time, but they were all in the range of about 2.4 to 3.2 cm (Brockhaus, 1966, p. 386).) This is equivalent to about 155 dB SPL. Mach & Kessel (1874) mentioned taking some measurements at a pressure about 6 dB less.

Lucae (1901) also observed eardrum vibrations visually under stroboscopic illumination. The stimuli were air-pressure variations with unspecified amplitudes and poorly defined waveforms (see Figures in Lucae, 1900b), with repetition rates up to about 35 per second. He did not present quantitative results, but said that the greatest displacements appeared to occur at the manubrium and in the posterior superior quadrant. These observations seem to be at variance with his statement in another paper (Lucae, 1900a) that the motions of the manubrium are smaller than those of the drum itself, in agreement with Helmholtz' principles, but he did not elaborate. Note that Lucae's observations were made on waking patients.

5.2.3 Mechanical probe. Mader (1900) used a mechano-electrical probe to study eardrum vibration. The probe consisted of a small rod attached to the movable plate of a variable-resistance microphone. The amplitude of the microphone output was estimated on the basis of the threshold of detectability in a telephone ear-piece in another room. The pressure exerted on the eardrum was adjusted to be the same in all measurements. In response to tones of 240 Hz and 600 Hz, as well as to a pulse of unspecified duration and shape, Mader found the greatest amplitude to be in the posterior inferior quadrant of the human cadaver eardrum (see Fig. 5.1). He also used the probe at three points in a line extending downwards from

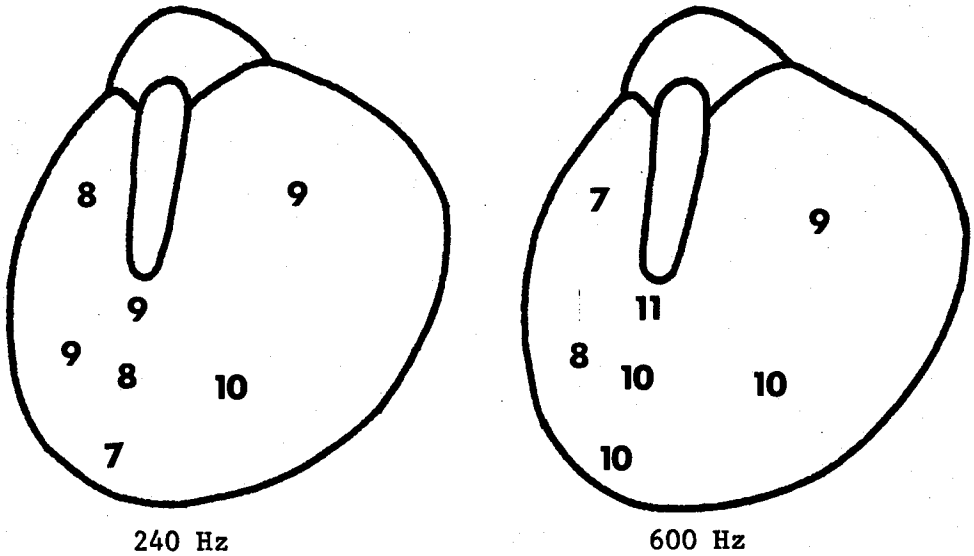

Pure-tone stimulus

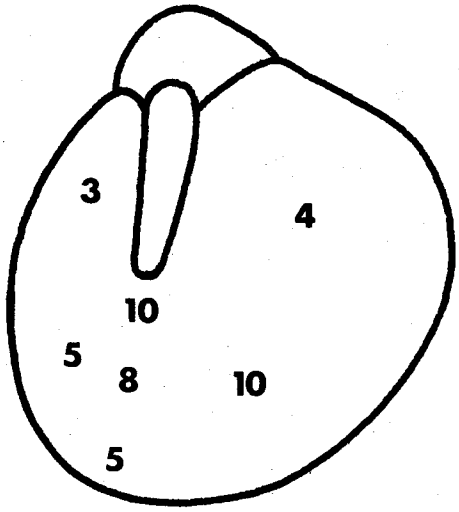

Pulse stimulus

Fig. 5.1. Relative probe outputs found by Mader (1900). The values here have been obtained by normalizing with respect to the value in the posterior inferior quadrant. In addition, I have taken the reciprocals of the values given by Mader for the pulse stimulus, since for that series of experiments his measured variable was inversely proportional to the amplitude of the microphone output. As noted in the text, these numbers are not necessarily directly related to eardrum displacements because of differences in coupling to the probe.

the tip of the manubrium. The probe output was greatest from the inner third and least from the outer third. However, the output from the middle third contained a distortion which he interpreted as indicating large displacements there that were poorly coupled to the probe. Thus, the conclusion is that the greatest drum displacements occur in the posterior inferior quadrant and that they are smaller near either the manubrium or the periphery than they are part way between.

From Mader's published data one cannot calculate either the sound pressures that he used, or the impedance with which his probe loaded the eardrum.

5.2.4 Mirrors. As early as 1874, Kessel suggested observing eardrum and ossicular displacements by fixing tiny mirrors to the surface under question, and using the angle of reflection of a beam of light as a measure of the motion of the mirror. Köhler (1910) used this method for measuring malleolar displacements but did not investigate the vibration pattern of the drum itself. Wada (1924) used the method on the eardrum, but published vibration-pattern data only for non-mammalian species.

Dahmann (1929, 1930) used mirrors on human cadaver eardrums, with the stimulus being a static pressure change. Fig. 5.2a shows his only published data. The black marks superimposed on the sketch of an eardrum represent the loci of the reflected beams of light from the nine mirrors positioned approximately where the numbers are written. The length of each mark is a measure of the angular deflection of that mirror, that is, it is a measure of the slope of the displacement function at that point.

In interpreting these patterns one must pay attention to the sign of the displacement slope. For example, the mirrors 7, 6, 2 and 3 are all rotating from side to side with little vertical rotation, but from the illustration one cannot tell whether these rotations are in or out of phase with one another, and Dahmann did not specify this in his discussion. The lines labelled *b* to *e* in the Figure are my calculations of the eardrum displacement function in a horizontal line through the tip of the manubrium, including mirrors 7, 6, 1, 2 and 3. (My method is presented in Appendix 2.)

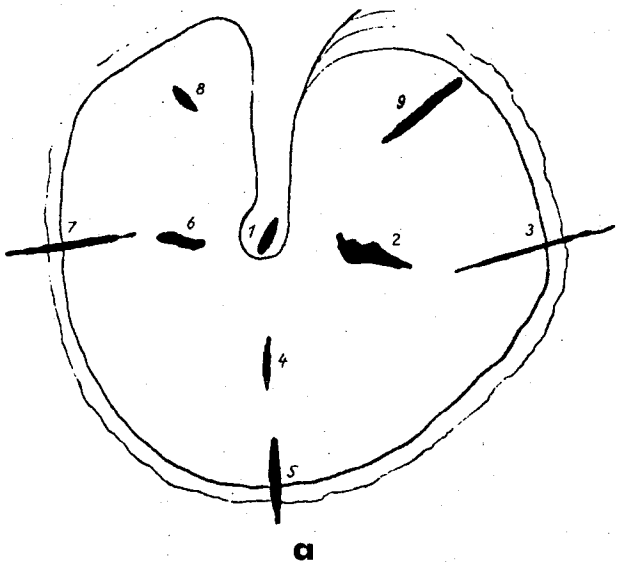

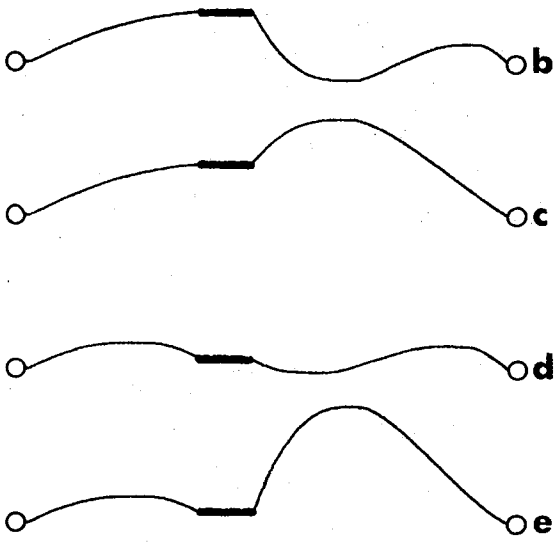

Fig. 5.2. Results of Dahmann's experiment. Part *a* is from Dahmann (1930). Parts *b* to *e* are horizontal displacement profiles through the umbo. See text for explanation.

For all four lines I assumed that the slope was positive (that is, displacement amplitude increases toward the right) at mirror 7 and negative at mirror 3, but each line represents a different combination of slope signs for mirrors 6 and 2. Evidently lines *b* and *d* are not realistic, since part of the right half of the drum is displaced in the wrong direction. Lines *c* and *e* show qualitatively similar shapes for the right half, but the left half presents a maximum between the periphery and the manubrium in line *e* and not in *c* . Wever & Lawrence (1954, pp. 83-85) interpreted Dahmann's results as meaning that neither side exhibited such a maximum. Dahmann himself however (1930, pp. 350-351) interpreted them as meaning that the middle parts had larger displacements than the manubrium as in line *e* .

The pressures used in these experiments were about 60 mmHg in each direction (Dahmann, 1929), equivalent to about 170 dB SPL. Wever & Lawrence (1954, p. 86) pointed out that this pressure is too high to be representative of normal operation of the eardrum, and suggested that it is "a hundred times or more what the ear can safely withstand." They were presumably thinking of the safety of the inner ear, which can sustain immediate damage at intensities in the range of150 to 160 dB SPL (Beranek, 1954, p. 397). It would be more appropriate to compare Dahmann's pressures with those that can damage the eardrum: Kobrak (1959, p. 7) gives a drum-bursting pressure of less than twice Dahmann's pressure. Zalewski (1906, cited by Sudderth, 1974) found that static pressures of 5.4 to 43.2 psi, equivalent to 182 to 200 dB SPL, caused rupture of eardrums of human cadavers. White (1967, cited by Sudderth, 1974) found ruptures occurring in half of his dogs and goats at shock overpressures of about 190 dB SPL. Thus, Dahmann's pressures were definitely less that what would cause drum rupture. However, the safety margin was perhaps as small as a factor of two, and it seems safe to agree with Wever & Lawrence that his observations are of little value for describing normal eardrum vibrations.

5.2.5 Capacitive probe. The next observations of drum vibration patterns were those of Békésy (1941), who used a capacitive probe on human cadavers. In his case also, only one illustration of his results was published. In Figure 5.3a I have reproduced his drawing showing the vibration pattern that occurs below 2 kHz. In Fig. 5.3b I have redrawn it, removing the contour labelled *1* so that the remaining contour lines represent equal increments of amplitude. As shown in Fig. 5.3c, he found that the central portion of the drum underwent almost no bending in the direction perpendicular to the manubrium. However, as shown in Fig. 5.3d, a section along the direction of the manubrium indicates considerable bending of the drum inferior to the manubrial tip. This is not consistent with the usual interpretation of his findings, which is, in his words, that "the whole eardrum except the extreme periphery vibrates as a stiff surface along with the manubrium". My interpretation of his equal-amplitude curves is that the part of the drum inferior to the umbo is stiff in one direction only, and bends quite a bit in the orthogonal direction.

This inconsistency is perhaps caused by inaccuracy in his Figure showing iso-amplitude curves. It is noteworthy that the flat portions of the contours are not quite parallel to the rotation axis as drawn, which is most unexpected. Unfortunately, no actual data were given which would permit clarification of his findings.

It is also impossible to decide with certainty whether his observations were made at intensities within the normal operating range of the ear, since he published neither the sound pressures used nor the actual displacements measured. However, he indicated that his probe could measure down to about 10 nm. In his Fig. 5-5 (1941) the iso-amplitude contour lines cover a range of 1 to 15 (arbitrary units) so one can guess that the maximum displacement was at least 150 nm. By comparison, Tonndorf & Khanna (1970) found a maximal drum displacement of 800 nm at 121 dB SPL (at 525 Hz, in human cadaver). On this basis, one can conclude that Békésy's measurements could have been performed at intensities as low as about 110 dB SPL, which is starting to be uncomfortably loud, but is still within the linear range of the middle ear.

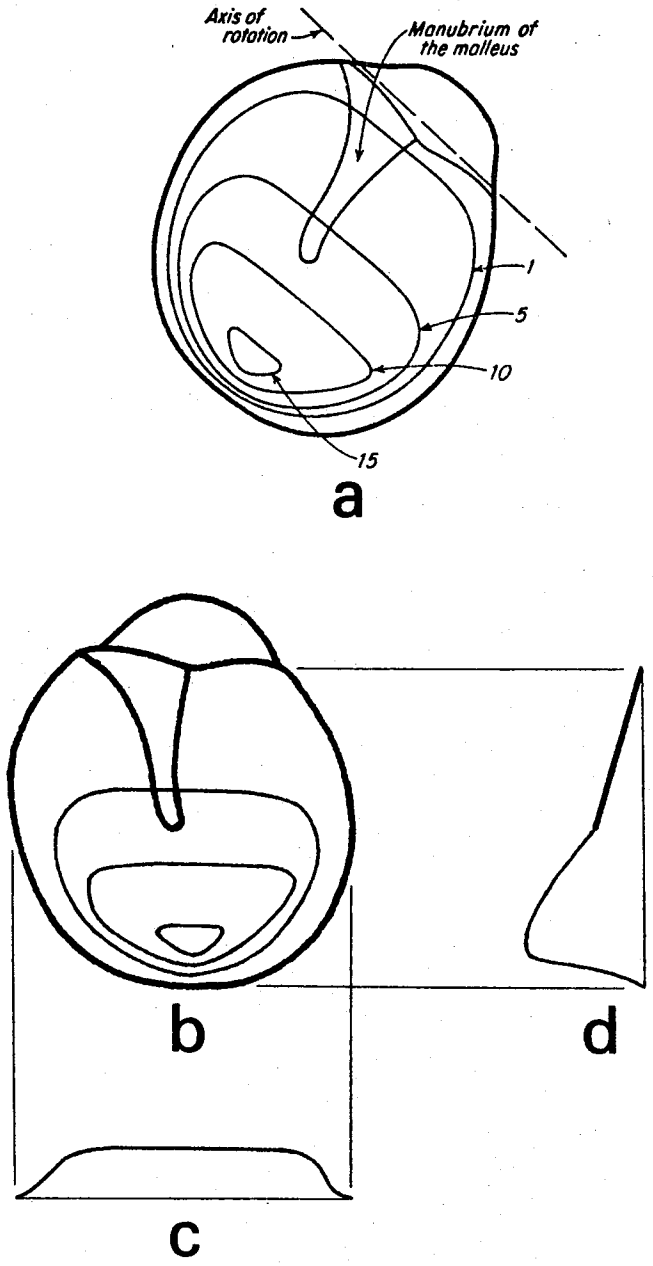

Fig. 5.3. Vibration pattern measured by Békésy in human cadaver, at frequencies below 2 kHz. Part *a* is from Békésy (1941). Part *b* has been redrawn based on *a*. Part *c* is a horizontal displacement profile through the umbo. Part *d* is a vertical displacement profile through the manubrium; the interpolation between contour lines is based on the assumptions that the displacement is zero where Békésy indicates the axis of rotation to be, and that the manubrium is rigid.

5.2.6 Visual observations II. Kobrak (1941) described the observation of the eardrums of human cadavers using high-speed cinematography, and later (1943) discussed the use of stroboscopic illumination with both cadavers and living subjects. In neither of these papers did he actually give the results of his observations. Kirikae (1960) cited the 1941 paper as having said that the amplitude of the intermediate part of the drum was greater than that of the central and peripheral parts. In his much later book (1959), Kobrak said that "the fold described by Békésy, around which the drum membrane vibrates, was observed" (p. 40).

Kobrak (1959, p. 40) mentioned a sound intensity of about 110 dB at 60 Hz, which was "not too unpleasant" and could easily be tolerated by the waking subject. It is not clear whether his intensity measurement was dB SPL, dB hearing level, or dB loudness level. 110 dB HL at 60 Hz is equivalent to about 160 dB SPL; 110 dB loudness level (that is, 110 phons) at 60 Hz is equivalent to 110 - 130 dB SPL (Beranek, 1954, Fig. 13.9 and 13.10).

Perlman (1945) described results using the same stroboscopic method as Kobrak. He reported that observations on cadavers indicate that the amplitudes of vibration of the anterior and posterior parts are about the same, although observations in the living ear (because of the difficulties involved) seem to indicate much smaller amplitudes in the anterior part. The greatest amplitude appeared to be "halfway between the umbo and the postero-superior part of the annulus", and the smallest amplitude was seen on the manubrium. No quantitative results were given.

Owada (1959) published sketches of his observations of the vibration patterns of the eardrums of the cat and rabbit, observed under stroboscopic illumination at frequencies of 500 to 1000 Hz. His results are reproduced in Fig. 5.4. In both species the greatest amplitudes are found midway between the manubrium and the periphery, anteriorly and posteriorly as well as inferiorly. (He attributed the differences between the two species to differences in the arrangements of the fibres of the drums.) The stimuli were in the range of 100 to 120 phons, equivalent to 100 to 130 dB SPL (see Beranek, 1954, Fig. 13.9 and 13.10).

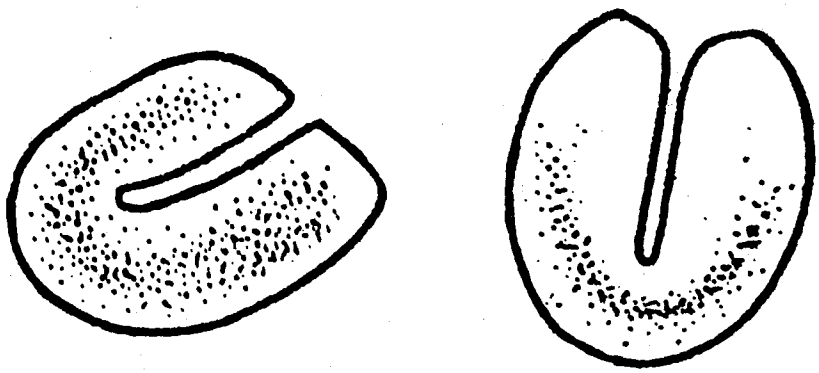

Cat *Rabbit*

Fig. 5.4. Vibration patterns in cat and rabbit. The density of the stippling indicates vibration amplitude. (After Owada, 1959)

Kirikae (1960) also used microscopy and microphotography under stroboscopic illumination to observe the vibrations of human cadaver eardrums. He used frequencies of 100 to 800 Hz, and loudnesses of 100 to 120 phons (100 to 140 dB SPL according to Beranek, 1954, Fig. 13.9 and 13.10). His observations are summarized in Fig. 5.5. Part *a* indicates his conceptual division of the drum into central, intermediate and peripheral parts. The largest displacements occur in the intermediate part, as shown in part *b* , with the displacements in the posterior superior quadrant being larger than those in the other quadrants. Kirikae concurs with Békésy in saying that "the central part vibrates as a rigid cone" (Kirikae, 1960, p. 53), but according to the curve of Fig. 5.5b this rigid central part is hardly wider than the manubrium itself.

Kirikae's published photograph showing the motion of the entire malleus (1960, Fig. 53) indicates a medial-to-lateral translation as well as a rotation. Kirikae does not comment on this, but it may well be a result of the large displacements observed. Perlman (1945) mentioned a "posteromedial displacement of the whole malleus handle".

5.2.7 Holography. Khanna (1970) reported the first use of laser holography to study eardrum vibrations. This is an interferometric technique which immediately produces complete iso-amplitude contour maps of a vibrating surface, rather than requiring interpolation among point displacement measurements. The absolute amplitudes corresponding to the various contour lines are precisely defined in terms of the wavelength of the laser light used, the smallest amplitude being 0.12 μm in Khanna's case. The contour spacing is not quite uniform: it is expressed in terms of a Bessel function, and is 0.121 μm between contours 0 and 1,0.157 μm between 1 and 2, and 0.158 μm from there on. Except for the most detailed quantitative study, this nonuniformity need not be considered.

The contour lines (or dark fringes) produced by this technique are not thin and sharp. They may be more or less broadened to indicate areas of approximately equal displacement, and the contrast between them and the light background decreases at higher amplitudes.

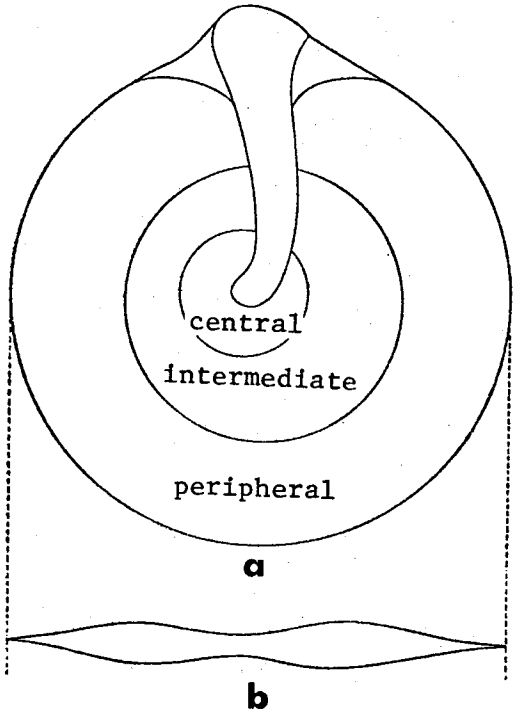

Fig. 5.5. Vibration pattern of human eardrum. In part *a* is shown an outline of the eardrum, indicating the division into central, intermediate and peripheral zones. Part *b* indicates vibration amplitudes in a horizontal section through the drum at the level of the umbo. (After Kirikae, 1960)

These observations were made at frequencies from about 400 to 6000 Hz. The sound intensities were adjusted to provide good contour patterns, and were as low as about 90 dB SPL in some cases.

Khanna (1970) presented results observed in cat cadaver ears. It was later shown (Khanna & Tonndorf, 1972a) that the patterns are not significantly different in live cats. A typical low-frequency pattern is shown in Fig. 5.6. The displacements are greatest partway between the manubrium and the periphery, and are greatest in the posterior segment of the drum.

The same technique was later used to investigate human cadaver ears (Tonndorf & Khanna, 1972). A typical low-frequency pattern is shown in Fig. 5.7. Again the displacements on the manubrium are smaller than those of the surrounding eardrum, and the largest displacements occur in the posterior segment.

5.2.8 Mössbauer technique. Manley & Johnstone (1974) applied the Mössbauer technique to the study of the vibrations of the guinea-pig middle ear. This technique involves placing a very small gamma-ray source on the vibrating structure, and produces a measure of velocity which can then be converted to displacement if the frequency of vibration is known. The sound pressures used were in the range of 85 to 110 dB SPL.

Manley & Johnstone investigated eardrum vibrations by measuring displacements at seven points on the drum. They plotted contour lines based on interpolation of these data at three frequencies, as shown in Fig. 5.8. (The positions of the seven measurement points are indicated in part *a* of the Figure.) Here again, the manubrial displacements are smaller than those of the surrounding eardrum surface. The greatest displacements occur in the inferior region.

5.2.9 Discussion. The general picture resulting from the experiments discussed above is that, at low frequencies, the displacements of the manubrium are less than those of the surrounding eardrum. In the human and cat the largest displacements are found in the posterior half of the eardrum, while in the guinea pig and rabbit (where the eardrums are very nearly

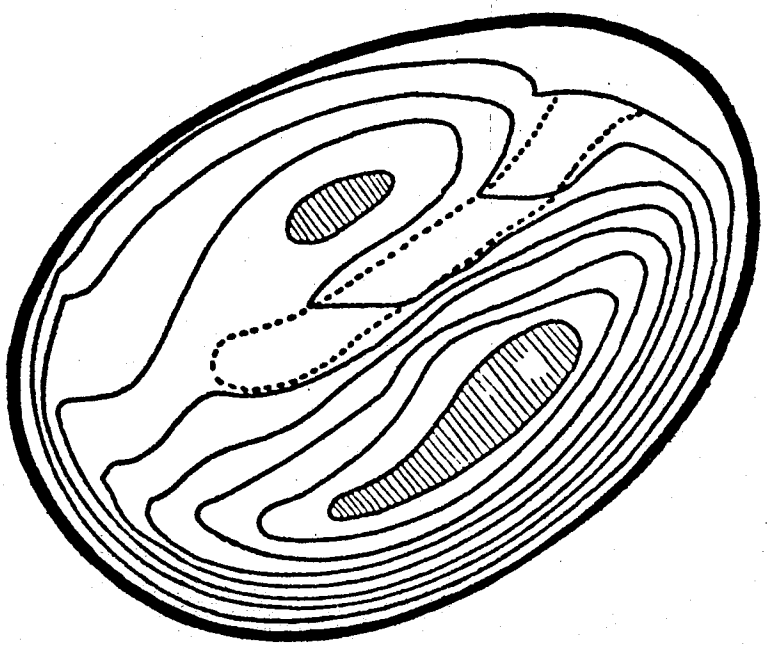

Fig. 5.6. Vibration pattern of cat eardrum. (After Khanna, 1970)

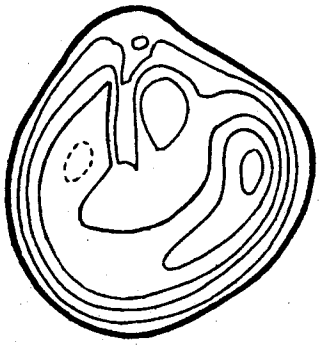

Fig. 5.7. Vibration pattern of human eardrum. (Based on Fig. 1 of Tonndorf & Khanna, 1972)

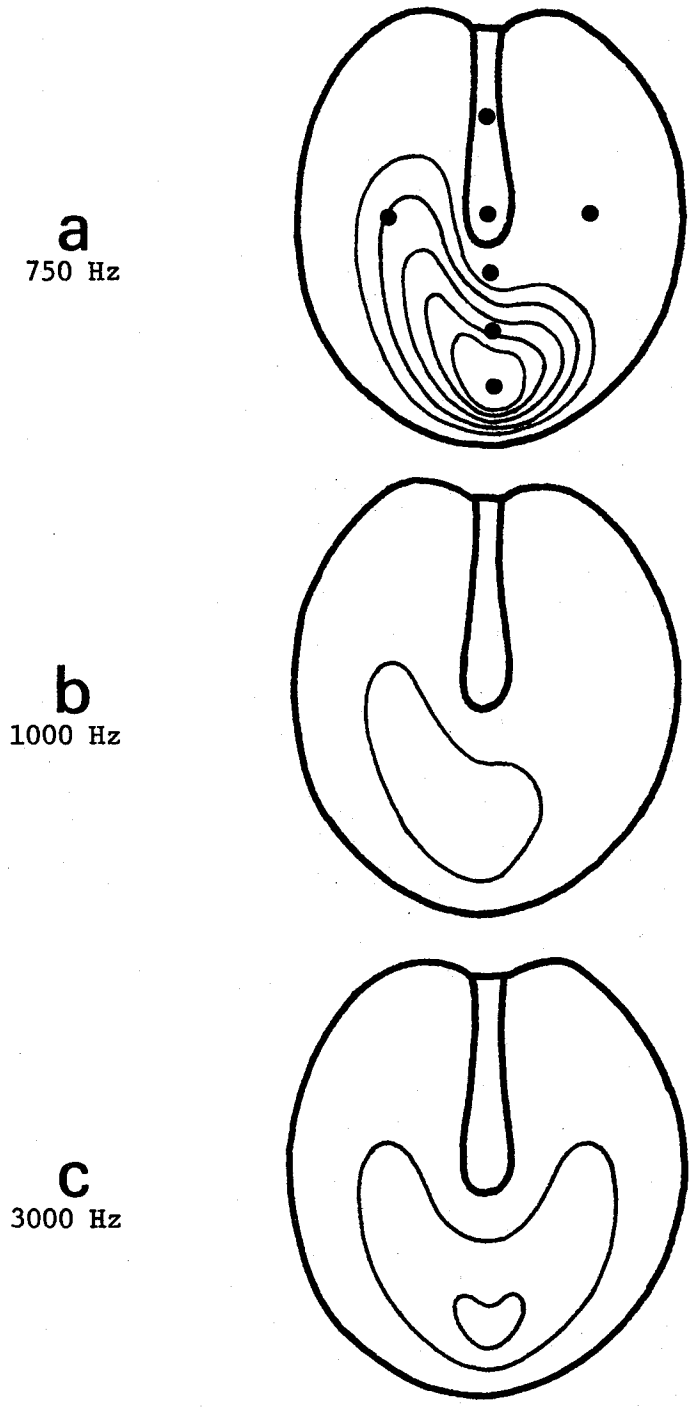

Fig. 5.8. Vibration patterns of guinea-pig eardrum at three frequencies. Based on Fig. 6 of Manley & Johnstone (1974), with contour lines added (*a*) and removed (*a*, *b* and *c*) to make the contours uniformly spaced in amplitude and directly comparable between frequencies. The seven dots in part *a* denote the points where actual displacement measurements were made.

symmetrical) the largest displacements occur in the inferior region.

Békésy's observations are the only ones that do not agree with this general picture. (Kirikae (1960, p. 53) cited Stuhlman (1937, 1943) as having pointed out that "the central part vibrates as a rigid cone". In fact, however, in the 1937 paper Stuhlman did not mention drum vibration patterns at all, and in the 1943 book he just gave some theoretical speculations which in any case were not consistent with Békésy's ideas.) Even in Békésy's results, the inferior region follows the pattern of having an amplitude maximum part-way between the manubrium and the periphery. In the anterior and posterior regions, however, he indicated that the drum displacements were the same as or less than the manubrial ones.

As discussed by Tonndorf & Khanna (1972), it is unlikely that post-mortem changes could account for Békésy's findings; most other observations on human eardrums have also been on cadavers. Nonlinearity also is probably not responsible for Békésy's disagreement: as mentioned above, Békésy's method was probably sensitive enough to permit the use of sound intensities within the linear range of the eardrum. In any case, other workers using very high intensities found vibration patterns similar to the recent low-level ones.

Four other possible factors may be proposed. First, Tonndorf, in the discussion period after the presentation of a paper (Tonndorf & Khanna, 1971b), suggested that the discrepancy may be due to departures of the ear canal and eardrum from the ideal environment for the use of a capacitive probe. The fact that both the canal walls and the drum itself have finite electrical resistances might have a considerable effect on the probe's output, especially since the geometry of the system is so irregular.

Second, it is possible that the size of the tip of Békésy's probe was too large to permit reliable determination of the details of the vibration pattern. Békésy (1941, p. 3) mentioned an electrode diameter of 1 mm. The same figure was given in a translation of the article (Békésy, 1960, p. 55), but the translation also mentioned parenthetically a tip *radius* of 1 mm. In Fig. 5.9, I have superimposed circles of these two sizes on a sketch of the eardrum, to give an idea of the resolution obtainable. (Békésy found that

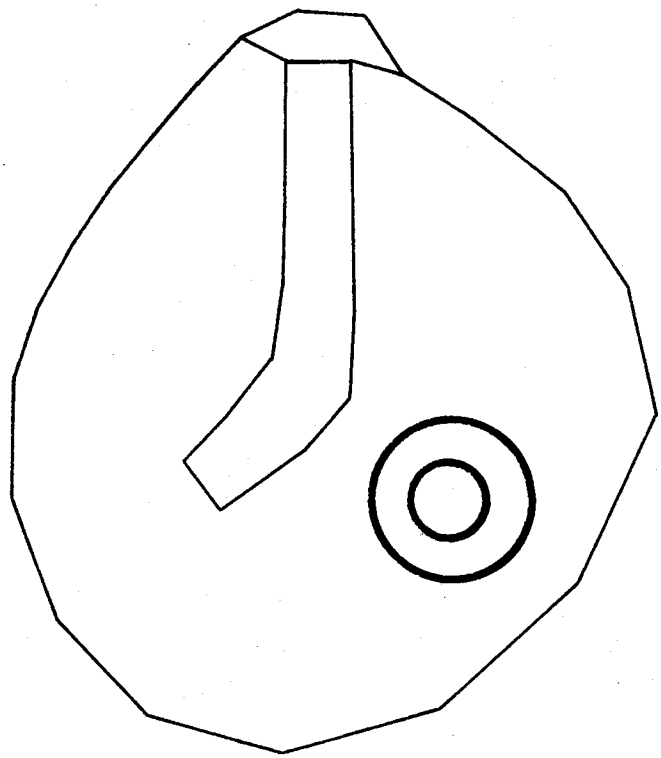

Fig. 5.9. Relative size of Békésy's capacitive probe. Superimposed on an outline of the human eardrum are two circles representing diameters of 1 and 2 mm, as discussed in the text.

the probe output was determined by an area of the vibrating surface approximately equal to that of the probe.) Since Békésy gave no details about how many points he measured, or where they were, it is difficult to decide whether his resolution was good enough to differentiate positively between the type of pattern he proposed and that proposed by other workers.

Third, it is known that Békésy's measurements were done on cadavers obtained from a children's hospital (Tonndorf & Khanna, 1972, citing a personal communication from Békésy), and that he preferred to use the temporal bones of newborns, at least for cochlear studies (Békésy, 1960, p. 20). In the absence of any mention of the ages of the cadavers used for his eardrum measurements, one can speculate that the drums may have been immature. It is not known how much this might have affected his results, if at all. See Section 2.4 for a discussion of the development of the human eardrum.

Fourth, it is conceivable that Békésy's use of low (unspecified) ambient temperatures, in an attempt to slow down post-mortem changes, could have affected the mechanical properties of the eardrum; as mentioned in Section 3.4.4, the effects of low temperatures on collagenous tissues have not been studied.

5.2.10 Conclusions. For the purposes of comparison with the models in Chapters 10 and 12, the low-frequency patterns shown in Figures 5.6, 5.7 and 5.8 will be taken as representative of cat, human and guinea-pig eardrum vibrations, respectively.

Apart from the general shapes of the contour lines, two numerical quantities that will be used to compare experimental and model results are (1) the amplitude of the maximal drum displacement, and (2) the ratio of that displacement to the displacement of the tip of the manubrium. The former is a measure of the over-all displacement of the drum, and the latter is a measure of the coupling of the drum to the ossicles and of the degree of sound transmission to the middle ear. The actual values of these properties will be discussed below in the appropriate sections of Chapters 10 and 12.

5.3 Higher-Frequency Vibration Patterns

Békésy (1941) stated that above 2400 Hz "the conical portion of the eardrum loses its stiffness, and the manubrium in its motion lags behind the motion of the adjacent portion of the membrane" (English translation in Békésy, 1960, p. 102), but no further details were given. Fumagalli (1949, p. 294) interpreted this as meaning that above 2400 Hz Békésy had observed drum vibrations like those predicted by Helmholtz, that is, vibrations with a smaller amplitude on the manubrium than on the adjacent drum.

The stroboscopic method of Khanna and Tonndorf provides detailed vibration patterns up to 6 kHz. A series of such patterns observed in one cat is shown in Fig. 5.10. The simple low-frequency vibration pattern is still present at 2.5 kHz, but above that it progressively breaks up as the frequency increases, until by 4 or 5 kHz most of the surface of the drum is only very poorly coupled to the manubrium. The details of the vibration patterns above 3 kHz vary from animal to animal: Fig. 5.11 shows typical examples of the differences between individuals at three frequencies. Tonndorf & Khanna (1972) observed a similar pattern break-up in human cadaver ears, at about the same frequencies.

The point velocity measurements of Manley & Johnstone (1974) do not provide complete vibration patterns, particularly if the patterns become more complex. However, their observations on the guinea-pig eardrum indicate that the basic low-frequency pattern may not be much changed until the frequency is as high as 6 to 8 kHz.

5.4 Middle-Ear Acoustical Input Impedance

As mentioned above, the acoustical input impedance of the middle ear depends more on the behaviour of the eardrum than on any other single factor. Thus, it serves as an easy-to-measure indicator of eardrum function, although of course it does not give the same detail as the holographic method, for example.

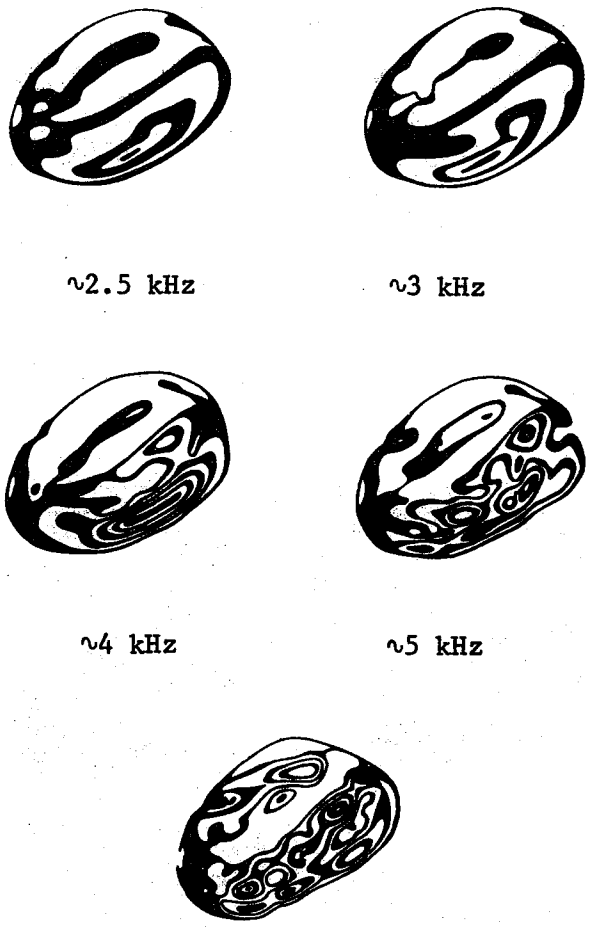

Fig. 5.10. Measured vibration patterns of the cat eardrum at five high frequencies. This Figure is a rearranged and heavily retouched version of part of Fig. 7 in Khanna & Tonndorf (1972a).

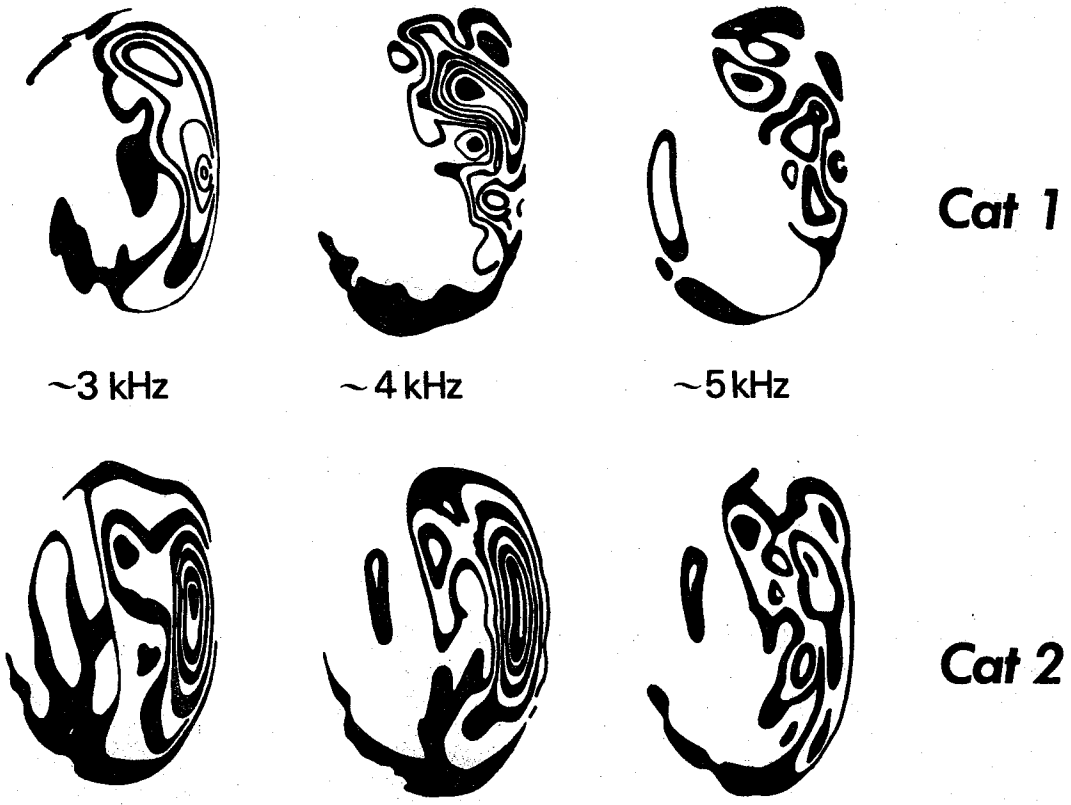

Fig. 5.11. Measured vibration patterns for two cats at each of three frequencies, indicating typical variability between individuals. This is a heavily retouched version of Fig. 9 in Khanna & Tonndorf (1972a).

In Chapter 10 below I shall compare the output of the guinea-pig membrane model to some impedance measurements reported earlier (Funnell, 1972; Funnell & Laszlo, 1972). In this section I shall briefly review the basis and results of these measurements.

The input impedance of the guinea-pig middle ear was measured by presenting a sound to the eardrum through a high-impedance driver, and measuring the resultant sound pressure with a high-impedance probe microphone. The set-up is shown in Fig. 5.12. The driver and probe were both half-inch condenser microphones with damped tubes attached. They were fixed to the ear of the anaesthetized animal after most of the external ear had been removed.

The high-impedance driver acts approximately as a constant-volume-displacement source. The acoustical impedance is calculated simply by converting the pre-calibrated volume displacement to a volume velocity, and dividing it into the measured sound pressure. The frequency characteristics of both the driver and the microphone probe tube are taken into account. The measured impedance includes the effect of the small residual volume of the external ear canal between the driver and the eardrum; this can easily be corrected for if the volume is measured.

Fig. 10.5a shows a typical measured impedance curve of an intact guinea-pig ear. This curve includes the effects of the middle-ear air cavities. These effects can be isolated by measuring the input impedance after complete removal of the eardrum.

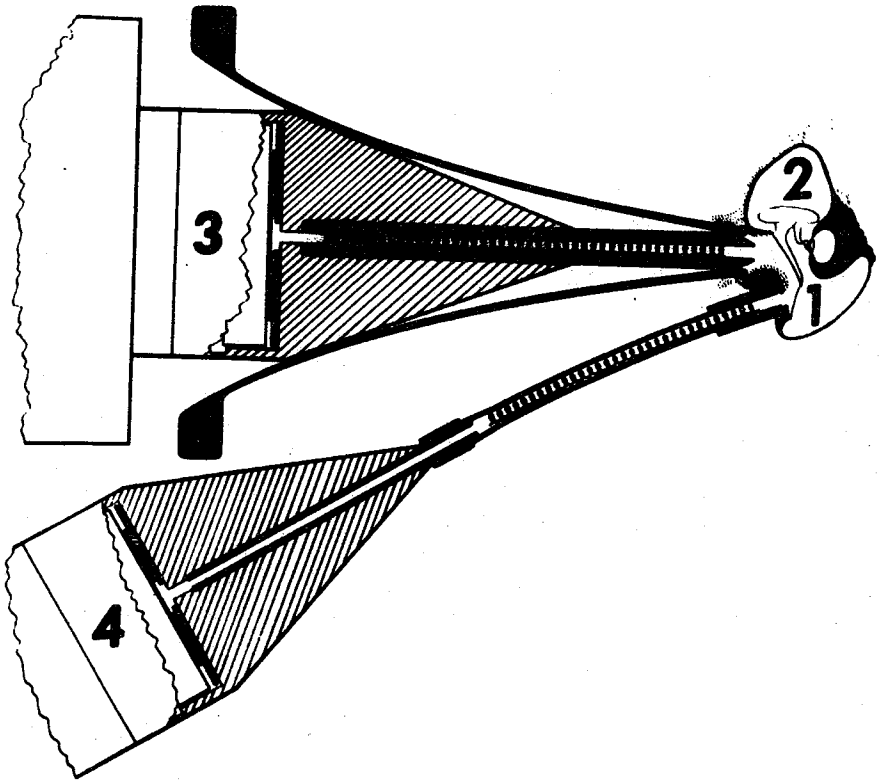

Fig. 5.12. Schematic drawing of the arrangement for measuring acoustical input impedance. *1* is the tympanic cavity of the guinea-pig middle ear, and *2* is the epitympanic cavity. *3* is a high-impedance acoustic driver, and *4* is a probe microphone.

CHAPTER 6

THEORIES OF EARDRUM FUNCTION

6.1 Introduction

The main function of the middle ear is that of an impedance-matching transformer. It transforms low-pressure, large-displacement acoustical vibrations in air into high-pressure, small-displacement vibrations in the cochlear liquid. The main contribution to this transformer action is made by the ratio of the area of the eardrum to that of the oval window of the cochlea: the air pressure acting on the large eardrum generates a large force which is then concentrated onto the small oval window. A second contribution to the transformer action is made by the ratio of the lever arm of the malleus to that of the incus.

The actual values of the transformer ratios, or lever ratios, arising from these two sources depend on the precise way in which the eardrum functions. (In fact, a third lever mechanism was hypothesized by Helmholtz which resulted entirely from the action of the eardrum.) There have been four main models suggested for eardrum function: curved-membrane, hinged-plate, plane-membrane, and plane-plate.

The curved-membrane hypothesis was proposed by Helmholtz in an attempt to account for the peculiar shape of the eardrum; it was also in accord with the results of one of his own experiments. (These results have since turned out to be erroneous.) Esser later extended the mathematical analysis of the theory, but it fell into disrepute when Békésy's observations of the eardrum vibration pattern did not agree with Helmholtz' prediction, and when Wever & Lawrence were unable to duplicate Helmholtz' experiment.

The hinged-plate model was put forward by Békésy simply as a description of his experimental results, and dominated thinking about the eardrum for many years. As discussed in the previous Chapter, other observations of eardrum

vibrations did not agree with Békésy's findings, but they had little impact on the theory. These other observations were generally non-quantitative and were suspected of being outside the normal range of operation of the eardrum. However, more recent results have also contradicted Békésy's, and in fact are closer to the predictions of Helmholtz. In consequence, Helmholtz' curved-membrane theory has been revived, albeit in a somewhat modified form.

The curved-membrane and hinged-plate theories are discussed in Sections 6.2 and 6.3, respectively.

The plane-membrane and plane-plate models have no particular basis in experiment, and do not take into account the obvious shape of the eardrum. They have been considered worthy of some consideration, however, because of their analytical simplicity. They are discussed briefly in Sections 6.4 and 6.5.

In this thesis I suggest what may be called a curved-shell model of eardrum function. This stands in the same relation to the curved-membrane model as the plane-plate does to the plane-membrane model. The curved-shell model is investigated in Chapter 12.

6.2 Curved-Membrane Model

6.2.1 Helmholtz (1869) observed that the eardrum is "almost inextensible", describing its behaviour when torn by pins on a flat surface as more like that of a collodion film than like that of rubber. Noting the curvature of the walls of the drum, his basic hypothesis was that this curvature served to provide a lever action of the sort illustrated in Fig. 6.1, with the structural elements (namely, the radial fibres) being inextensible. Fig. 6.1a shows a simple lever system: it can be shown that a displacement x_i gives rise to a smaller displacement x_o, the lever ratio increasing with decreasing α and increasing θ. This transformation from large input to small output displacement is just what is required to augment the transformer action of the middle ear.

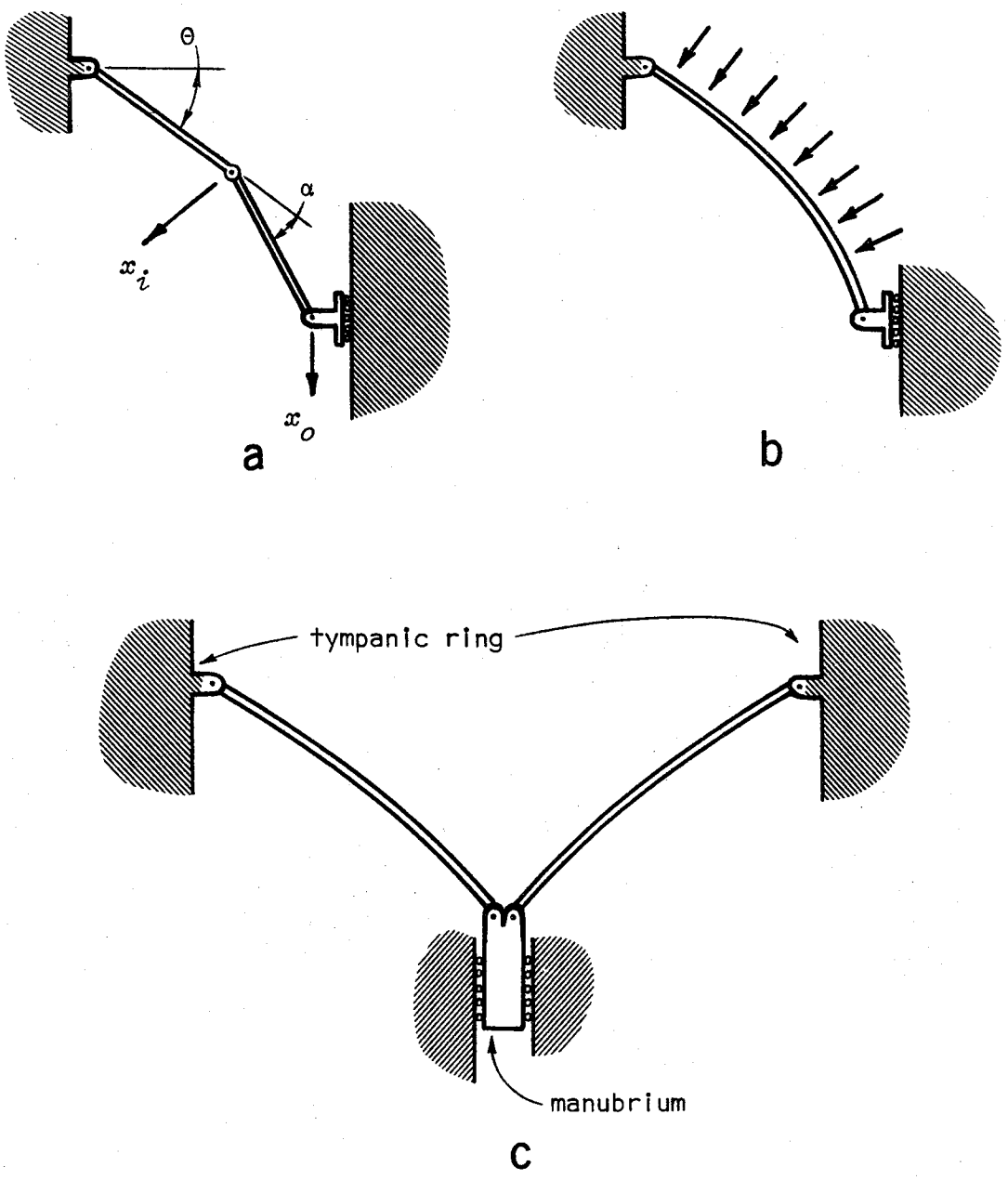

Fig. 6.1. Schematic illustration of the curved-membrane principle. See text for explanation.

If one implements the same principle using a larger and larger number of smaller and smaller rods, one arrives in the limit at the situation shown in Fig. 6.1b: the lever consists of a single inextensible but flexible fibre. Fig. 6.1c shows how the ear can be interpreted in terms of such a system, the upper supports representing the tympanic ring and the lower ends of the fibres being attached to the manubrium, whose direction of displacement is restrained (by ligaments, and possibly by symmetry).

Helmholtz analyzed this single-fibre system and showed that the lever ratio increases with decreasing curvature, as for the two-rod system. However, the single-fibre system (as well as any multi-rod system except the two-rod one) is not stable since its lack of bending stiffness prevents it from maintaining its shape under any but very special loading conditions. Helmholtz solved this problem by assuming that the fibre is under tension. This then requires some transverse structure to maintain the curvature. Helmholtz assumed that a large number of these fibres are arranged radially, with extensible circular fibres maintaining the shape of the structure. The tension is applied around the tympanic ring and at the manubrium. Physiologically, he believed that the tension was maintained by the malleolar ligaments and by the "elasticity of the tensor tympani".

Further analysis of this system requires some knowledge about either the exact form of the curvature, or the stress distribution among the circular fibres, neither of which is known. Helmholtz pointed out that the system would transmit air-pressure variations to the manubrium optimally *if* its shape were the same as would be produced by a positive air pressure acting on the medial surface of a similar system without circular fibres. He therefore calculated what that shape would be, and then assumed it to be the actual shape in obtaining an expression for the lever ratio of the system. These same results were re-derived by Esser (1947) within a more general framework.

Note that Helmholtz' model would explain not only the existence of the drum's curvature, but also the fact that the drum is conical, since this shape is required if the curvature is to give rise to a lever action.

6.2.2 Esser (1947) did a more general analysis of the same system considered by Helmholtz: a circular curved membrane under tension, clamped at the periphery, and with a force applied to a disk (or point) at the centre representing the malleus, as shown in Fig. 6.2. He did not immediately make assumptions about the extensibility of the fibres.

Consideration of the equilibrium requirements of an element of the surface gives two differential equations:

$$\begin{cases} \dfrac{d(r\gamma_r)}{dr} - \gamma_c = 0 \\ \gamma_r \dfrac{d\ \cos\alpha}{dr} + \gamma_c \dfrac{\cos\alpha}{r} = p\ , \end{cases}$$

where r = radial coördinate (cm);
p = applied pressure (dyn cm^{-2});
α = local slope of drum (see Fig. 6.2);
and γ_r, γ_c = radial and circular components of tension (dyn cm^{-1}).

The tension distributions, $\gamma_r(r)$ and $\gamma_c(r)$, and the eardrum shape, $\alpha(r)$, are all unknown functions of r. Thus, there are two equations in three unknowns, and a third equation is needed to permit solution of the problem. Some assumption is necessary, and Esser considered four different cases.

Esser's first case was to assume γ_c = constant. Given this assumption, one can then calculate the stress distributions and the shape function. In particular, Esser calculated the resting shape, that is, the shape when $p = 0$.

Esser's second case was to assume $\gamma_c = \gamma_r$, that is, equal tensions in the radial and circular directions. This would be the case for amorphous or isotropic membranes. The resting shape turns out to be the same as for the first case.

Esser's third case was the adoption of Helmholtz' assumption, namely that the resting shape is the same as it would be for $\gamma_c = 0$ but $p \neq 0$. This is the situation that Helmholtz showed to be "optimal" for transmitting pressure variations to the malleus. Esser used the conditions $\gamma_c = 0$ and $p \neq 0$ to calculate the same shape function as obtained by Helmholtz, and then, with

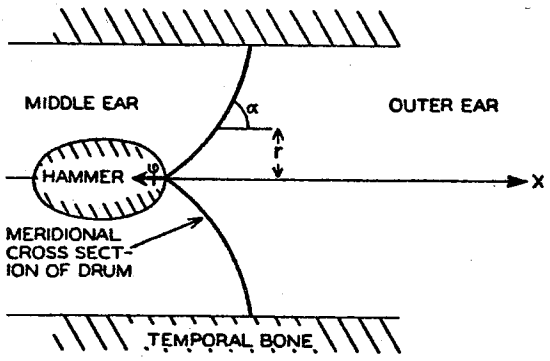

Fig. 6.2. Diagram of the system analyzed by Esser. See text for explanation. (After Esser, 1947)

$p = 0$, went on to calculate the tension distributions γ_c and γ_r. The equation he obtained for γ_c showed it to be increasing towards the periphery, which he took as agreeing with the increasing density of the circular fibres toward the periphery.

Esser then showed that Helmholtz' hypothesis of inextensible radial fibres makes it particularly simple to study the force transformation of this lever system because, if the malleus is held fixed, the shape of the drum does not change when the applied pressure p is changed. This is because the shape due to the circular fibres is the same as the shape due to the air pressure. Thus, one can calculate the force-transformation ratio, which increases for decreasing curvature or increasing tension. The system is equivalent to a rigid lever.

Esser's fourth case was to assume that γ_c does not change during drum motions. This is equivalent to assuming either that circular-fibre elongations are much smaller than radial-fibre ones, or that circular fibres are very yielding so that their elongation produces small tension changes. This was similar to Helmholtz' hypotheses in that he took the circular fibres to be more extensible than the radial ones, but instead of taking the radial fibres as inextensible, he took the circular ones as very extensible. Esser pointed out that his assumption was "made for mathematical simplification, but is not justified by physical or anatomical considerations."

A considerable amount of algebra, valid only for small displacements, shows that the system is equivalent to a non-rigid lever combined with a spring. (The spring also applies to case 3, with Helmholtz' hypotheses.) The lever ratio again increases with decreasing curvature. Esser also found that the lever ratio is less than one for very stretchable radial fibres, but can increase to very large values for sufficiently stiff radial fibres and small curvatures.

His analysis resulted in a number of multiple integrals. In order to evaluate them he first had to assume that the shape was that predicted by Helmholtz, and for some of them had to ignore the curvature altogether.

6.2.3 Khanna (1970, Appendix III) estimated a value for the effective lever ratio by making a further assumption: he assumed that the drum is constructed so that the work it performs on the malleus is spread evenly along the manubrium. He further assumed that the work done on the malleus equals the work done on the drum by the air pressure, neglecting the work involved in stretching the radial and circular fibres. Taking the work done on the eardrum as the product of the total force (due to pressure) and of the average drum displacement, and using anatomical measurements and his experimental results from the cat, he calculated a ratio of $\frac{\text{force on malleus}}{\text{force on drum}}$ equal to 1.96. Note that the value he took for the ratio $\frac{\text{average drum displacement}}{\text{malleus-tip displacement}}$ was based on measurements of the component of drum displacement perpendicular to the plane of the tympanic ring. It would be more correct to use the total displacements perpendicular to the surface of the drum.

6.2.4 Recent modifications. Tonndorf & Khanna (1972) proposed two modifications to the curved-membrane theory, to remove certain conflicts with experimental observations. The first modification is simply a reduction of the expected value of the effective lever ratio due to the curved-membrane mechanism. This is consistent with an error found in Helmholtz' calculations (Hartman, 1971) and with their recent experimental results concerning the ratio of drum to malleolar displacement.

The second modification concerns Helmholtz' and Esser's assumption of greater elasticity for the circular fibres than for the radial ones. Tonndorf & Khanna (1972) felt that the two sets of fibres should be similar, and that they should both be considered to be inextensible since they appear to be collagenous. They proposed that the required elasticity might be found in the mucopolysaccharide ground substance between the layers of fibres. They suggest that the circular fibres might slide as much as two fibre diameters (about 10^{-3} cm) along the radial fibres in the region of maximal displacement (about half way between the manubrium and the periphery). It should be noted that this is equivalent to a circumference change of $2\pi \times 10^{-3}$ cm (neglecting a small downward correction due to the slope of the eardrum), compared to a

circumference of about 2π x 0.25 cm. In other words, the circular fibres, if fixed to the radial ones, would undergo a stretch of about 0.4%. This is considerably less than the ultimate strain of about 5% reported for collagenous tendon (Wilkes *et al.*, 1973, for example), so it may not be necessary to assume that all of the yielding takes place in the ground substance.

As concerns the assumed greater elasticity of the circular fibres as compared to the radial ones, it should be noted that the circular-fibre layer is generally thinner than the radial-fibre layer, so that the effective stiffness of the former will be less even if the elastic moduli of the component fibres are the same.

6.2.5 Objections. Tonndorf & Khanna (1972) answered a number of objections that had been raised against the curved-membrane theory, partly by means of the proposed modifications mentioned above. In addition, they felt that arguments against the theory that are based on the effects of drum perforations in different positions are not conclusive because of the small size of the differences measured.

More recently, Marquet *et al.* (1973) raised five points against the curved-membrane theory as presented by Tonndorf & Khanna. Their first point was that there is no justification for considering the circular fibres to be more extensible than the radial ones. This is discussed above. Their second point was that the theory as presented involved only static considerations. This is true, but it should be noted that inertial effects are insignificant up to about 1 kHz.

Their third and fourth points concerned the details of the analysis presented by Tonndorf & Khanna (1970). That presentation, however, was very much simplified in order to explain the basic principles of the type of lever action proposed. The analyses of Helmholtz and Esser take care of the more involved aspects of the theory.

Finally, Marquet *et al.* presented some experimental results intended to demonstrate that the effective lever ratio of the eardrum does not change

when the curvature changes as a result of static pressures. However, Tonndorf & Khanna (1972) pointed out that this lever-ratio change is likely to be quite small. Marquet *et al.* did not indicate the resolution of their apparatus, but their results were plotted on a linear pressure scale with an upper limit of 120 mm H_2O, which corresponds to about 150 dB SPL. This indicates that their resolution was probably not adequate to determine details of behaviour within the normal, linear operating range of the eardrum.

6.3 Hinged-Plate Model

The measured vibration patterns on which Békésy (1941) based his stiff-plate description are discussed above in Chapter 5. He estimated that about 65% of the drum is "stiffly coupled to the manubrium" in man. He described the drum as acting like a "stiff piston" ("starrer Kolben") but he did not mean "piston" in the conventional sense, since it rotated rather than just moving back and forth.

This description led to the common use of the term "effective area" in discussions of middle-ear lever ratios. Khanna (1970) pointed out that, in calculating a value for the ossicular lever ratio, one should not take the air pressure as acting at the tip of the manubrium, since the pressure is acting uniformly across the "effective area". Note also that in specifying an effective area one should take into account the fact that the pressure acting on the "lower fold" will have some influence on the malleus, albeit reduced.

Békésy felt that the conical shape of the eardrum provided a close coupling between the drum and the manubrium. This presumably would be a result of the greater effective stiffness of a conical diaphragm as compared to a flat one. Except for its rotation about one edge, the eardrum in Békésy's conception behaved very much like a loudspeaker diaphragm, stiffened by its conical shape, loosely supported at its edges and vibrating like a piston. The geometric stiffening mechanism provides a rigid piston with very low mass.

Békésy (1949) made some measurements on a stretched, circular membrane made of rubber, and concluded that an embedded disk (representing the manubrium and the part of the drum stiffly coupled to it) provided more sensitivity than did an embedded rod (representing the case of a drum not stiffly coupled to its manubrium).

There is no clear anatomical indication that the eardrum is built to function like a stiffened cone with a flexible periphery. Békésy admitted that the "lower fold" is only weakly developed in many specimens, and suggested a particular susceptibility of this part of the drum to disease and drying. It is not clear whether he believed that the greater flexibility of the lower fold was due to structural differences, or to its shape, or both. Fumagalli (1949) interpreted the fibre structure of the eardrum as consistent with behaviour as a stiffened cone, but the discussion was very qualitative. He suggested that the mode of attachment of the radial fibres to the tympanic ring, including the presence there of some elastic fibres, provides the necessary flexibility.

6.4 Plane-Membrane Model

Frank (1923) modelled the eardrum as a plane membrane under tension. For simplicity, the drum was assumed to be circular, and the manubrium was taken to be a symmetrically located rigid rod, hinged at the circumference. The rod had infinitesimal width.

Even with these simplifications, approximate numerical techniques were required to calculate natural frequencies and vibration patterns. Indeed, even in the static case, the problem becomes difficult to handle analytically as soon as the length of the embedded rod is made to be anything other than half of the diameter. Békésy (1949) made some experimental measurements on a physical model consisting of a circular stretched membrane, made of rubber.

With so many oversimplifications, the quantitative results of the model are of relatively little interest. In Chapter 10 below I shall present the results of a plane-membrane model, studied numerically, which does not require

most of the assumptions needed by Frank. Even so, it must be realized that no plane-membrane model is a realistic representation of the mammalian structure.

6.5 Plane-Plate Model

Gran (1968) recognized that Békésy's observations of low eardrum tension and significant bending stiffness indicated a need to model the drum as a plate rather than as a stretched membrane. He ran into difficulty in analyzing such a system, however, even though he was considering only the geometrically simplified case of a plane circular plate with a radially positioned manubrium hinged at the circumference. Such an arrangement becomes difficult to analyze if one assumes fully clamped boundaries (as defined in Section 4.2 above) since the malleus is thereby prevented from rotating. Gran, however, felt that it was necessary to consider the boundaries as fully clamped, based on Békésy's example when calculating Young's moduli in his 1949 paper. (As discussed in Section 4.2, Békésy did not actually imply a fully clamped eardrum boundary.)

Gran handled the problem introduced by the clamped boundaries by decomposing the eardrum vibrations into two components: one component which did not involve any displacement of the malleus, and a second component which made up the remainder of the vibration. He did not attempt to handle the difficulties involved in analyzing the second component.

For his analysis of the first component, he assumed the drum to be uniform and isotropic, and also had to assume a simplified shape for the manubrium, namely, that of a sector of the circle. Even so, all that he was able to accomplish was an approximation of the first few natural frequencies, taking into account the effect of the closed tympanic cavity. He attempted to use his model to predict a bending-stiffness value based on impedance measurements, but obtained a range of values 60 to 250 times the value measured by Békésy.

Gran used the Rayleigh-Ritz procedure for his numerical calculations, which is the procedure that forms the basis of the finite-element method used here.

CHAPTER 7

SIMULATION METHODS

7.1 Introduction

This chapter is a general discussion of methods for simulating physical systems which are defined mathematically as boundary-value problems. That is, these systems are continua with certain constraints imposed by boundary conditions. Particular attention will be paid to mechanical systems of two or three spatial dimensions.

Section 7.2 will present a quick over-view of approaches to the solution of practical boundary-value problems, and will discuss briefly the reasons for choosing to use the finite-element method. Section 7.3 reviews the concepts of the finite-element method, and then Sections 7.4 and 7.5 present general pictures of the particular finite-element formulations used in this work for the plane-membrane and shell models, respectively. The details of the methods used here are given in more detail in the next chapter.

The final section in this chapter considers the range of validity of the present methods, and indicates how they might be extended.

7.2 Approaches to Boundary-Value Problems

The simplest boundary-value problems may be solved by writing down the differential equations from consideration of the physical system, and then solving the equations (with their associated boundary conditions) analytically, using separation of variables to reduce a multidimensional problem to several one-dimensional ones. Separation of variables is only possible for a few simple boundary shapes, however, and for arbitrary boundaries approximate analytical methods are required, such as variational

techniques, perturbation techniques and conformal mapping. For more complicated shapes, or in the presence of inhomogeneities, numerical methods become necessary. The main numerical methods for solving differential equations are numerical integration, the finite-difference method and the finite-element method. The first is generally not used for multidimensional problems.

The finite-difference method consists of replacing the differential operators by difference operators. Graphically this is equivalent to placing a grid over the structure and considering only points at intersections of grid lines. The finite-element method involves conceptually dividing the structure into elements of finite size whose geometries are simple enough to permit analytical intra-element solutions of the differential equations. One takes into account inter-element effects by considering the various elements to be connected only at specific nodes on their boundaries. Both the finite-difference and finite-element methods result in systems of simultaneous algebraic equations that can be solved by standard numerical methods.

There are a number of features that make the finite-element method particularly attractive. First, in even its simplest form it handles irregular boundary shapes very conveniently. Second, it is relatively easy to handle inhomogeneities, nonlinearities, and complex geometries and boundary conditions systematically. Third, one need never analyze the behaviour of the whole system. All of the analysis is done on simple elements, and even there one need not be able to write down the governing differential equations. The elements can be formulated using any method that is convenient, such as the variational method often used for plates and shells.

Another reason for the popularity of the finite-element method is that it can be understood on a physical, or intuitive, basis. Its use is essentially an extension of the very common technique of analyzing mechanical or electrical systems as networks of interconnected discrete components.

7.3 Concepts of the Finite-Element Method

7.3.1 Introduction. This section is not intended to be a complete description of the finite-element method. Rather, it is a brief introduction to some of the concepts involved, in order that the reader may understand the significance of the element formulations discussed in Sections 7.4 and 7.5, and the implementation details presented in the next chapter. A number of texts are available concerning the finite-element method. The first such was that of Zienkiewicz & Cheung (1967), but recently several others have been published (Zienkiewicz, 1971; Desai & Abel, 1972; Martin & Carey, 1973; Norrie & de Vries, 1973; Ural, 1973; Brebbia & Connor, 1974).

When using the finite-element method, the physical system to be analyzed is divided into a number of discrete two-dimensional or three-dimensional elements which may or may not correspond to natural subdivisions of the actual structure. For example, for an assembly of plates and beams, the elements may consist of the individual plates and beams themselves, if these are easy enough to analyze individually. On the other hand, a single homogeneous plate of irregular shape may be considered to be composed of a number of triangular or rectangular plate elements which together make up the over-all irregular shape, but which individually are easy to analyze. Once one has divided the structure into elements, the mechanical behaviour of each element is analyzed, and its response to applied loads is expressed in terms of the displacements of its edges. This analysis is often based on the Ritz-Rayleigh procedure, which is discussed in Section 7.3.2. An example of a particularly simple element formulation is presented in Section 7.3.3.

The result of the element analysis is a matrix equation relating the behaviour of the element to the applied forces. The components of the matrix are functions of the shape and properties of the element. If all of the elements in the structure are of the same type, such as triangular membrane elements, or quadrilateral thin-plate elements, then after the initial

element analysis has been done once one need only substitute the shape and property definitions for each element into the formulae obtained for the matrix components. In fact the user seldom needs actually to do the preliminary analysis at all, since such analyses have been published in the literature, and included in computer programmes, for a wide variety of element types.

Once the element matrix equations are ready, they are all combined together into one over-all system matrix equation, as discussed in Section 7.3.4. (The boundary conditions are also included in the system matrix equation.) Since the behaviour of each element has been described in terms of its behaviour at its edges, and in fact at certain discrete nodes along its edges, this assembly of element matrices is simply a statement of the fact that a node shared by two elements must have the same displacement when considered as part of either element, and of the assumption that the elements can only interact at these discrete nodes.

The actual solution of the system matrix equation is discussed in Section 7.3.5.

7.3.2 Ritz-Rayleigh procedure. The Ritz-Rayleigh procedure was introduced by Ritz in 1908 as a generalization of a technique described by Rayleigh in 1877. It is the most common procedure used for formulating finite-element approximations. The following discussion is based on Stakgold (1968, pp. 332-335).

The procedure is based on the theorem of minimum potential energy in mechanics. This theorem states that if one obtains a functional giving the potential energy of a system, then the "admissible" function which minimizes that functional is the solution of the system. An admissible function is one which satisfies the boundary conditions of the boundary-value problem, as well as certain continuity conditions.

In practice it will be difficult or impossible to find the one function which actually minimizes the functional. Thus, one must limit the set of functions over which one will attempt to minimize the functional. The Ritz-Rayleigh procedure consists of restricting the search to a

particularly simple subset of admissible functions, namely, the space of linear combinations of n independent admissible basis functions $w_1(\mathbf{x}),\ldots, w_n(\mathbf{x})$. The value of n is chosen to be as small as is consistent with the accuracy required of the answer. The particular set of basis functions used is more or less arbitrary, as long as they are independent and admissible.

Since each of the basis functions is admissible, every function in the space of linear combinations will also be admissible. These functions can be expressed as

$$w(\mathbf{x}) = \sum_{i=1}^{n} c_i w_i(\mathbf{x}) \ ,$$

where the c_i are n constants defining $w(\mathbf{x})$. Now, minimizing the functional $F(w)$ over this set of functions evidently requires choosing the c_i such that F (which is now a function of the c_i) is minimal. Thus, taking the partial derivatives of F with respect to each c_i in turn and setting it to zero, one ends up with a set of n algebraic equations in c_i:

$$\frac{\partial}{\partial c_i} F\left(\sum_{j=1}^{n} c_j w_j\right) = 0, \quad i = 1,2,\ldots n.$$

Thus, the boundary-value problem is reduced to the solution of n linear equations in n unknowns.

7.3.3 A simple element analysis. As an example of the type of analysis involved in the formulation of finite elements, this section will consider the analysis of a very simple case: a triangular plane-membrane element using only three basis functions.

The differential equation governing a plane membrane under tension, vibrating sinusoidally, is (Rayleigh, 1877)

$$T\nabla^2 w + \sigma\omega^2 w = p \ ,$$

where w is the membrane displacement (cm); σ is the area density (gm cm^{-2});

ω is angular frequency (sec^{-1}); T is tension (dyn cm^{-1}); and p is applied pressure (dyn cm^{-2}). This can be rewritten as

$$\nabla^2 w + \lambda^2 w = g \ .$$

It can be shown (Forsythe & Wasow, 1960, Chap. 3) that the energy functional corresponding to this system is

$$F(w) = \tfrac{1}{2}\iint |\nabla w|^2 dS + \tfrac{1}{2}\iint \lambda^2 w^2 dS - \iint w g dS,$$

where the integrals are over the entire region of interest, in this case the triangular element. The three integral terms on the right-hand side represent energy due to membrane tension, inertia, and the applied pressure, respectively.

This functional is the one to be minimized using the Ritz-Rayleigh procedure. As for what basis functions to use, the simplest choice is to choose a set which permits the displacement field over the element to be a general linear function of x and y. For this, three basis functions are needed. There are two ways of formulating them, one based on Cartesian coördinates and the other on so-called "natural" coördinates. The ultimate result is the same, but in some circumstances one or the other formulation may be superior. I shall present both methods below.

The Cartesian-coördinate method involves choosing as basis functions the set $\{1, x, y\}$. The displacement at any point (x,y) in the element is then given by a linear combination of these three functions, namely,

$$w(x,y) = c_1 + c_2 x + c_3 y \ .$$

Following the Ritz-Rayleigh procedure, one then replaces w by this expression in the equation for $F(w)$, carries out the double integrations, and differentiates with respect to each of the c_i in turn. Setting the derivatives equal to zero then results in a set of algebraic equations for the c_i:

$$\mathbf{A}\mathbf{c} = \mathbf{B}\mathbf{g},$$

where the components of **g** represent the nodal values of the pressure field $g(x,y)$. The components of the matrices **A** and **B** are functions of the vertex coordinates of the triangular element, $(x_1,y_1,x_2,y_2,x_3,y_3)$, and of λ.

This equation is the one that would have to be solved if the element were alone. If it is part of a larger system, however, the equation must be transformed so that it can be combined with similar equations representing other elements. Specifically, one uses the transformation

$$\begin{pmatrix} w_1 \\ w_2 \\ w_3 \end{pmatrix} = \begin{pmatrix} 1 & x_1 & y_1 \\ 1 & x_2 & y_2 \\ 1 & x_3 & y_3 \end{pmatrix} \begin{pmatrix} c_1 \\ c_2 \\ c_3 \end{pmatrix}$$

or, in matrix notation,

$$\mathbf{w} = \mathbf{X}\mathbf{c}.$$

The w_i are the nodal displacements, and this equation represents simply the expression of the nodal displacements as linear combinations of the basis functions. Using the inverse transformation, the algebraic equations describing the behaviour of the element become

$$\mathbf{A}\mathbf{X}^{-1}\mathbf{w} = \mathbf{B}\mathbf{g}.$$

Changing notation, we may write

$$\mathbf{S}\mathbf{w} = \mathbf{B}\mathbf{g}.$$

Note that the right-hand side is actually a vector of nodal forces, so that we may also write the equation as

$$\mathbf{S}\mathbf{w} = \mathbf{f}.$$

The components of the matrix **S** are evidently ratios of forces over displacements, and **S** is known as the element stiffness matrix.

The natural-coördinate method (Desai & Abel, 1972, pp. 88-91) expresses the location of any point in the triangular element by the area

coordinates $(\zeta_1, \zeta_2, \zeta_3)$, where $\zeta_i = A_i/A$; A is the total area of the triangle, and the A_i are as shown in Fig. 7.1. (Note that the three ζ_i are not independent, since $\zeta_1 + \zeta_2 + \zeta_3 = 1.$) It can be shown that the relationship between Cartesian coördinates and these "natural" coördinates is given by

$$\begin{pmatrix} 1 \\ x \\ y \end{pmatrix} = \begin{pmatrix} 1 & 1 & 1 \\ x_1 & x_2 & x_3 \\ y_1 & y_2 & y_3 \end{pmatrix} \begin{pmatrix} \zeta_1 \\ \zeta_2 \\ \zeta_3 \end{pmatrix} = \mathbf{x}'\boldsymbol{\zeta} .$$

We may now use $\{\zeta_1, \zeta_2, \zeta_3\}$ as the set of basis functions. It can easily be seen that in this case the coefficients c_i become the nodal displacements w_i. Following the Ritz-Rayleigh procedure again leads to an equation of the form

$$\mathbf{S}\,\mathbf{w} = \mathbf{f} .$$

7.3.4 Assembly of system equation. The previous section has outlined the analysis for a simple triangular element. Suppose that a system to be studied consists of two such elements interconnected as shown in Fig. 7.2. For the first element, substituting the vertex coordinates and material properties into the formulae obtained from the analysis gives the stiffness (**S**) matrix components a_{ij} for the equations relating the nodal displacements to the nodal loads:

$$\begin{pmatrix} a_{11} & a_{12} & a_{13} \\ a_{21} & a_{22} & a_{23} \\ a_{31} & a_{32} & a_{33} \end{pmatrix} \cdot \begin{pmatrix} w_1 \\ w_2 \\ w_3 \end{pmatrix} = \begin{pmatrix} f_1 \\ f_2 \\ f_3 \end{pmatrix} .$$

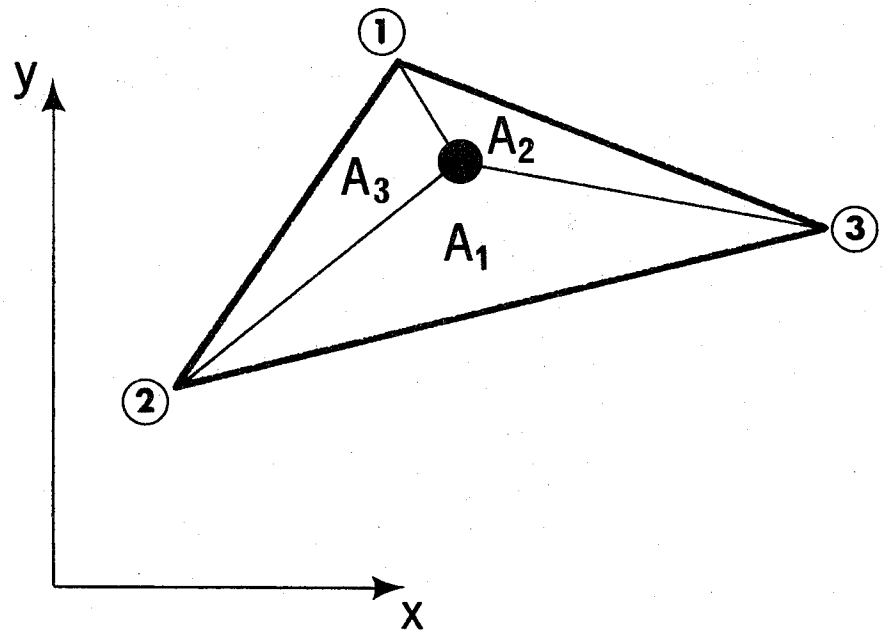

Fig. 7.1. Natural coördinate system. A_1, A_2 and A_3 are the natural coördinates of the point shown in the triangle. See text for explanation.

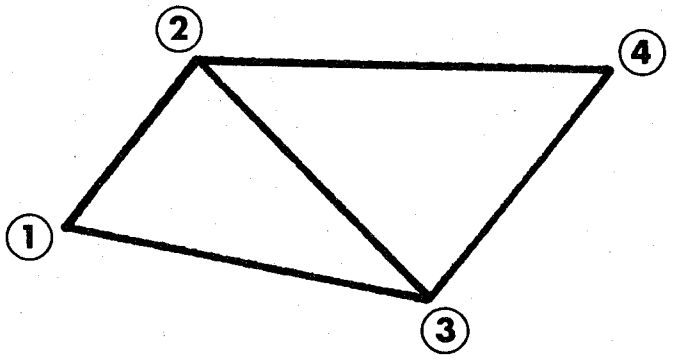

Fig. 7.2. Simple two-element system, showing two triangular elements coupled at nodes *2* and *3*.

Similarly, for the second element one obtains the matrix equation

$$\begin{pmatrix} b_{11} & b_{12} & b_{13} \\ b_{21} & b_{22} & b_{23} \\ b_{31} & b_{32} & b_{33} \end{pmatrix} \begin{pmatrix} w_2 \\ w_3 \\ w_4 \end{pmatrix} = \begin{pmatrix} g_2 \\ g_3 \\ g_4 \end{pmatrix}.$$

Now, since the elements are connected at nodes 2 and 3, the w_2 and w_3 in the first equation are the same as the ones in the second equation. Therefore one can combine the two equations as follows:

$$\begin{pmatrix} a_{11} & a_{12} & a_{13} & 0 \\ a_{21} & a_{22}+b_{11} & a_{23}+b_{12} & b_{13} \\ a_{31} & a_{32}+b_{21} & a_{33}+b_{22} & b_{23} \\ 0 & b_{31} & b_{32} & b_{33} \end{pmatrix} \begin{pmatrix} w_1 \\ w_2 \\ w_3 \\ w_4 \end{pmatrix} = \begin{pmatrix} f_1 \\ f_2+g_2 \\ f_3+g_3 \\ g_4 \end{pmatrix}.$$

The system boundary conditions now consist of prescribed values for some of the w_i. These are implemented in the usual way, as discussed in Section 8.5 below.

The force terms on the right-hand side of this equation represent nodal forces due to body or surface forces acting on the various elements, as discussed above. One can also add further nodal force terms representing specified point loads on the system. The equation then represents the entire boundary-value problem, and is solved as discussed in the next section.

7.3.5 Solution of system equation. The actual nodal displacements are obtained by solving the system matrix equation, which is equivalent to a system of linear algebraic equations. There are a number of ways to do this (see discussion in Ural, 1973, for example), but the most common methods are Gauss-Jordan elimination and Cholesky's method. The former requires a smaller number of computational steps. The latter uses less computer memory, but takes

more time and is less accurate because it involves taking square roots. For problems of the size treated in this thesis, either method is adequate.

7.4 Membrane Elements

In Section 7.3.3 above is presented a membrane element using the set of linear basis functions $\{\zeta_1, \zeta_2, \zeta_3\}$. One may develop higher-order elements based on more complex functions of the ζ_i. In particular, Silvester (1969) has developed an element based on polynomial functions of the ζ_i which permits very efficient calculations of element stiffness matrices. This is the method used in the programme adapted for use in the plane-membrane analysis reported in this thesis.

I shall not repeat the theory behind these high-order-polynomial elements here. Two points should be mentioned, however. The first is that the coefficients of the basis functions (the c_i) include, in addition to the displacements at the vertices of the triangle, the displacements at a number of extra nodes along the edges and in the interior of the triangle. For example, a third-order element has two extra nodes on each edge and one in its interior. These extra nodes do not add to the difficulty of defining the physical problem to the computer since they can easily be generated automatically.

The second point is to justify the use of more complex high-order elements instead of a larger number of simple low-order elements. The order of the system of equations to be solved is the same if one uses nine first-order elements, for example, instead of one third-order one. It has been shown, however (Silvester, 1969; George, 1971), that the accuracy in the latter case will be considerably superior. This is analogous to the fact that if one wishes to use three degrees of freedom to approximate an arbitrary curve, then it is generally better to use one second-order polynomial than to use two straight-line segments.

7.5 Shell Element

The formulation of shell elements is considerably more complicated than is the case for membrane elements. The main reason for this is that in addition to the transverse displacements, w, one must also consider in-plane displacements. These are denoted by u and v, parallel to the x and y axes respectively. A further reason is that the governing equations involve higher-order derivatives of the transverse displacement than is the case for the membrane. Finally, since the shell has a non-zero thickness, one must use volume integrals instead of surface integrals.

The elements used here are those described by Mufti & Harris (1969). Each element is a thin, plane triangular plate. I shall present only enough of their derivation to relate them to the membrane elements in Sections 7.3.3 and 7.4.

The potential energy functional for the element is

$$F(\mathbf{u}) = \iiint \boldsymbol{\varepsilon}'\boldsymbol{\sigma}\, dV \; - \iiint \mathbf{u}'\mathbf{g}\, dV \; .$$

This expression is analogous to the one given earlier for membranes, but the scalar displacements and forces have become vectors with x, y and z components. Thus, $\mathbf{u} = (u\ v\ w)$. The two integrals represent energy due to strains and to the applied forces, respectively. The strains, $\boldsymbol{\varepsilon}$, are given by derivatives of the components of $\mathbf{u}$; the stresses, $\boldsymbol{\sigma}$, are related to the strains by Hooke's law which embodies the material properties of the plate. Note that there is no inertial-energy integral, since we are considering only static displacements.

In this formulation, the basis functions used to describe u and v are the set $\{1, x, y\}$, as for the membrane. For w, however, the set is $\{1, x, y, x^2, xy, y^2, x^3, (Px^2y+Qxy^2), y^3\}$. This is equivalent to the use of third-order polynomials in Section 7.4, except that the x^2y and xy^2 terms have been combined; the constants P and Q are both equal to one except under certain conditions described by Mehrotra *et al.* (1969). There are thus 15 constants, c_i, to be found: three for u, three for v, and nine for w.

Application of the Ritz-Rayleigh procedure again leads to a matrix equation in $\mathbf{c}$. We then transform $\mathbf{c}$ to a vector of nodal displacements, $\mathbf{w}$. This

displacement vector contains u, v and w for each node, plus the derivatives $-\frac{\partial w}{\partial y}$ and $\frac{\partial w}{\partial x}$ at each node.

Note that in the element formulation used by Mehrotra and Mufti, any coupling between in-plane (membrane) and out-of-plane (bending) action is neglected, in order to simplify the problem. This requires the assumption that the displacements are much smaller than the thickness of the element, which is acceptable for the eardrum under normal acoustical stimulation.

The elements used here are 'non-conformable', that is, there will in general be discontinuities of displacement and slope when crossing from one element to another. This problem is not necessarily serious, and plate elements which are conformable usually have other disadvantages. Mehrotra (1969) and Mufti (1969) gave examples comparing the behaviour of conformable and non-conformable elements.

7.6 Range of Validity

7.6.1 Introduction. There are upper limits on the displacements and frequencies that the methods used here can handle. These are discussed in the following two sections. Section 7.6.4 then discusses the restriction of homogeneity.

7.6.2 Displacements. The problem formulations and solution procedures used in this thesis are all linear. Large nodal displacements introduce both geometric and physical nonlinearities.

Geometric nonlinearities arise when the deflections are no longer small compared to the dimensions of the system. At this point the deflections significantly change the actual shapes and orientations of the elements, and invalidate the problem formulation based on the undeformed geometry. The usual way to attack such a situation is with iteration: for example, the problem may be repeatedly reformulated to match the displaced geometry, and the displacements be recomputed based on the new geometry, until the displacements converge to a stable value.

Physical nonlinearities arise when parts of the system become distorted beyond the linear ranges of their elastic properties. Again, iteration is generally used in this case. Note that physical and geometric nonlinearities often, but not necessarily, occur together.

A third constraint on the displacements permissible to the shell model presented here is that they must be much smaller than the thickness of the shell (which is 10 to 50 μm). This was assumed to simplify the formulation of the finite element, as mentioned in Section 7.5 above.

The displacements of the eardrum under normal acoustical stimulation are small enough that they do not raise the question of nonlinearity. The same is not true, however, of the displacements due to large static pressure changes such as are used in tympanometry, nor is it true of the effects of middle-ear-muscle contractions. In both these cases the displacements are so large as to visibly change the shape of the eardrum. The methods presented in this thesis, then, are not adequate to model these situations. The finite-element method itself, however, is very suitable for studying such large displacements. The book by Oden (1972) is devoted specifically to the treatment of nonlinear problems by the finite-element method.

7.6.3 Frequency. The models presented here have an upper frequency limit because of the assumption that the sound pressure is uniform across the surface of the eardrum (and throughout the middle-ear cavity). To give an idea of the seriousness of this limitation, Fig. 7.3 shows the human eardrum in comparison with a sine wave representing the wavelength of sound in air at 10 kHz, the highest frequency used in this study. It can be seen that the pressure falls off by only a few decibels toward the outside of the drum. This is negligible compared to the other possible sources of error in the model. When such refinements do become necessary, it will be possible to use the finite-element method itself to compute sound-pressure distributions within the external ear canal and middle-ear cavities.

Another frequency limit is imposed on the present models by the fact that, as the vibration patterns become more complex at higher frequencies, they will

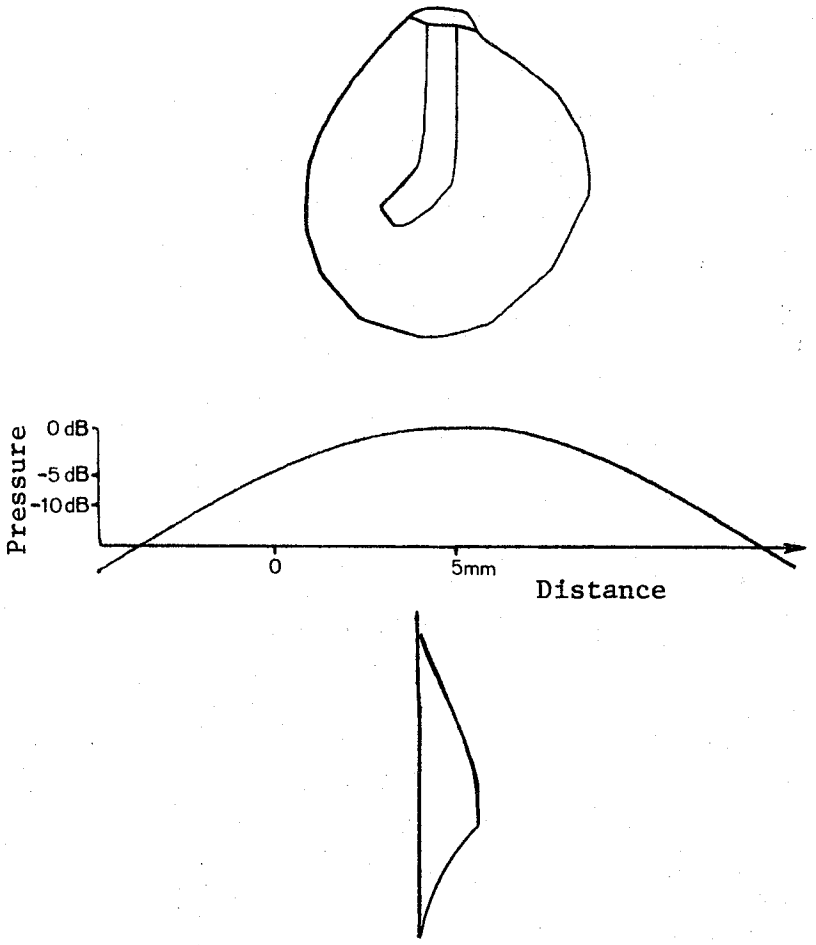

Fig. 7.3. Comparison of acoustical wavelength with dimensions of eardrum. At top and bottom are plan and side views, respectively, of the human eardrum. In the centre is a sinusoid representing the wavelength of a 10-kHz plane wave in air.

ultimately become too complicated to be faithfully reproduced by the limited resolution of the finite-element subdivision used. As will be seen in Chapter 10, however, the patterns do not become overly complicated in the frequency range considered here.

7.6.4 Homogeneity. As described in Section 2.3 above, the eardrum is composed of a number of layers with different characteristics. The two layers that are presumably most important structurally are each highly anisotropic, having strong 'grains' in different directions, much like plywood. In an analysis of the behaviour of plywood in which the grain directions of the inner and outer layers are mutually perpendicular, Hearmon (1961, pp. 37-38) found that in general a single Young's modulus could not be used to describe the behaviour of the plywood under both in-plane (membrane) and out-of-plane (bending) stresses. In the present work, however, I have assumed the eardrum to be homogeneous throughout its thickness, and characterized by a single Young's modulus. This is partly for simplicity and partly because there are not enough experimental data available to provide a more detailed representation of the drum. The finite-element method itself has been used to analyze laminated structures, and materials that consist of fibres embedded in a matrix.

CHAPTER 8

IMPLEMENTATION OF FINITE-ELEMENT METHOD

8.1 Introduction

This chapter presents details of the computer implementation of the plane-membrane and shell eardrum models considered in this work. Sections 8.2 to 8.6 discuss in turn the reading of the model definition into the computer, the formulation of the individual element stiffness matrices, the assembly of the element matrices into one system stiffness matrix, the inclusion of the boundary conditions, and the solution of the system equation. All of these items are based on the methods used in the programmes of Mehrotra *et al.*, for the shell model, and of Konrad & Silvester (1971) for the membrane model. The latter was written in the Department of Electrical Engineering (McGill University) for electromagnetic-field studies, the equations for which are the same as those for plane membranes. The programme used here for the shell model was based on one written in the Department of Civil Engineering (McGill University) by Mehrotra (1969), and subsequently modified somewhat by Mufti (1969); it has been described in the literature by Mufti & Harris (1969).

Sections 8.7 to 8.9 describe the modifications to the programmes that were made to include the effects of the rigid manubrium, the ossicular forces, and the middle-ear air cavities, respectively. Section 8.10 discusses the calculation of acoustical input impedance for the membrane model.

Section 8.11 discusses the methods used in plotting the iso-amplitude contours based on the displacements calculated for the membrane and shell models. These methods are based in part on the plotting programme of Csendes & Silvester (1972) from the Department of Electrical Engineering (McGill University).

Finally, Section 8.12 presents the computer hardware requirements for these programmes, and some execution times.

More complete descriptions of the computer programmes used in this work are available in a separate report (Funnell, 1975).

8.2 Definition of Models

The procedures used here for reading the model definitions into the computer are essentially the same as those used in the original programmes, although certain changes in data format and arrangement have been made to suit the particular problems being solved and the particular computer being used.

An important adjunct to the finite-element programme itself is the use of interactive graphics programmes to prepare the data files used to define the models. Special programmes have been written for both the membrane and shell models which display node positions and element definitions. These aid in checking the problem definitions for correctness, and in modifying them. The details of the programmes will not be presented here. There are no significant innovations in them from the point of view of interactive graphics, and the particular methods used depend strongly on the particular computer hardware available.

One feature of the graphics programme used with the shell model involves the three-dimensional curvature of the eardrum. As described in Section 11.3 below, the eardrum's radial fibres are assumed to be circular arcs. The user does not have to calculate and type in the coördinates of each node on these fibres, however. Given the end points of the fibres, and a specified degree of curvature, the programme automatically calculates the coördinates of the intermediate nodes. The algorithm places the nodes so as to divide the fibre into segments of equal arc length. The user is warned if any of the intermediate nodes falls above the plane of the tympanic ring, indicating an anatomically unreasonable geometry caused by specifying too small a radius of curvature.

8.3 Calculation of Element Matrices

The procedures used for this step are little changed from the original programmes. Note, however, that in the membrane model most of the calculations must be done with complex numbers since the model involves damping. The original programme of Konrad & Silvester (1971) used real numbers.

The calculations for the shell model have been accelerated somewhat by

using analytical inversions of some of the simpler intermediate matrices, rather than numerical inversions.

8.4 Assembly of System Equations

Again, the methods of the original programmes have not been much altered. Note that because of the size of the problem, the shell programme requires the system matrix to be partitioned, and the submatrices are stored in disk files; this was also done in the original programme, since it is uneconomical to do everything in main memory even if the computer is large enough. The membrane problem requires much less storage since there is only one degree of freedom at each node instead of six.

8.5 Boundary Conditions

The boundary conditions in these models all consist simply of constraining certain displacements to be zero. In the programme for the shell model, each of these prescribed displacements is forced into the matrix equation by multiplying the corresponding diagonal element of the matrix by a very large number, k, and then replacing the corresponding term of the force vector by the product of k and the prescribed displacement value. This has the effect of making the equations corresponding to constrained nodes dominate the system so that their displacements will not be affected by other nodes.

This method is rather wasteful, since it means that all of the constrained nodes remain in the system equation as though they were free, and thus add to the computations required for the solution. However, the method is very easy to programme.

A more sophisticated procedure is used to handle constrained nodes in the programme for the membrane model. The nodes are renumbered so that all of the constrained nodes are put together, and then the system equation is partitioned:

$$\begin{pmatrix} S_{11} & S_{12} \\ S_{21} & S_{22} \end{pmatrix} \begin{pmatrix} w_1 \\ w_2 \end{pmatrix} = \begin{pmatrix} f_1 \\ f_2 \end{pmatrix} ,$$

where w_1 represents free nodes and w_2 represents fixed ones. It is then easy to show that

$$S_{11}w_1 = f_1 - S_{12}w_2 .$$

Thus, to find w_1, one need invert only S_{11}. The order of the system is reduced by the number of constrained nodes.

The methods described above are the ones used in the original programmes. It will be possible to make the shell programme more efficient by rewriting it to use the same method as the membrane programme.

8.6 Solution

The techniques used for the actual solution of the matrix equations are quite conventional. More sophisticated methods could be used to take more advantage of the sparseness and bandedness of the matrices, but the extra complexities might outweigh the benefits for problems of the size considered here. The shell programme, which is by far the slower of the two, already takes advantage of the special banded nature of the system-matrix partitions. This is done at the expense of user convenience, since to ensure the bandedness requires attention to the ways in which the nodes and partitions of the problem are defined and numbered.

A potential problem in solving large systems of equations is round-off error. In the shell programme, whose system matrix is much larger than that of the membrane programme, this source of error was routinely checked by multiplying the calculated displacement vectors by the original matrices and comparing the result with the original force vector. The errors were generally a few per cent or less, although they sometimes became as large as 10 to 15%. This is not considered excessive for the present purposes.

8.7 Manubrium

In the shell-model programme, the rigidity of the manubrium is represented simply by using a very high Young's modulus. This is wasteful since the displacements of all of the nodes on the manubrium could be represented by a single degree of freedom, thus reducing the order of the system. The reprogramming would be quite involved for the shell model and has not yet been done. For the membrane-model programme, however, I have reduced all of the manubrial degrees of freedom to a single one using an extension of the method described in Section 8.5. Here again, the system matrix is partitioned, this time with the three partitions representing free, manubrial and fixed nodes, respectively. The system equation then becomes

$$\begin{pmatrix} \mathbf{S}_{11} & \mathbf{S}_{12} & \mathbf{S}_{13} \\ \mathbf{S}_{21} & \mathbf{S}_{22} & \mathbf{S}_{23} \\ \mathbf{S}_{31} & \mathbf{S}_{32} & \mathbf{S}_{33} \end{pmatrix} \begin{pmatrix} \mathbf{w}_1 \\ \mathbf{w}_2 \\ \mathbf{w}_3 \end{pmatrix} = \begin{pmatrix} \mathbf{f}_1 \\ \mathbf{f}_2 \\ \mathbf{f}_3 \end{pmatrix} .$$

Now, since the manubrial nodes must all be displaced as a rigid assembly, one can write

$$\mathbf{w}_2 = u\,\mathbf{b} ,$$

where u is a dimensionless variable representing the angular displacement of the manubrium, and $\mathbf{b}$ is a vector whose components represent the perpendicular distances between the axis of rotation and the manubrial nodes. Substituting this into the system equation, and premultiplying the second row by $\mathbf{b}'$, one obtains

$$\begin{pmatrix} \mathbf{S}_{11} & \mathbf{S}_{12} & \mathbf{S}_{13} \\ \mathbf{b}'\mathbf{S}_{21} & \mathbf{b}'\mathbf{S}_{22} & \mathbf{b}'\mathbf{S}_{23} \\ \mathbf{S}_{31} & \mathbf{S}_{32} & \mathbf{S}_{33} \end{pmatrix} \begin{pmatrix} \mathbf{w}_1 \\ u\mathbf{b} \\ \mathbf{w}_3 \end{pmatrix} = \begin{pmatrix} \mathbf{f}_1 \\ \mathbf{b}'\mathbf{f}_2 \\ \mathbf{f}_3 \end{pmatrix} .$$

In this way, the set of equations in $\mathbf{w}_2$ has been collapsed to a single equation in u.

8.8 Ossicular Forces

As mentioned in the previous section, the manubrium in the shell model is represented simply by elements with very high stiffness. In this case, the simplest way of simulating the forces acting on the manubrium due to the rest of the ossicular chain is to introduce a spring acting at one of the nodes about half-way down the manubrium. This is done in the programme by adding an extra stiffness term to the appropriate component of the system stiffness matrix. If the added stiffness is too large, the manubrium will tend to bend in spite of its stiffness, because of the concentrated nature of the load. As shown in Section 12.7 below, however, this is not a serious problem for reasonable values of the ossicular forces.

In the membrane programme, the forces on the ossicles are represented by adding an angular stiffness term to the component of the system matrix corresponding to the angular displacement of the manubrium, after the manubrial nodes have been collapsed as described in the previous section. Since the membrane model takes dynamic effects into account, the angular stiffness term added is a complex number given by

$$\left(\frac{1}{C} - \omega^2 L\right) + j\omega R \ ,$$

where R, L and C represent resistive (damping), inertial and compliance effects, respectively.

8.9 Middle-Ear Air Cavities

The effects of the middle-ear air cavities are not included in the shell model.

To find the effects of these cavities on the membrane model, we first note that the pressure change (assumed to act uniformly over the eardrum) of a simple cavity is given by

$$dP = \frac{\gamma P_o}{V_o} dV \ ,$$

where P_o is the resting pressure of the air in the cavity; V_o is the volume of the cavity; and dV and dP are the changes in volume and pressure due to the displacement of the membrane (see Kinsler & Frey, 1962, for example); γ is a constant (a ratio of specific heats) determined by the type of gas filling the cavity.

Now, using the notation of Section 7.3 above, the volume displacement of the eardrum is given in terms of the nodal displacements by

$$\mathbf{e'Bw},$$

where $\mathbf{e'}$ is a vector filled with ones. (This expression is based on equation 36 of Silvester, 1973. My $\mathbf{B}$ is equivalent to his $\mathbf{T}$.) Thus, in addition to the original pressure term loading the drum, there is another pressure term with the opposite sign:

$$\mathbf{Sw} = \mathbf{B}\,(\,\mathbf{g} - k\,\mathbf{e}\,\mathbf{e'Bw}\,),$$

where $k = \dfrac{\gamma P_o}{V_o}$, and $\mathbf{e}$ serves to expand the scalar $\mathbf{e'Bw}$ to a column vector.

Rearranging, the system equation becomes

$$(\,\mathbf{S} + k\mathbf{Bee'B}\,)\mathbf{w} = \mathbf{Bg}.$$

The effects of the cavities are thus included by adding the appropriate amount to every component of the system stiffness matrix. The fact that the middle-ear cavities consist of two cavities with a narrow passage between them means that the constant k becomes complex, its value being determined by the constants R, L, C_{b1} and C_{b2} introduced in Section 4.6 above.

8.10 Acoustical Input Impedance

For the purposes of comparison with experimental impedance data in Section 10.3.2, it is necessary to calculate the acoustical impedance of the eardrum based on the nodal displacements. This is done by calculating the volume displacement using the expression given in the preceding section. This is then converted to a volume velocity by multiplying by frequency, and divided into the sound pressure to give impedance. The impedance of the small ear-canal volume mentioned

in Section 4.6, namely C_e, is inserted in parallel with the eardrum impedance in order to simulate the conditions of the experimental measurement.

It is inefficient to calculate the complete vibration pattern when all that is required is the over-all volume displacement. The computation becomes especially time-consuming when one wishes to obtain a complete frequency response for the volume displacement. Silvester (1973) has presented a method which requires only the calculation of a number of eigenvalues and eigenfunctions (that is, natural frequencies and modes). To calculate the volume displacement for any particular frequency then requires only a simple algebraic computation. Although I have applied this procedure to a simplified form of the present model, it unfortunately cannot be used when the system stiffness matrix contains frequency-dependent terms such as those representing ossicular and air-cavity stiffness.

8.11 Plotting

The method used for plotting the iso-amplitude contours of the membrane model is based on the programme of Csendes & Silvester (1972). This involves dividing each element into second-order subelements and then solving a series of quadratics to trace out the contour lines. The result for a given contour line is then a number of disconnected curved line segments. In order to make the actual plotting of these segments more efficient (at the expense of computation time) I store all of the points to be plotted for each contour in a disk file, and then rearrange them to form a single continuous curve. The actual plotting is done from the rearranged points. (The rearrangement is done by repeatedly sweeping through the list of points, and picking the closest point to the current one to be the next point. This practically eliminates the problem of resolving different branches of given contour lines referred to by Csendes & Silvester.)

Similar plotting methods were used for the results of the shell model, except that the elements were not subdivided. As discussed in Chapter 7, the triangular shell elements involve cubic interpolation functions. Fig. 8.1 shows an example of contour lines calculated from the nodal displacements using the full cubic functions. It can be seen that the contours are more convoluted than

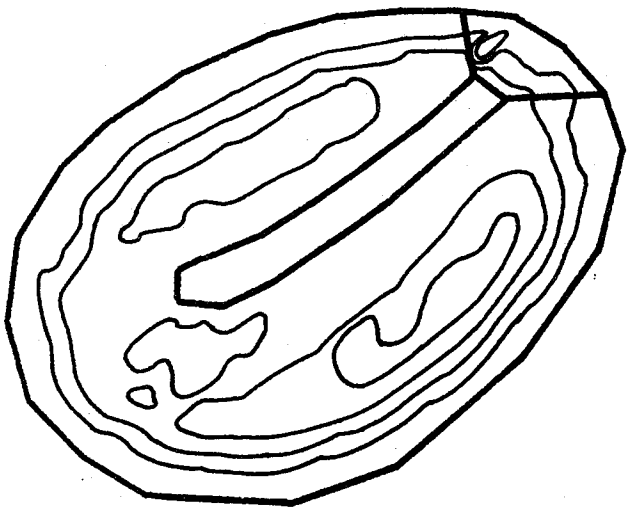

Fig. 8.1. Example of contour lines calculated for cat eardrum model using cubic interpolation functions.

is physiologically reasonable. This problem with the model is not entirely unexpected, both because of the non-conformable nature of the elements used (see discussion in Section 7.5) and because of the coarseness of the finite-element grid. Since the fine details of the contours are unreliable, there is no point in using cubic interpolation for the plotting, especially since one can save considerable time by using a simpler function. (Using the cubic function means that one has to extract the three roots of a cubic polynomial at every step along every contour line.) Therefore, I have used linear interpolation functions in preparing the contour plots presented in Chapters 11 and 12.

In each of the Figures showing iso-amplitude contours in Chapters 9 to 12, the contours were plotted for five displacement values evenly spaced between the minimum and maximum values. Thus, all of the vibration patterns are normalized with respect to peak drum displacement. The actual contours themselves in all of the Figures in Chapters 9 to 12 are exactly as plotted by the computer; they are unretouched except for the addition of dotted lines in some cases, to close gaps left by the programme or to join lines of equal amplitude for clarity.

For the membrane model, which includes dynamic effects, each displacement is a complex quantity. The contour patterns presented in Chapters 9 and 10 therefore represent either displacement magnitude, or the real and imaginary components of the displacement, as appropriate.

8.12 Computer Hardware Requirements and Timings

These programmes have been implemented on a PDP-12 minicomputer that has 28k words of 12-bit main memory and a single removable-cartridge disk. It also has a separate floating-point-arithmetic processor that can run in parallel with the main processor. The programmes have been written mainly in FORTRAN, but several critical subroutines have been manually streamlined at the assembler-language level to make up for inefficient code produced by the compiler. This was done mainly to reduce execution times.

The actual times required for problem solution obviously depend largely

on the size of the model used as well as on the particular computer hardware available. For the models used here, the plane-membrane programme requires about 22 seconds to calculate the displacements for a single set of parameter values; about 5 seconds of this is for the assembly of the system equation and the rest is for the actual solution. The shell model requires on the order of 20 minutes for a single set of parameter values, about equally divided between assembly and solution. These figures do not include the times for the plotting of the results, which are determined almost entirely by the type of plotter used.

Both programmes use almost all of the main storage available, mostly for storage of matrices and vectors. The amount of memory required has been considerably reduced by the use of programme overlays from disk files. The disk is also used for a number of data-storage files for both intermediate and final results.

CHAPTER 9

DESCRIPTION OF MEMBRANE MODELS

9.1 Introduction

This chapter presents the actual eardrum models used in calculating the results of the next chapter. The cat and guinea-pig models are described in Sections 9.2 and 9.3, respectively. Section 9.4 discusses the adequacy of the finite-element subdivision.

The actual parameter values used are those given in Chapters 2 to 4, except for the membrane tension and resistance which are discussed in the next chapter.

9.2 Cat

Fig. 9.1 illustrates the shapes of the anatomical structures as they are modelled for the cat. The position and orientation of the ossicular axis of rotation are as given by Khanna (1970, Fig. 21). Fig. 9.2 shows the way in which the model has been divided into elements: the 24 triangles around the circumference are first-order elements, and the rest are second-order (as discussed in Section 7.4 above).

9.3 Guinea Pig

Figures 9.3 and 9.4 present the guinea-pig model, in the same formats as Figs. 9.1 and 9.2, respectively. Again, the triangles around the circumference (21 this time) are first-order elements, and the remaining triangles are second-order.

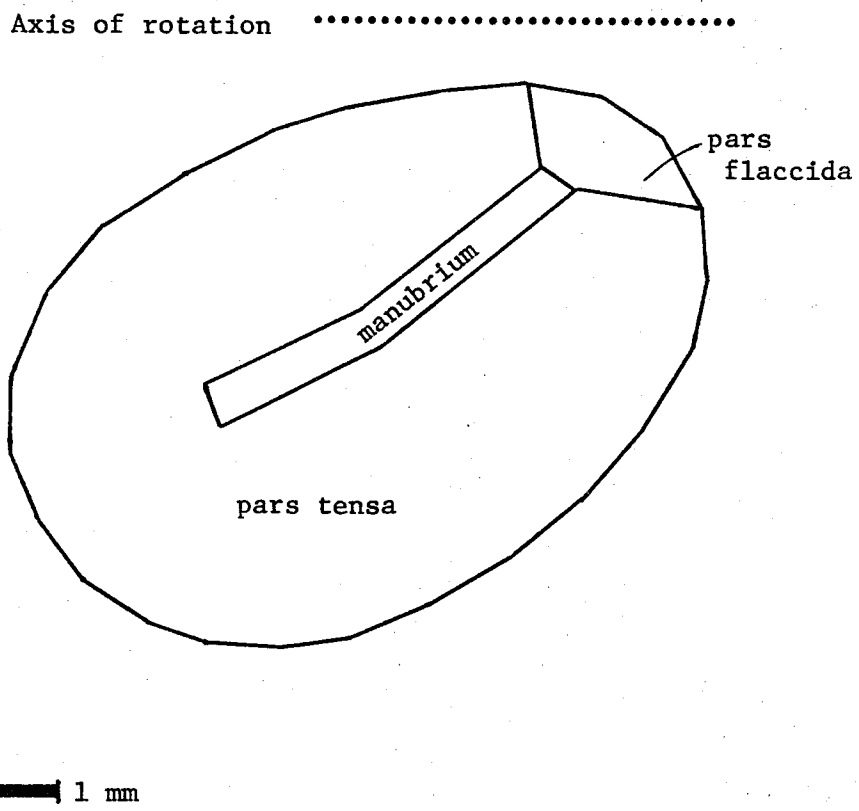

Fig. 9.1. Shape of plane-membrane model for cat.

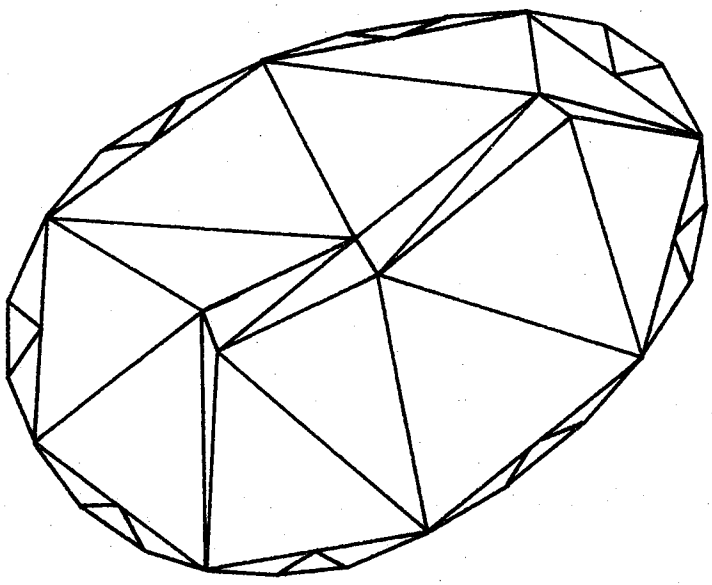

Fig. 9.2. Subdivision of cat plane-membrane model.

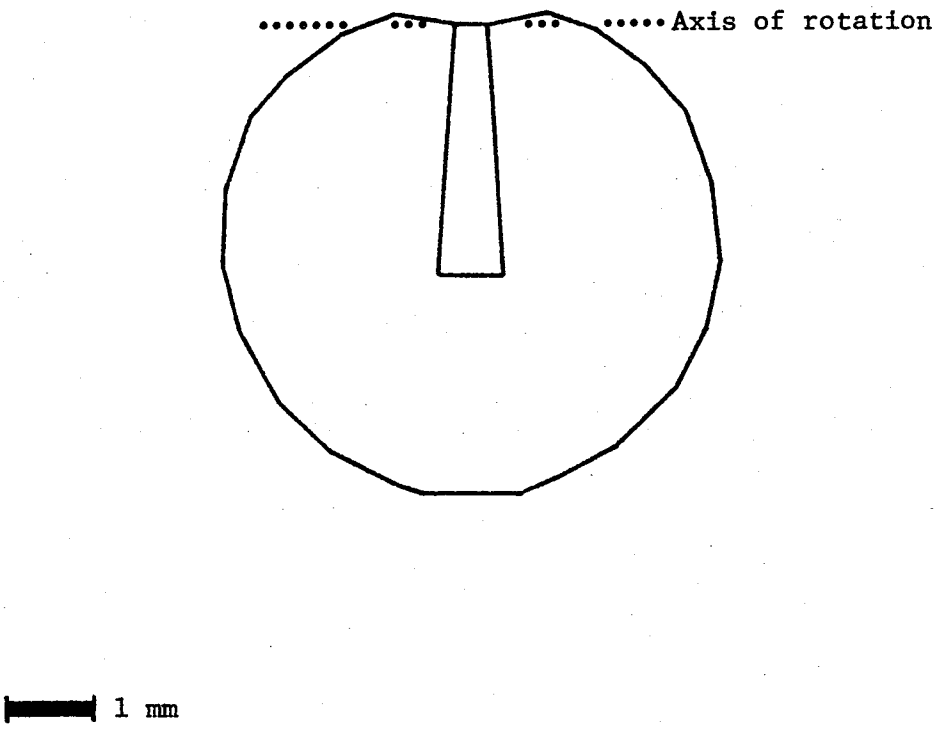

Fig. 9.3. Shape of plane-membrane model for guinea pig.

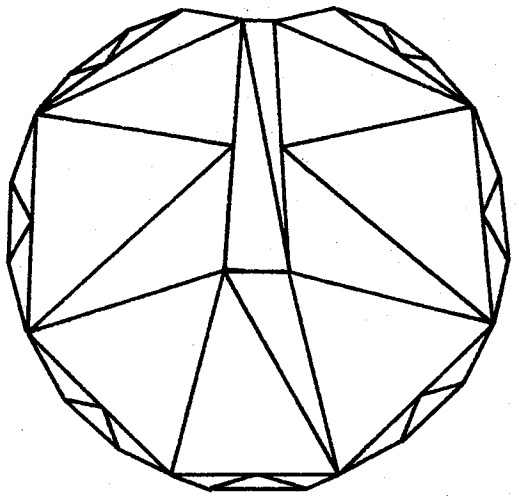

Fig. 9.4. Subdivision of second-order guinea-pig plane-membrane model.

9.4 Adequacy of Subdivision

The elements have been limited to first order and second order to save computer time. To estimate the accuracy of this second-order model, I have done some calculations using the third-order model represented in Fig. 9.5. Fig. 9.6 shows two contour plots computed using each model, for comparison. At the top are vibration patterns at 100 Hz and 7.5 kHz, from the second-order model. The former is a typical low-frequency pattern, and the latter is a more complicated high-frequency pattern which would be expected to be more sensitive to the limited resolution of the simpler model. In part *b* of the Figure are patterns at the same frequencies calculated using the third-order model. Although there are differences between the patterns calculated using the different models, the patterns do not really change significantly. For a more quantitative comparison, I have calculated that the peak eardrum displacements at 100 Hz are within 5%, and the over-all volume displacements (which are less sensitive to details of the vibration patterns) are within 0.2%. At 7.5 kHz these figures are higher, as expected, but still small: 7% and 4%, respectively. The ratios of $\frac{\text{peak displacement}}{\text{manubrial tip displacement}}$ are within 9% at 100 Hz, and even closer (1%) at the higher frequency.

From this I conclude that the second-order model is adequate for my present purposes.

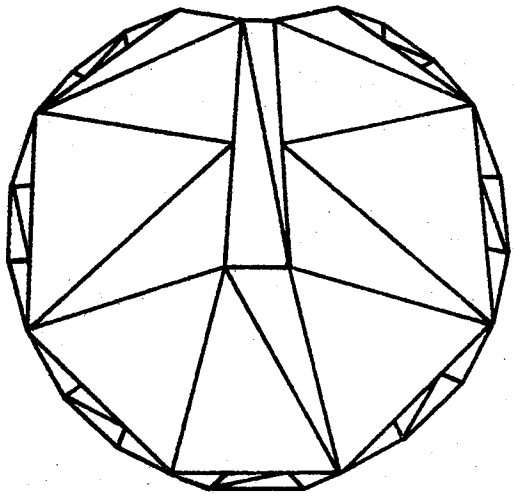

Fig. 9.5. Subdivision of third-order guinea-pig plane-membrane model. This is the same as the second-order subdivision (Fig. 9.4) except for the small elements around the periphery, which must be rearranged because the interior elements are now third-order instead of second-order, and thus have four nodes/side instead of three.

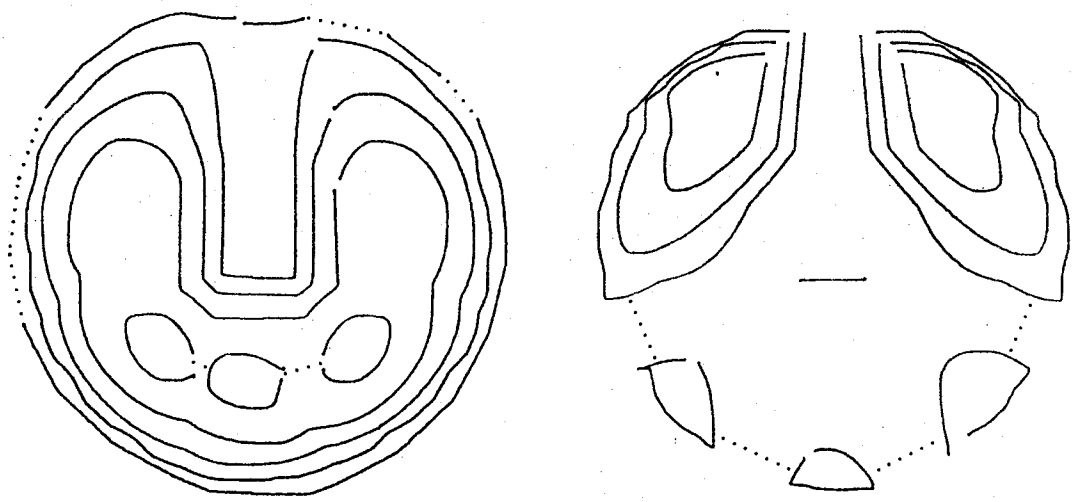

100 Hz 7500 Hz

a. second-order

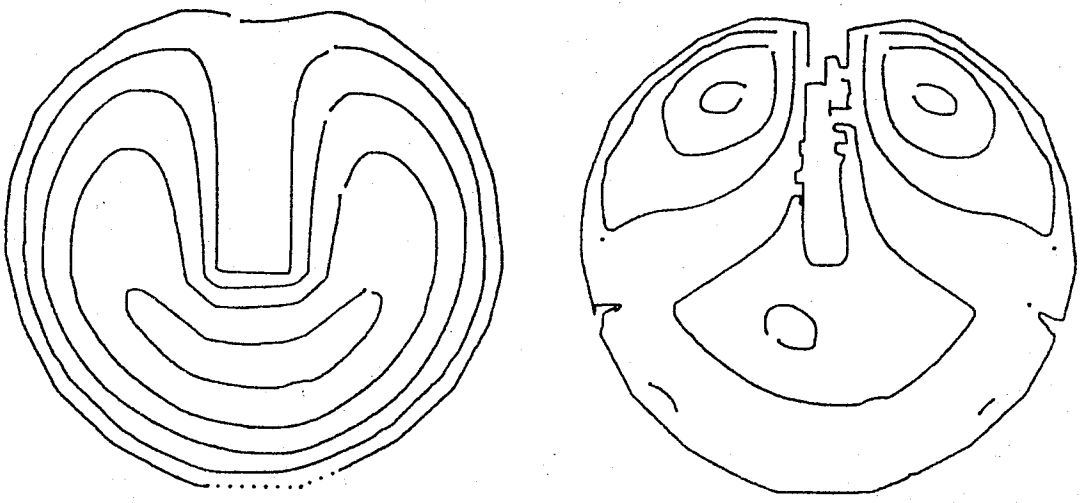

100 Hz 7500 Hz

b. third-order

Fig. 9.6. Comparison of second-order and third-order models, at 100 Hz and 7500 Hz. Contours represent real part of complex displacement.

CHAPTER 10

RESULTS OF MEMBRANE MODELS

10.1 Introduction

This chapter presents the results of calculations made using the membrane models described in the previous chapter. Sections 10.2 and 10.3 present results for the cat and guinea pig, respectively. The model outputs for both species are compared to experimental results with respect to (1) general shape and complexity of vibration patterns; (2) amplitude of the peak drum displacement; and (3) displacement of the tip of the manubrium and the ratio of this to the peak drum displacement.

For the guinea pig, the model results are also compared to some previous measurements of acoustical input impedance as a function of frequency (see Section 5.4). There are other experimental data available concerning middle-ear behaviour as a function of frequency: the recent transfer-function data of Nuttall (1972), for example. I have chosen to limit myself to the above-mentioned impedance data for three reasons. First, the frequency resolution of the impedance data is much better than that of the transfer-function data — Nuttall measured only five points between 4 kHz and 10 kHz, compared to about 30 points for the impedance data. Second, there apparently were some problems with equipment resonances in the transfer-function measurements, making the high-frequency curves unreliable (Nuttall, 1972, pp. 32-34). Third, middle-ear impedance is determined mainly by the eardrum, which is the focus of interest in the present work. By contrast, the middle-ear transfer function also depends heavily on the properties of the ossicular chain and the cochlea, and a proper comparison of the model to the data would require a more careful consideration of these properties than is within the scope of this thesis.

Most of the parameter values used for these calculations are based on the estimates presented in Chapters 3 and 4 above. The only exceptions

are the eardrum tension and resistance. There is no estimate available for the former, and in fact this parameter probably cannot be interpreted as an actual physical tension. The eardrum may actually function with no resting tension at all, as represented by the shell model presented elsewhere in this work. At least part of the "tension" in this membrane model serves to provide an effective bending stiffness which in fact is provided by the inherent stiffness of the eardrum. Values for the tension parameter have been arrived at by comparing the model results to experimental data.

An estimate for internal resistance was offered in Chapter 3 above, but it was not very convincing. It has been found to give unacceptable results in this model, and considerably lower values have been used, as described in Sections 10.2.1 and 10.3.1 below. Different values have been used for the two species: the significance of this is discussed in Section 10.4 below.

10.2 Results from Cat Model

10.2.1 Determination of parameter values. As mentioned above, two parameters were adjusted to make the model results fit the experimental data, namely, the tension and the internal resistance of the eardrum. The final values were chosen in two steps. First, the resistance was set to zero, and the tension was adjusted so that the break-up of the vibration pattern occurred at frequencies similar to those found by Khanna (1970). The value arrived at was 18×10^3 dyn cm^{-1}. If the tension was increased to 19 or 20×10^3, the patterns calculated were too simple, and if the tension was reduced much below 18×10^3, the break-up occurred at too low frequencies. The pattern complexity was taken to be the number of amplitude maxima in each of the anterior and posterior halves of the drum, and the pattern presented by Khanna & Tonndorf at their highest frequency, about 6 kHz, was interpreted to have two anterior peaks and four posterior ones (ignoring the very fine detail of their contour lines and considering only the major peaks).

Having established a value for the tension, the resistance was increased from zero as far as possible without destroying the complexity of the high-frequency patterns. The value decided on was 18×10^{-4} dyn sec cm^{-1}. This means a ratio of stiffness to resistance of 10^7 sec^{-1}, compared to 10^3 sec^{-1} mentioned in Section 3.7 above. Decreasing this ratio even to 10^6 sec^{-1} cut the number of peaks at 6 kHz in half.

As discussed in Section 10.4 below, not too much importance is to be attached to these parameter values.

10.2.2 Calculated patterns. Fig. 10.1 shows the vibration pattern calculated at 1 kHz. The patterns at lower frequencies were essentially identical. This pattern is obviously similar to the low-frequency patterns found by Khanna and Tonndorf. The only qualitative difference is that a separate peak does not quite form in the anterior region.

Fig. 10.2 compares calculated (*b* and *c*) and measured (*a*) vibration patterns at the five highest frequencies observed by Khanna and Tonndorf. Part *b* shows the iso-amplitude contours calculated from the model for the magnitude of the complex displacement, for direct comparison with the experimental data. Part *c* shows the contours for the real (that is, in phase with the applied pressure) and imaginary components of the displacement, in order to reveal more clearly the break-up of the vibration pattern.

The model does not duplicate the fine details of the experimental patterns, but it does show the main features: the posterior pattern starts to break up at about 4 kHz, and the anterior one at about 5 kHz. Note that, according to the model, the anterior peak is out of phase with the posterior one in the region of 3 to 4 kHz. This is opposed to the assumption used by Khanna and Tonndorf (1972a) in calculating eardrum volume displacements. It would not really make much difference at these frequencies, however, since the anterior displacements are quite small.

Another noticeable difference between the model and experimental results is that at about 5 kHz the maximal drum displacement in the model occurred in the anterior region, which was never observed experimentally.

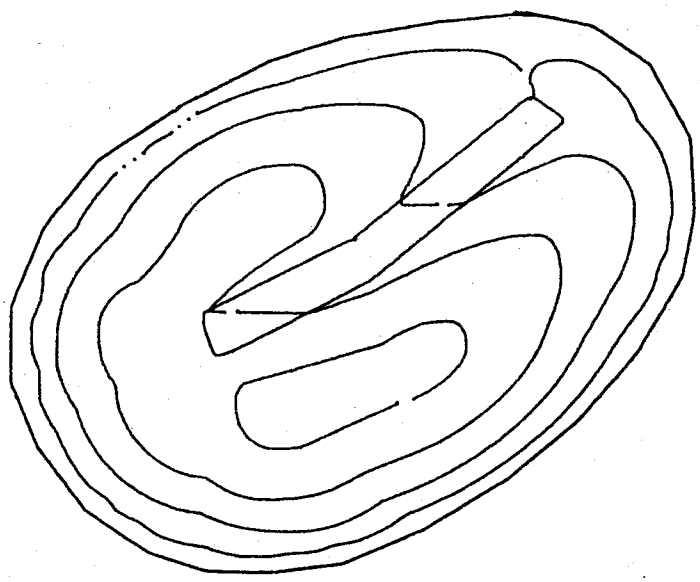

Fig. 10.1. Low-frequency (1 kHz) vibration pattern calculated for cat. Contours represent magnitude of complex displacement.

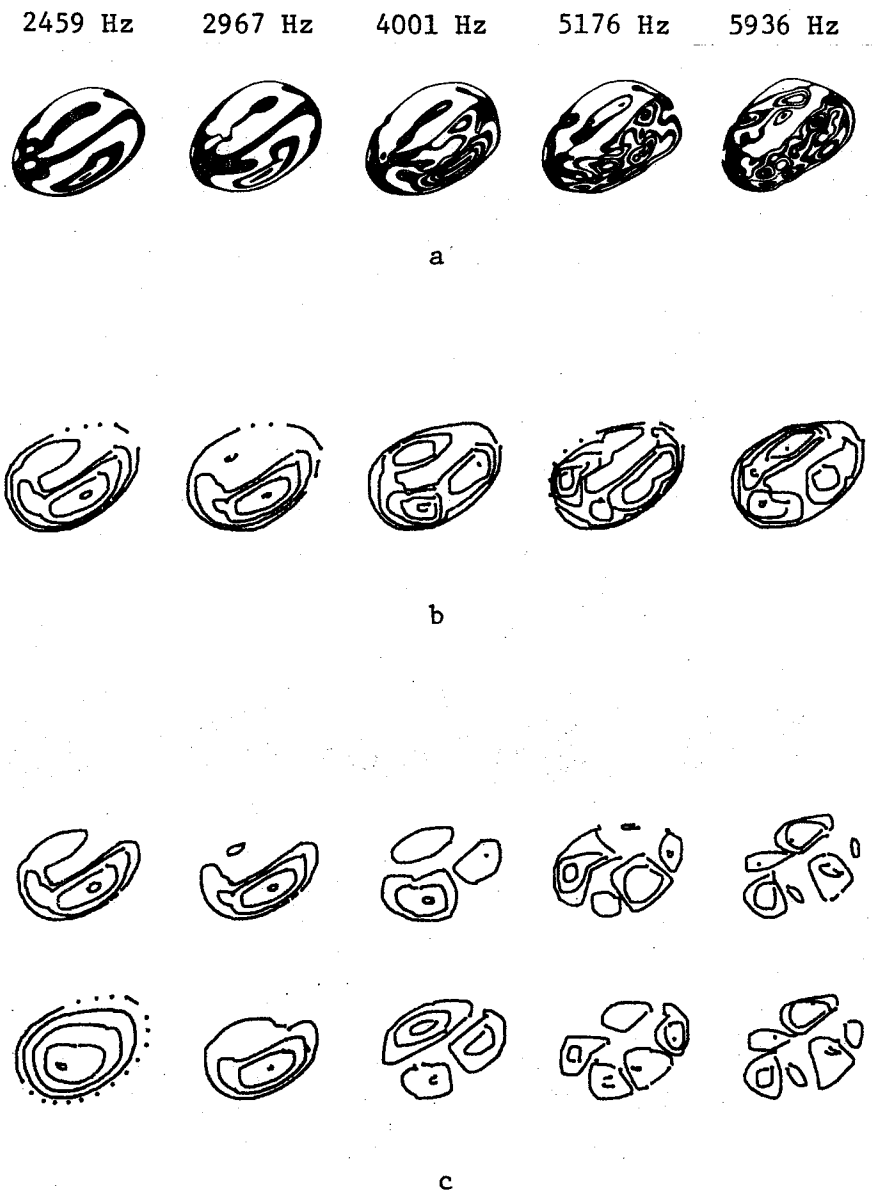

Fig. 10.2. Comparison of experimental and model results at five high frequencies. Part *a* represents the same experimental data as Fig. 5.10. Part *b* shows the contour lines (magnitude) calculated for the same frequencies. Part *c* shows contour lines for the real parts (top) and imaginary parts (bottom row) of the complex displacements for the same frequencies.

10.2.3 Drum displacement. Fig. 10.3 is a comparison of experimental and model data for maximal drum displacement at 100 dB SPL. Except for the points at 3 and 4 kHz, there is not much more difference between the model and one of the cats than there is between the two cats. The model outputs at 3 and 4 kHz, however, are much too large. This could indicate either peaks that were missed experimentally due to insufficient frequency resolution, or, more likely, insufficient damping of resonances in the model.

As noted in the previous section, at about 5 kHz the maximal drum displacement occurred in the anterior region rather than in the posterior one. The amplitude of the calculated posterior peak was about half that of the anterior one at this frequency.

10.2.4 Ratio of drum to malleolar displacement. Fig. 10.4 compares the model results to some values of the ratio of $\frac{\text{peak drum displacement}}{\text{malleolar-tip displacement}}$ measured by Khanna & Tonndorf (1972a). The values calculated from the model are similar to the experimental ones in that (1) they are in the range 2 to 4 in the low to medium frequencies, and (2) they increase to very high values above 3 kHz. The chief significant difference between the two sets of data is that the model results do not show a plateau between 600 and 2000 Hz. Note that the amplitude of the manubrial displacement, and thus the value of the ratio $\frac{\text{peak}}{\text{tip}}$, is strongly influenced by the properties of the ossicular chain, which properties have not been optimized for these calculations.

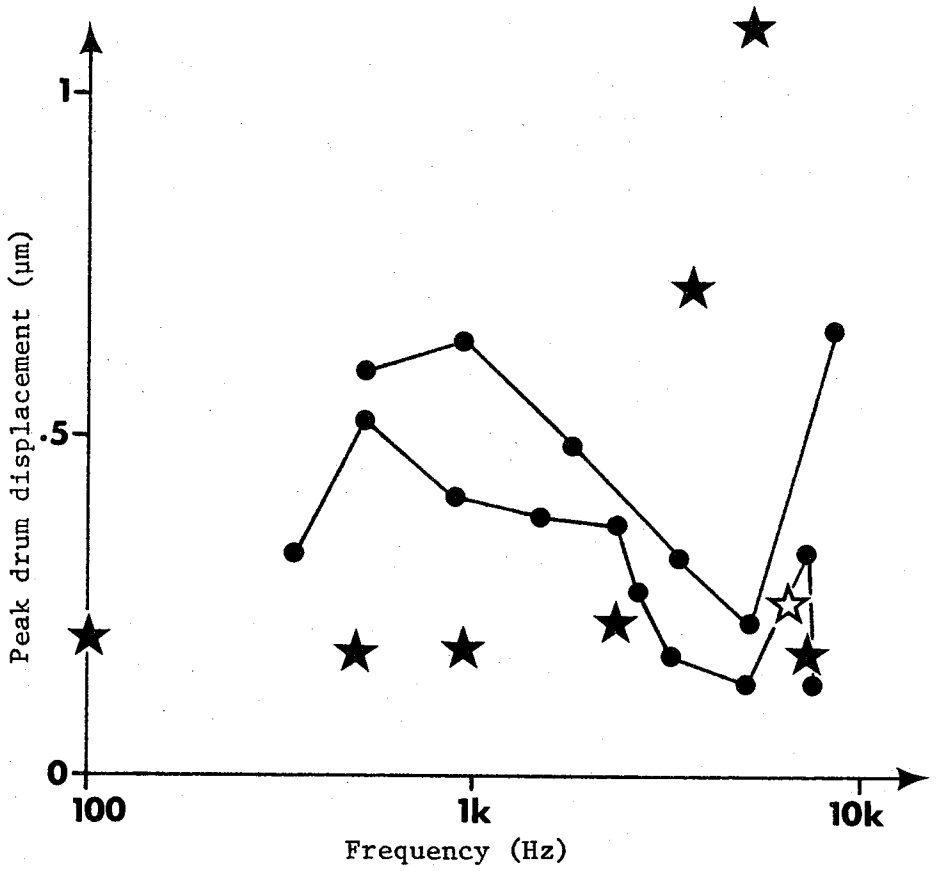

Fig. 10.3. Comparison of measured and calculated peak drum displacements. The filled circles represent experimental data for two different cats (Khanna, 1970, Fig. 31 & 32). The stars represent calculated values. The single unfilled star (near 5 kHz) indicates that at that frequency the peak displacement occurred in the anterior rather than the posterior region.

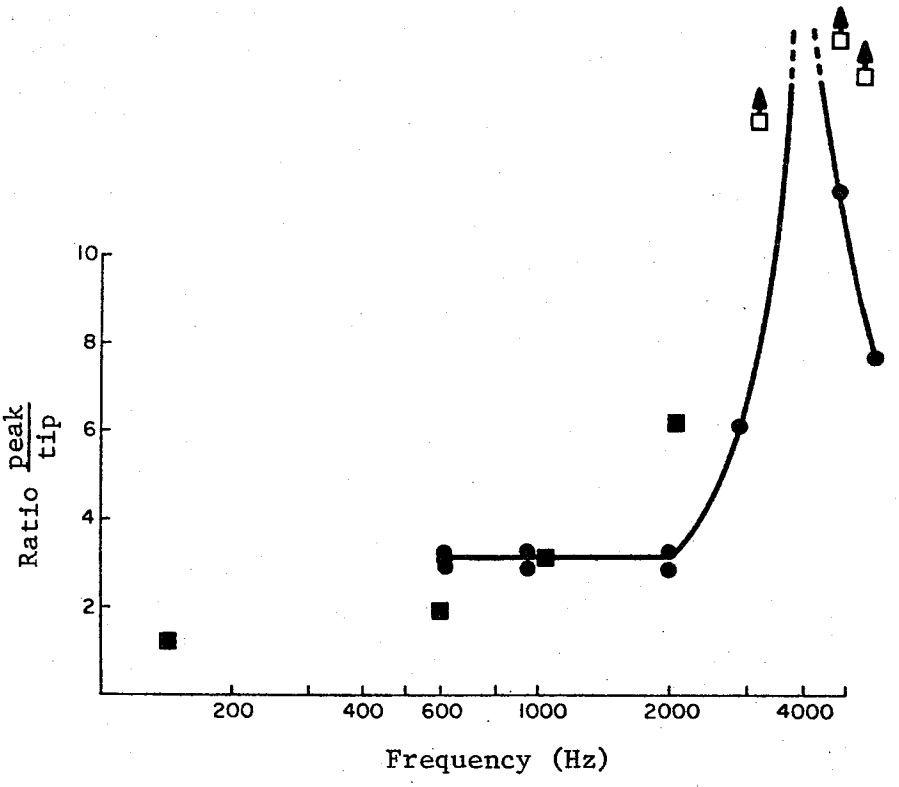

Fig. 10.4. Comparison of measured and calculated values of the ratio $\frac{\text{peak}}{\text{tip}}$. The filled circles are experimental data of Khanna & Tonndorf (1972a, Fig. 11). The squares are model data. The unfilled squares indicate values that fall off-scale.

10.3 Results from Guinea-Pig Model

10.3.1 Determination of parameter values. As for the cat, the two parameters to be chosen are the tension and resistance. The tension was selected on the basis of the low-frequency impedance of the middle ear. The impedance of the air cavities alone, with the eardrum removed, is 9.4×10^3 dyn sec cm^{-5} (that is, 9.4 kohm) at 100 Hz for the cavity volumes used in this model. Previous impedance measurements (Funnell, 1972, for example) have shown that the impedance of the intact guinea-pig middle ear is not much higher than that of the cavities below about 1 kHz. With this in mind, the tension was set to 2000 dyn cm^{-1}. This gives an impedance at 100 Hz of about 10.6 kohm.

The resistance of the drum was chosen to make the curve of impedance against frequency qualitatively similar to measured ones. The value decided on was 0.2 dyn sec cm^{-1}, for a ratio of stiffness (tension) to resistance of 10^4 sec^{-1}.

10.3.2 Calculated impedance curve. Fig. 10.5 shows, in part *a*, an experimentally measured impedance curve from Funnell (1972); and in part *b*, the impedance curve calculated from the present model, using the parameter values given above. The low-frequency slope and the resonance-antiresonance at 4 to 5 kHz are due to the middle-ear air cavities. The features due to the eardrum and ossicles are the height of the 4-to-5-kHz peak, and the depth of the 8-kHz trough. In these two respects the model output is similar to the measured curves. Fig. 10.6 shows the effect of varying the resistance by a factor of ten above and below the value used for Fig. 10.5. It can be seen that the higher value almost entirely obliterates the peaks and troughs, while the lower value makes the troughs too deep. Note that the degree of flattening of the impedance curve is unaffected by damping in the ossicular suspension: resistance there will damp the manubrial vibrations but not those of the surrounding drum.

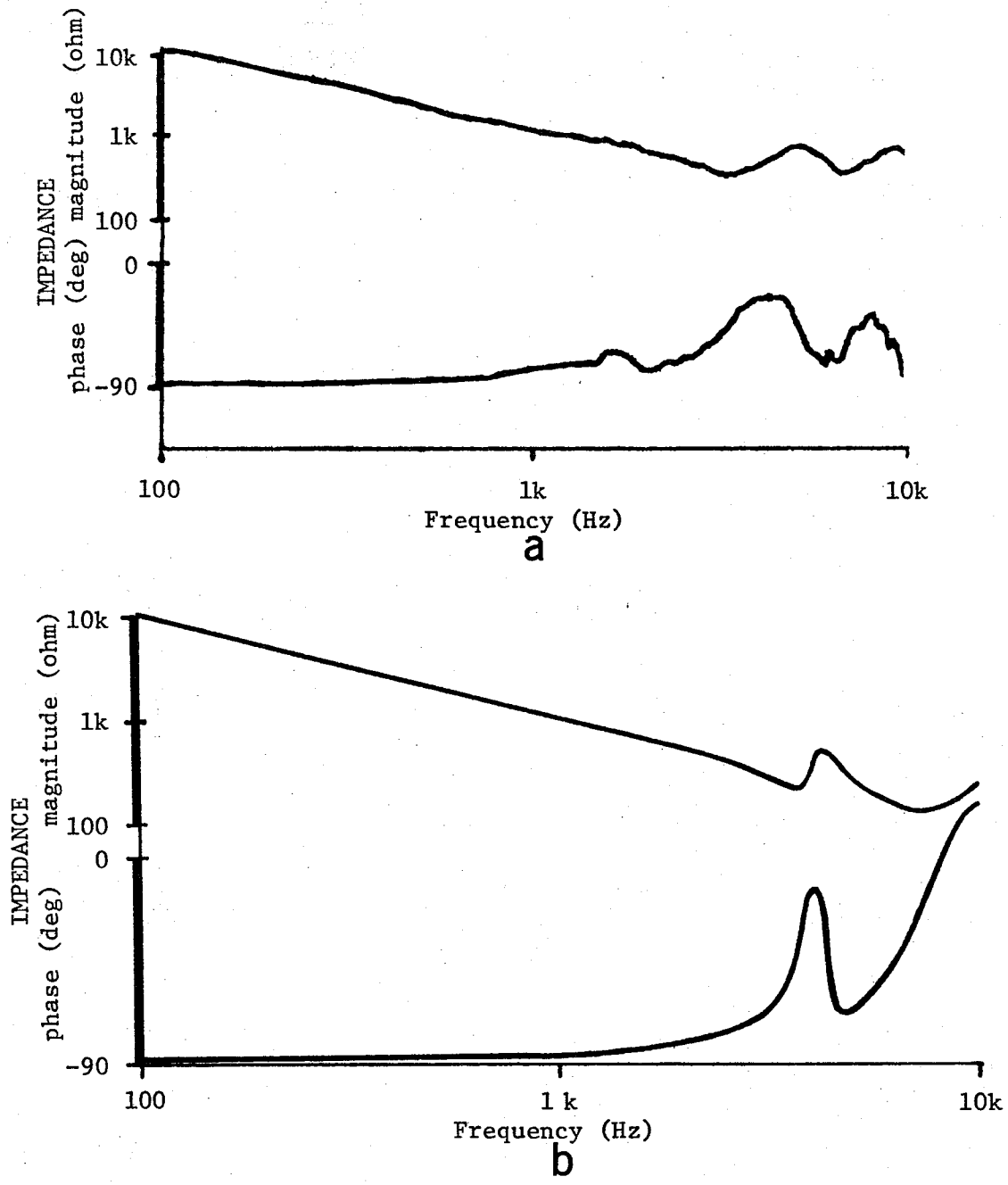

Fig. 10.5. Comparison of measured and calculated acoustical input impedance. Part *a* is measured curve (after Funnell, 1972). Part *b* is calculated from model.

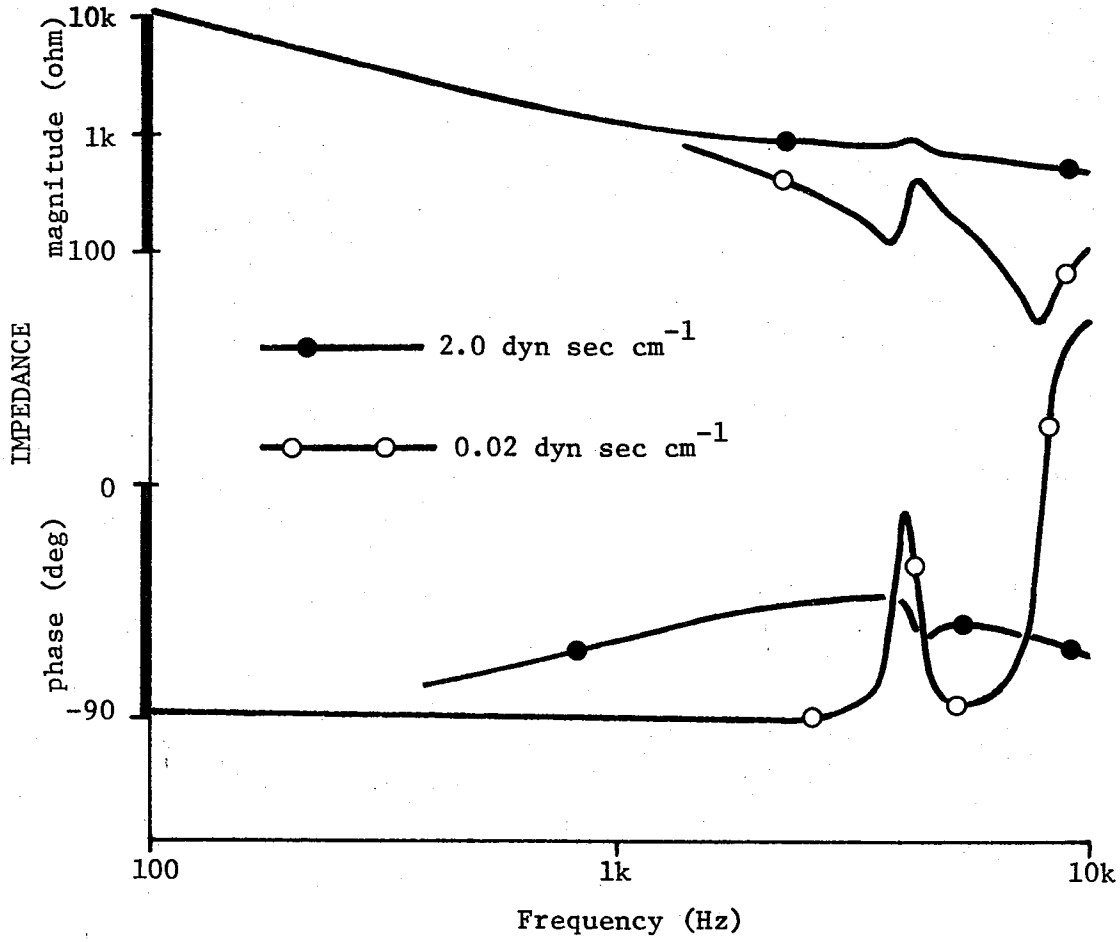

Fig. 10.6. Calculated impedance for two values of eardrum resistance.

10.3.3 Vibration patterns. Fig. 10.7 shows the vibration patterns calculated from the model at seven frequencies. The contour lines correspond to the real (in-phase) component of the displacement. The pattern changes little up to 7 kHz, except that the amplitude maximum splits into two and each half shifts upward. At 7.5 kHz the drum is divided into three segments, two superior ones in phase with each other and a low-amplitude segment out of phase with the other two. At 8 kHz the inferior peak has a larger amplitude than the superior ones. At yet higher frequencies the pattern simplifies again, becoming similar to the low-frequency patterns but with reversed phase.

At low frequencies damping is relatively unimportant, and the magnitude of the complex displacement is approximately equal to the real part. At high frequencies, however, the damping dominates and the imaginary part of the displacement is larger than the real part. Fig. 10.8 shows the vibration patterns at the six high frequencies, calculated from the magnitude of the displacement rather than from the real part. The patterns are almost identical, and are determined almost entirely by the imaginary component of the displacement.

There are no experimental data with which to compare the high-frequency patterns. However, the low-frequency pattern shown in Fig. 10.7 is qualitatively the same as the one inferred by Manley & Johnstone (1974) from their point measurements of eardrum displacement. The essential features are (1) that the amplitudes of the manubrium are always less than those of the neighbouring portions of the drum, and (2) that the over-all displacement maximum occurs in the inferior region.

10.3.4 Drum displacement. The peak drum displacement of the model at 100 Hz is 0.14 μm, which is to be compared to a value of 0.45 μm measured by Manley & Johnstone (1974).

10.3.5 Ratio of drum to malleolar displacement. The ratio $\frac{\text{peak}}{\text{tip}}$ at 100 Hz is 5.3 according to the model, compared to a range of about 2 to 9 measured by Manley & Johnstone (see Section 12.3).

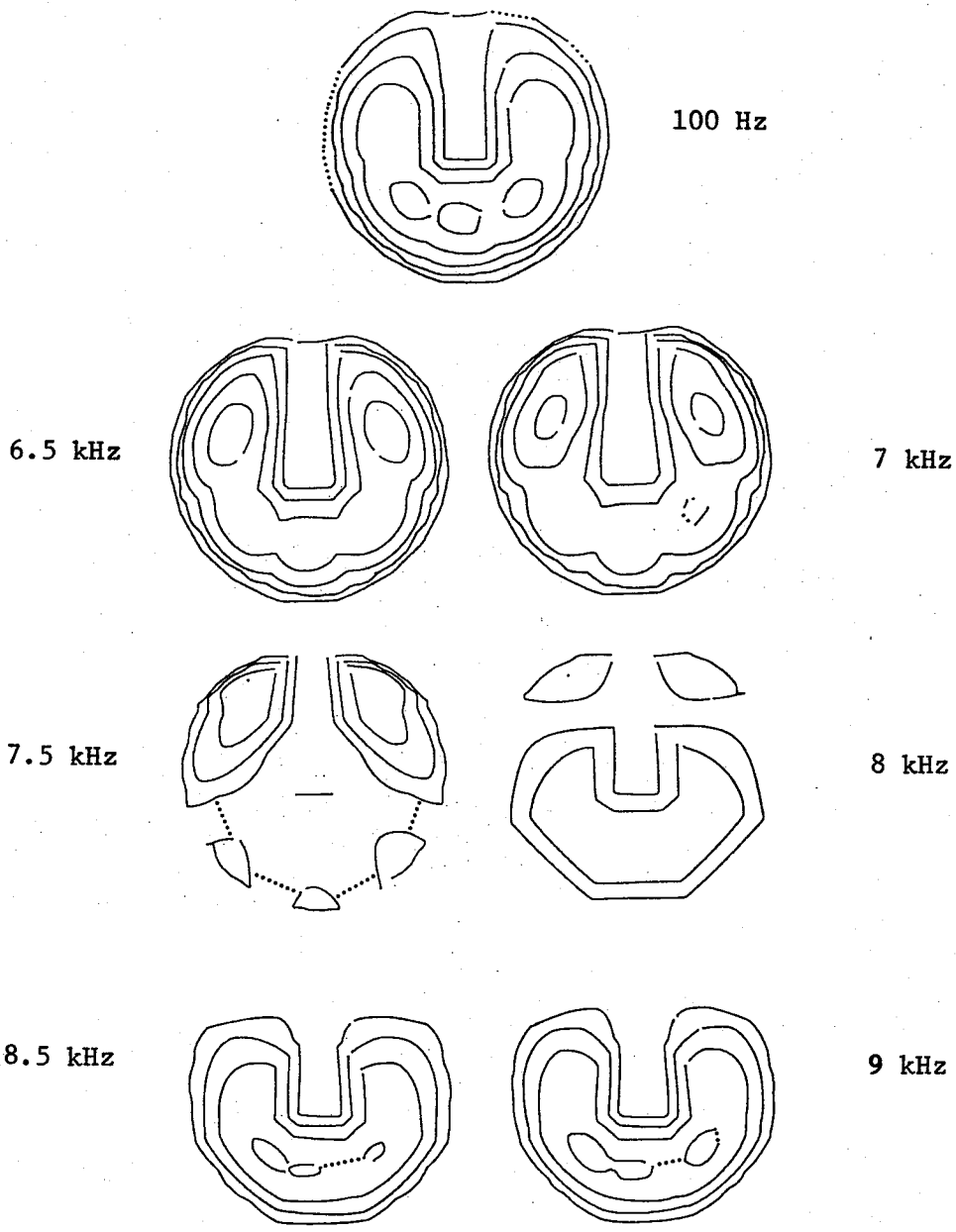

Fig. 10.7. Calculated vibration patterns for guinea pig. Contours represent real parts of complex displacements.

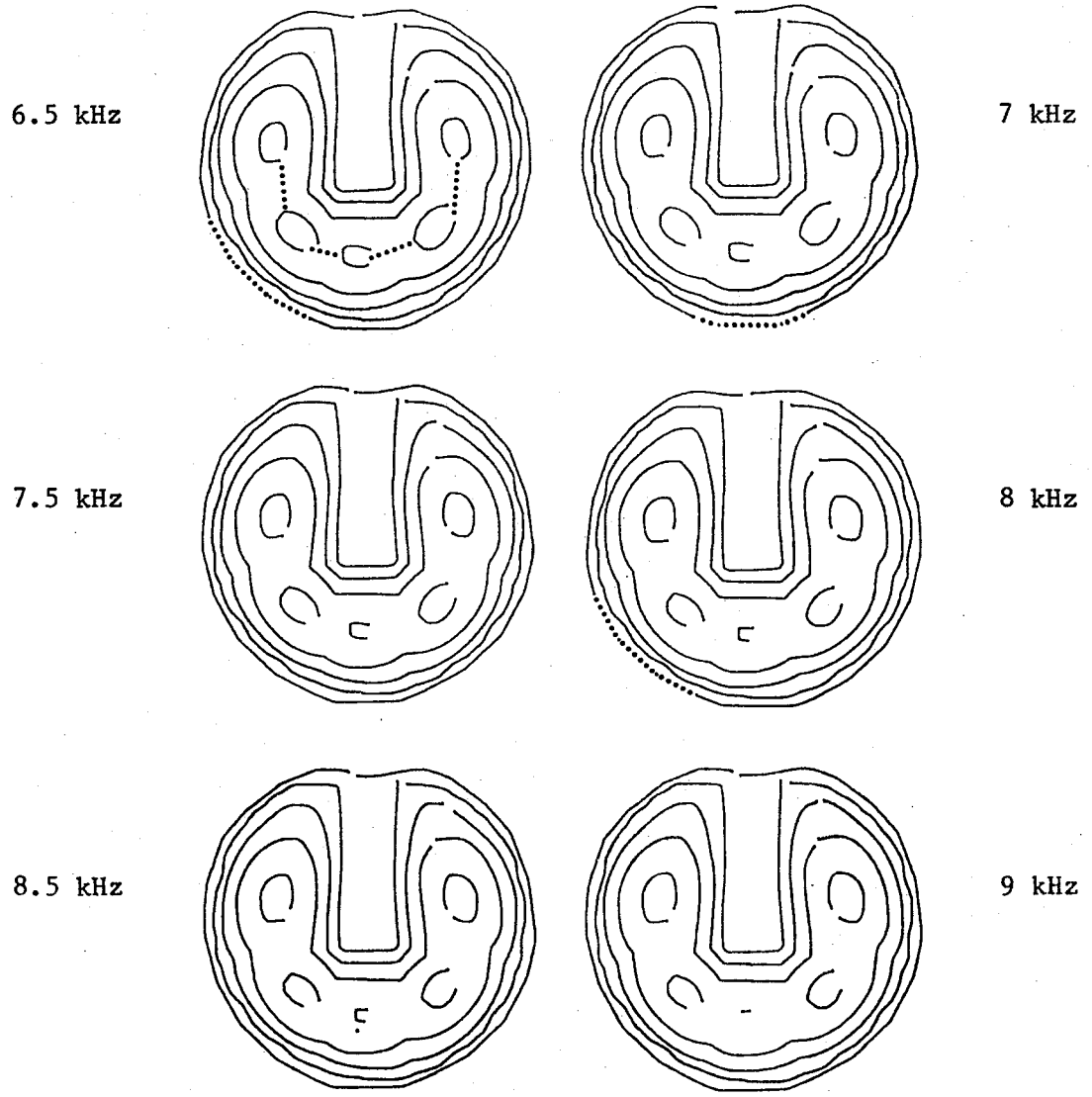

Fig. 10.8. Calculated vibration patterns for guinea pig. Contours represent the magnitudes of the complex displacements.

10.4 Conclusions

The plane-membrane eardrum model presented here displays a number of features similar, qualitatively at least, to those observed experimentally in the cat and guinea pig by different experimental methods. There are also discrepancies. Some of these could no doubt be reduced or removed by judicious adjustments of the parameters of the model, few of which can be predicted with confidence on the basis of independent experimental observations.

It is not to be expected, however, that the plane-membrane model can ever completely reproduce the actual behaviour of the eardrum. Quite apart from the question of whether tension is really the dominant factor in determining eardrum stiffness, the plane-membrane model does not attempt to represent the true shape of the mammalian eardrum. For this reason I have not felt it worthwhile to attempt parameter optimization with this model.

The parameter values describing the mechanical properties of the eardrum, namely the tension and resistance, were estimated in different ways for the two species considered: on the basis of vibration-pattern complexity in the case of the cat, and on the basis of the impedance-frequency curve in the case of the guinea pig. The values arrived at were also very different for the two cases. This might be ascribed to species differences, or it might be argued that further experimentation with different parameter values could resolve the differences. The discrepancy might also be due to a fundamental inability of the model to predict both aspects (pattern complexity and impedance curve) of eardrum behaviour, indicating that the features of drum structure left out of this model (including shape, bending stiffness and non-uniformity) are essential to its function.

CHAPTER 11

DESCRIPTION OF SHELL MODELS

11.1 Introduction

This chapter describes the specific eardrum models used to obtain the results presented in the next chapter. Section 11.2 concerns the shapes of the annular ring, manubrium and pars flaccida, and the positions of the radial fibres. The models for tne cat, guinea pig and human are described. Section 11.3 discusses the curvature of the sides of the cone formed by the eardrum. Section 11.4 discusses the question of whether the finite-element subdivision is sufficiently fine.

The material properties used are those given in Chapters 2 to 4.

11.2 Basic Shape

The essentials of the geometry of the eardrum model are shown in Fig. 11.1 for the cat. Fig. 11.1a shows a view of the drum model in the plane of the annulus: the outlines of the pars tensa, pars flaccida and manubrium are shown. Also visible are lines corresponding approximately to the orientations of the radial fibres of the drum. Fig. 11.1b is a section through the manubrium, showing the way it points medially. These two views define the model shape completely except for the drum curvature which is discussed in the next section.

Fig. 11.2 shows the actual subdivision of the cat model into triangular finite elements.

Fig. 11.3 to 11.6 present the models for the guinea pig and human, in the same formats as Fig. 11.1 and 11.2.

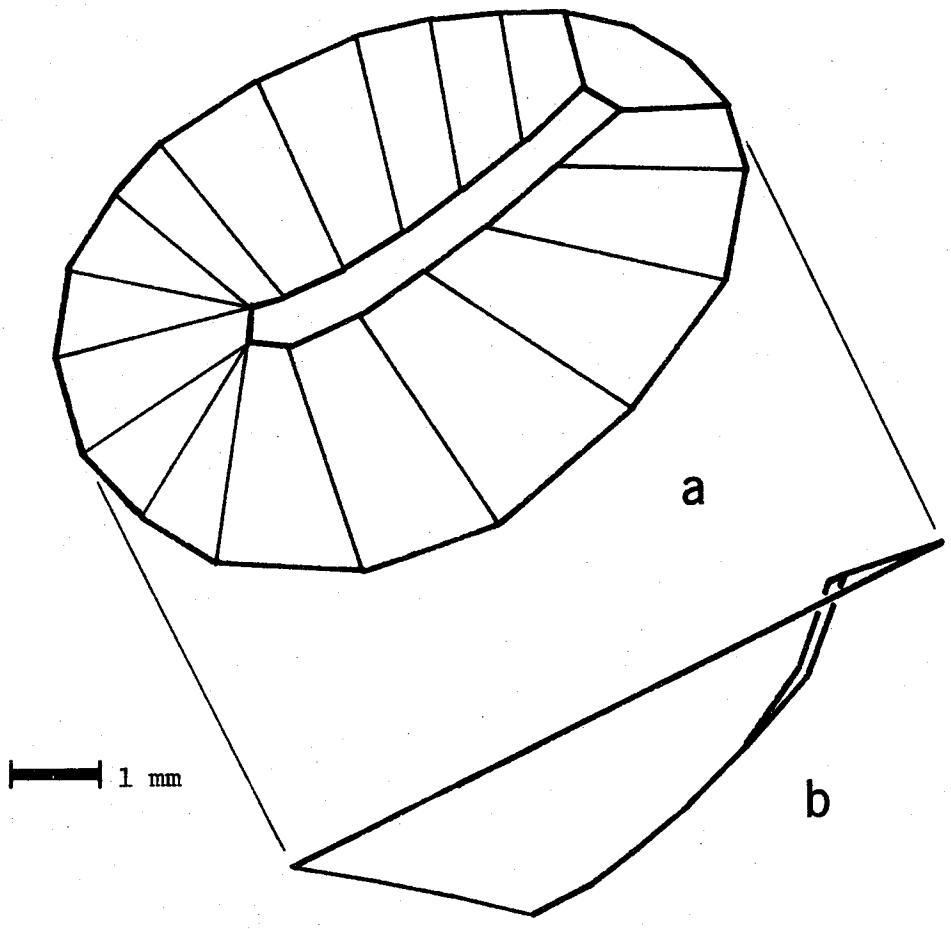

Fig. 11.1. Shape of shell model for cat. Part *a* is a plan view, part *b* is a side view. Curvature parameter *c* (Section 11.3) is 9.5.

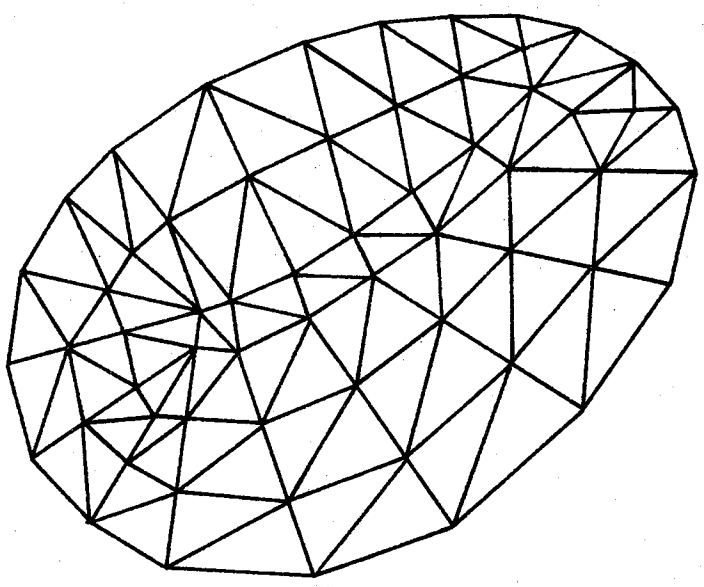

Fig. 11.2. Subdivision of cat shell model.

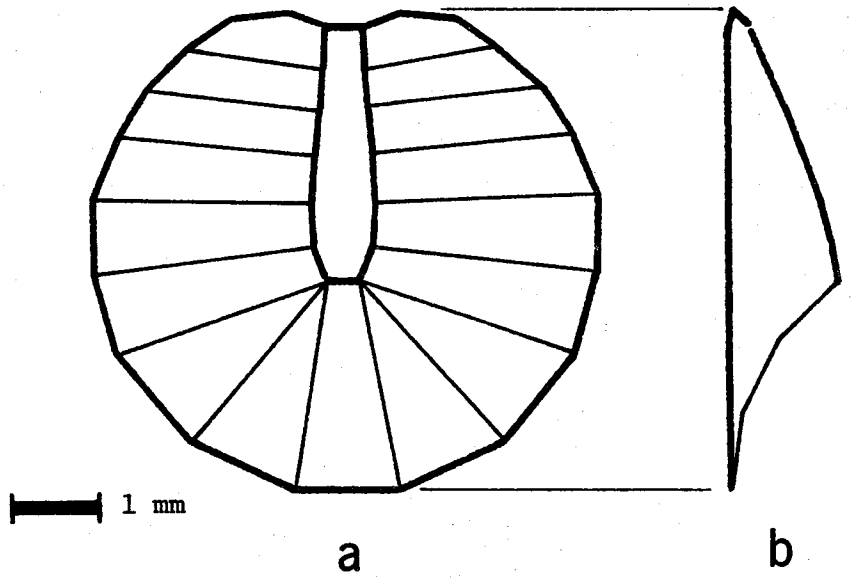

Fig. 11.3. Shape of shell model for guinea pig. Curvature parameter c is 1.12.

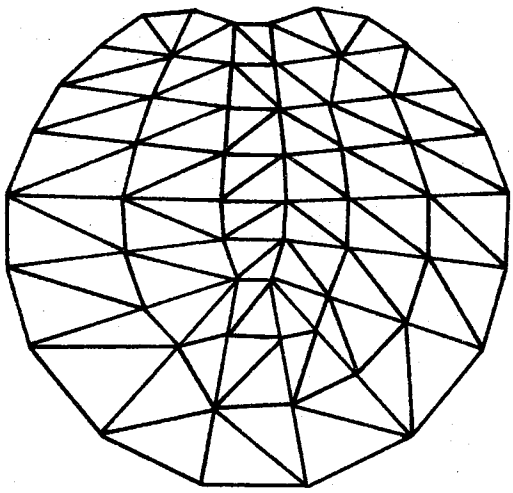

Fig. 11.4. Subdivision of guinea-pig shell model.

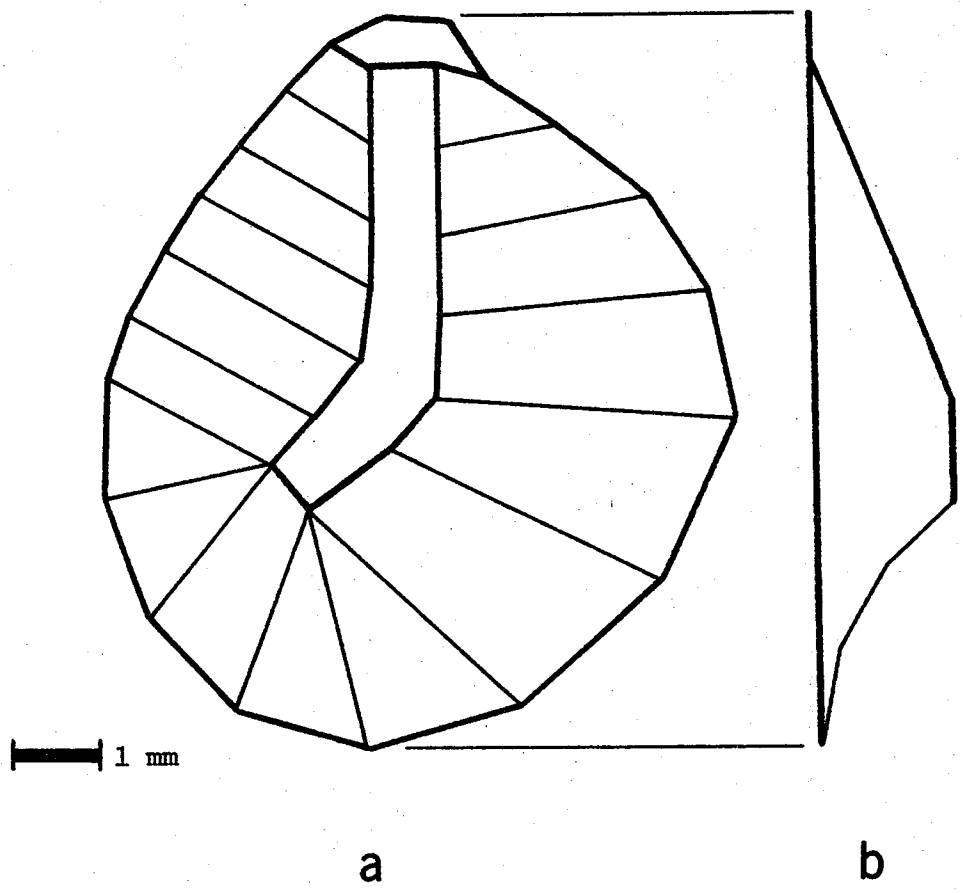

Fig. 11.5. Shape of shell model for man. Curvature parameter c is 1.12.

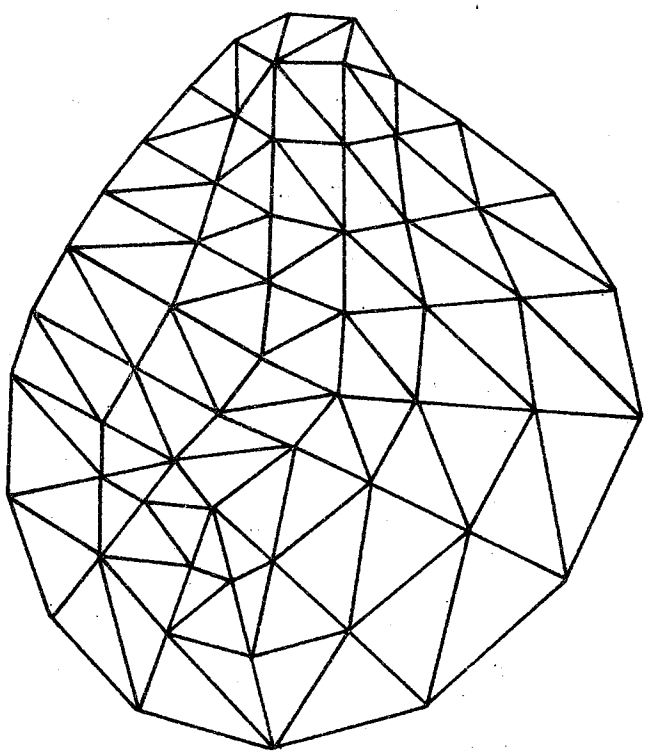

Fig. 11.6. Subdivision of human shell model.

11.3 Curvature

As discussed in Section 2.2.4, there are no good data available to quantify the curvature of the sides of the eardrum. Helmholtz (1869) presented a formula for the shape of the eardrum (Fig. 11.7a), but this was based on a theoretical analysis of how the eardrum might function (see Section 6.2) rather than on any quantitative observations of drum shape. Kirikae (1960) suggested an equation of the form

$$y = \frac{a^2}{x^2 + a^2} - b$$

to describe the drum's shape. Such a curve can be matched quite well to the measured shape. Its chief advantage over the equation given by Helmholtz, apart from simplicity, is that it is flat at the centre (see Fig. 11.7b), more reasonably representing the position and shape of the manubrium. For the purposes of investigating the significance of the curvature, however, the shape of the manubrium is not important, and from the available data one cannot conclude that the drum itself is flattened near the manubrium.

For the sake of simplicity, I have chosen to represent the curvature of the sides of the drum using circular arcs. (Esser (1947) calculated that one of the coefficients in his analysis changed by only 7% if circular arcs were assumed instead of Helmholtz' curve.) The over-all degree of curvature of the eardrum is specified in the models by a dimensionless constant c. The radius of curvature of any particular radial fibre f is then given by

$$r_f = c\, d_f ,$$

where d_f is the straight-line distance between the ends of the fibre as shown in Fig. 11.8. The circular arcs are taken to lie in vertical planes (the plane of the tympanic ring being horizontal).

In the model for each species I have used for c the smallest value that does not result in any nodes of the model lying above the plane of

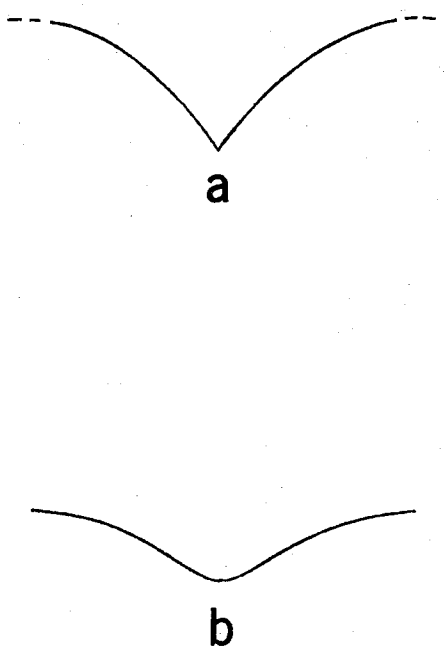

Fig. 11.7. Two suggested forms for eardrum curvature. Curve *a* is that of Helmholtz (1869), curve *b* is that of Kirikae (1960). See text for discussion.

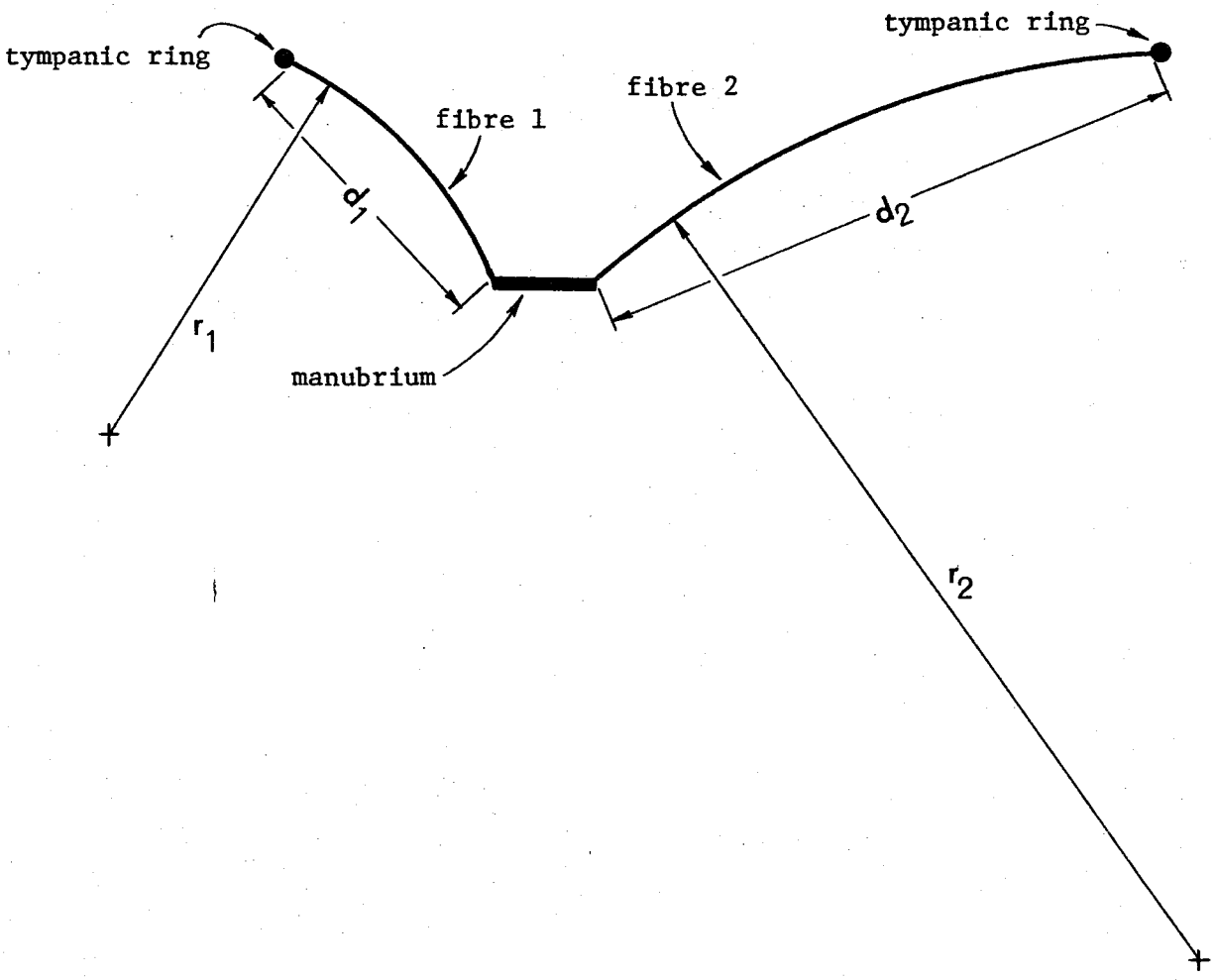

Fig. 11.8. Diagram illustrating radial fibres approximated by circular arcs. The curvature parameter c is 1.5 for this Figure. See text for discussion.

the tympanic ring. For the particular geometries used here, these minimum values turn out to be 0.93 for the cat, and 1.12 for both guinea pig and human. Fig. 11.3b and 11.5b give an idea of what these curvatures look like. They are similar to the curvatures found in the actual eardrums. Note that the values of these lower limits are not physiologically meaningful: they are determined by the particular way in which I introduce the curvature into the model.

As pointed out above, in this model the minimum values for the constant c are about 1. There is obviously no upper limit, but the curvature is practically gone by about ten, as demonstrated by the essentially straight side shown in Fig. 11.1b (at a value of 9.5).

Fig. 11.9 is a perspective view of the model of the cat eardrum, to give an idea of its over-all shape.

11.4 Adequacy of Subdivision

The eardrum models could be refined by using more nodes, but each node adds six degrees of freedom to the system, and the amounts of computer time and storage space required are proportional to the square of the number of degrees of freedom. The subdivisions shown above represent the outlines of the eardrum quite well. Their weakest feature is that each curved radial fibre is approximated by only two (in the anterior region) or three (in the posterior and inferior regions) straight-line segments.

One can estimate the effects of this approximation by looking at Fig. 12.2. That Figure shows the contour lines calculated for the guinea-pig shell model, which is symmetrical except for the use of two straight-line segments per radial fibre in the anterior region, as opposed to three in the posterior region. The posterior amplitudes are larger than the anterior ones, but never by more than a factor of about two and generally by much less. The contour lines are similar in the two halves in that they extend upwards but do not form separate peaks.

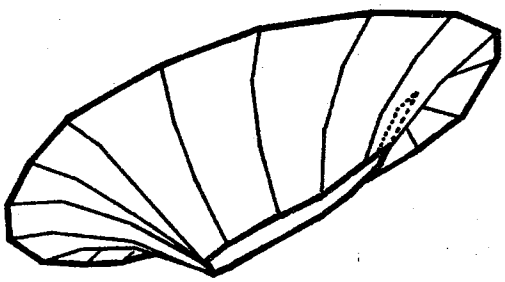

Fig. 11.9. Perspective view of the cat shell model.

A more quantitative estimate of the effects of the limited numbers of nodes was obtained by using three models of half of a guinea-pig eardrum, with two, three and four line segments per radial fibre, respectively. The resulting contour patterns are shown in Fig. 11.10, and all display the characteristic inferior peak. The first contour line falls about half-way down the manubrium in each case, indicating similar values for the ratio $\frac{\text{peak}}{\text{tip}}$. A secondary peak is present in part *c* (four segments/fibre) but is quite flat.

The actual value of peak drum displacement is about 10 dB higher with three segments/fibre than with two, and only about 7 dB higher with four than with three. In view of the uncertainties involved in determining the physical parameters of the model, the subdivision used in obtaining the results in the next chapter (equivalent to three segments/fibre) is considered to be adequate for the present purposes.

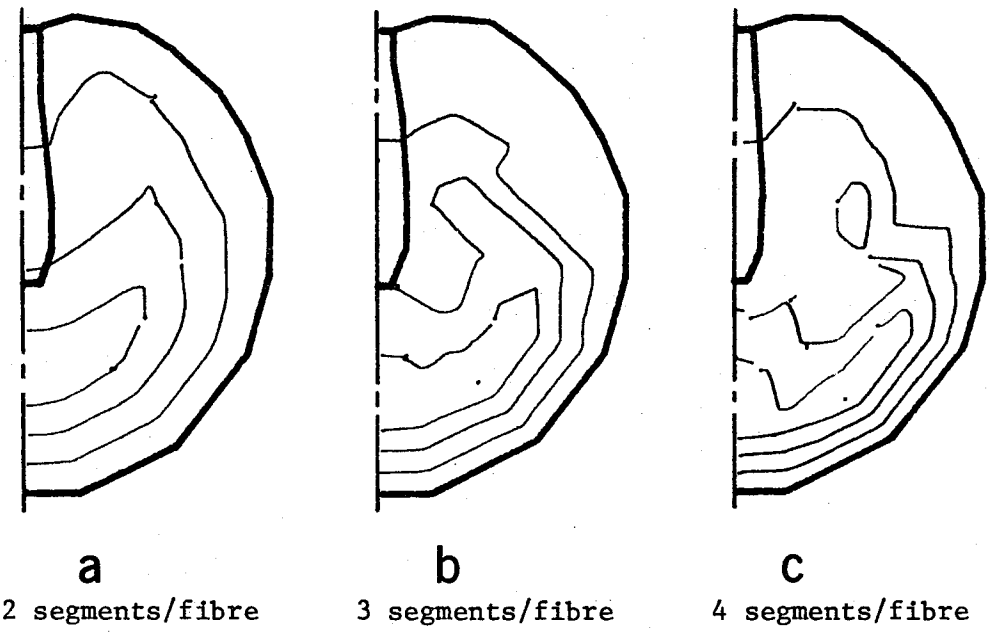

Fig. 11.10. Comparison of three shell models with different degrees of refinement. See text for discussion.

CHAPTER 12

RESULTS OF SHELL MODELS

12.1 Introduction

This chapter presents the results of calculations using the shell models described in the previous chapter. Sections 2 to 4 present results for the cat, guinea pig and human, respectively. Apart from the general shape of the contour lines, the two quantities to be compared between the experimental and the calculated results are (1) the amplitude of the maximal drum displacement, and (2) the ratio of that displacement to the displacement of the tip of the manubrium. The former is a measure of the over-all displacement of the drum, and the latter is a measure of the coupling of the drum to the ossicles and of the degree of sound transmission to the middle ear.

The parameter values used for Sections 12.2 to 12.4 are those estimated in Chapters 2 to 4, without regard to the results of the displacement calculations. No attempt has been made to find a set of parameter values to match a particular set of experimental data exactly. The main reason is that there is not yet enough information available to lead to a unique choice for the "best" values, so the results of such a search would have little meaning. To indicate the effects of changes in parameter values, Sections 12.5 to 12.9 present the results of varying several of the parameters, including stiffness, Poisson's ratio, ossicular-hinge stiffness, curvature, and depth. Finally, Sections 12.10 to 12.13 explore the effects of modifying some of the assumptions of the model, including those concerning isotropy, type of boundary condition, and position of ossicular axis. All of Sections 12.5 to 12.13 concentrate on one particular species, for simplicity and clarity. The cat was chosen because the available displacement data are better for this species than for any other.

12.2 Displacements for Cat

Fig. 12.1 shows displacement contours calculated for the cat model using the parameter values specified in Chapters 2 to 4. The vibration pattern is very similar to that observed experimentally by Tonndorf & Khanna (1972): the drum displacements are greater than those of the manubrium, and there is an amplitude maximum in the posterior region. The only qualitative difference between the calculated and experimental results is that the latter show a small amplitude peak in the anterior region while the former do not (although the displacements there are definitely greater than on the manubrium).

As mentioned in the introduction to this chapter, the two quantitative measures which I shall use to compare experimental and modelling results are (1) the maximum drum displacement, and (2) the ratio of maximum drum displacement to manubrial-tip displacement. Tonndorf & Khanna (1971a) reported a maximal drum displacement of 1.5 μm at 600 Hz and 111 dB SPL. This is equivalent to 0.42 μm at 100 dB SPL. (The frequency of 600 Hz is low enough that the displacement will be practically the same as at 0 Hz.) By comparison, the results presented in Fig. 12.1 show a maximal drum displacement of 0.43 μm at 100 dB SPL.

Tonndorf & Khanna (1971a) report a ratio of $\frac{\text{peak displacement}}{\text{tip displacement}}$ equal to 2.2 at low frequencies. Khanna & Tonndorf (1972a) show a value of about 3. The computed results in Fig. 12.1 have a ratio equal to 2.4.

Note that the experimental results considered here were measured with the middle-ear cavity closed, while the model as presently implemented does not account for the effect of the middle-ear cavity, that is, it assumes the cavity to be wide open. However, as discussed in Chapter 4 above, the middle-ear cavities in the cat have little effect on the drum's vibration since they are relatively large, and thus compliant.

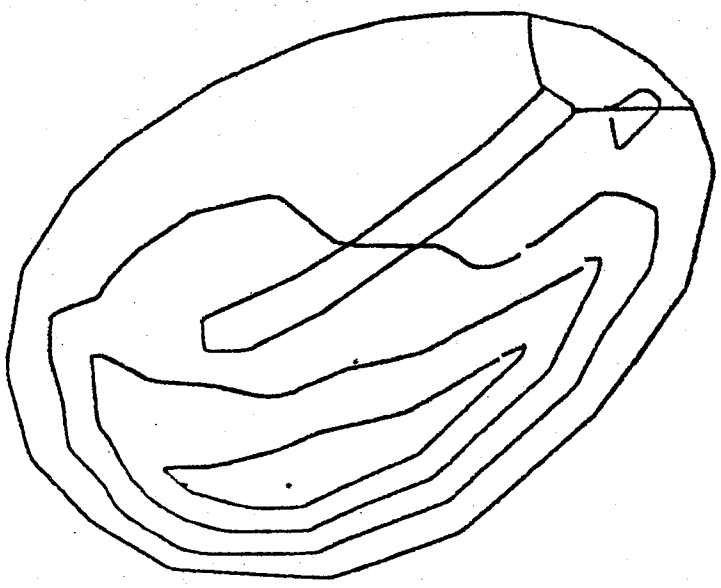

Fig. 12.1. Displacement contours for cat shell model.

12.3 Displacements for Guinea Pig

Fig. 12.2 shows a vibration pattern calculated with the guinea-pig model. The pattern is very similar to the one observed by Manley & Johnstone (1974), with the maximal drum displacement occurring below the tip of the manubrium. The fact that the model results are asymmetrical, in a way similar to the published contour plots of Manley & Johnstone, is entirely an artifact of the model, as discussed in Section 11.4 above.

Manley & Johnstone reported an average (3 animals) manubrial-tip displacement of 0.45 μm at 100 dB SPL at 100 Hz, the lowest frequency that they observed. (This measurement was taken with the bulla open, as assumed in this model.) Since they were not using a holographic technique one cannot derive precise values for the ratio $\frac{\text{peak}}{\text{tip}}$ from their data. However, they did measure displacements for three points on the drum below the tip of the manubrium in the region of the displacement peak. From their Fig. 1, it would appear that the largest of these three displacements is about 19 dB, 5 dB and 8 dB above the displacement of the manubrial tip, at 750 Hz, 1 kHz and 1.5 kHz, respectively. It is surprising that the value at 750 Hz is so much different from those at 1 and 1.5 kHz, since neither the manubrial-tip displacement (their Fig. 2) nor the over-all volume displacement (Funnell, 1972) changes that drastically at frequencies lower than 1 kHz. At any rate, the values 5 to 19 dB correspond to a range of 1.8 to 9 for the ratio $\frac{\text{peak}}{\text{tip}}$.

By comparison with the above experimental data, the model results of Fig. 12.2 show a manubrial tip displacement of 1.1 μm and a ratio $\frac{\text{peak}}{\text{tip}}$ of 3.2.

12.4 Displacements for Human

Fig. 12.3 shows the displacement contours calculated using the model for the human eardrum. Again, the contours are qualitatively similar to experimental results.

Tonndorf & Khanna (1972) suggested that their results at about 1 kHz

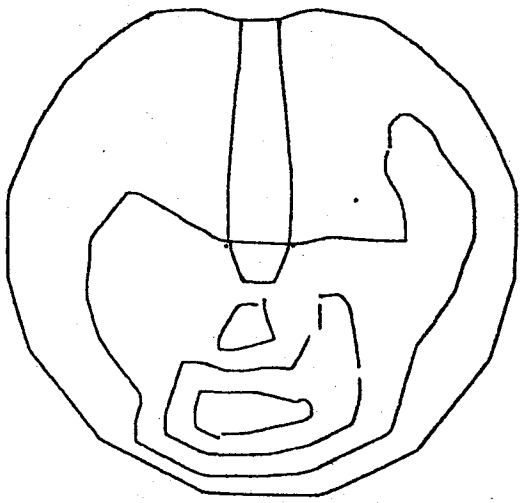

Fig. 12.2. Displacement contours for guinea-pig shell model.

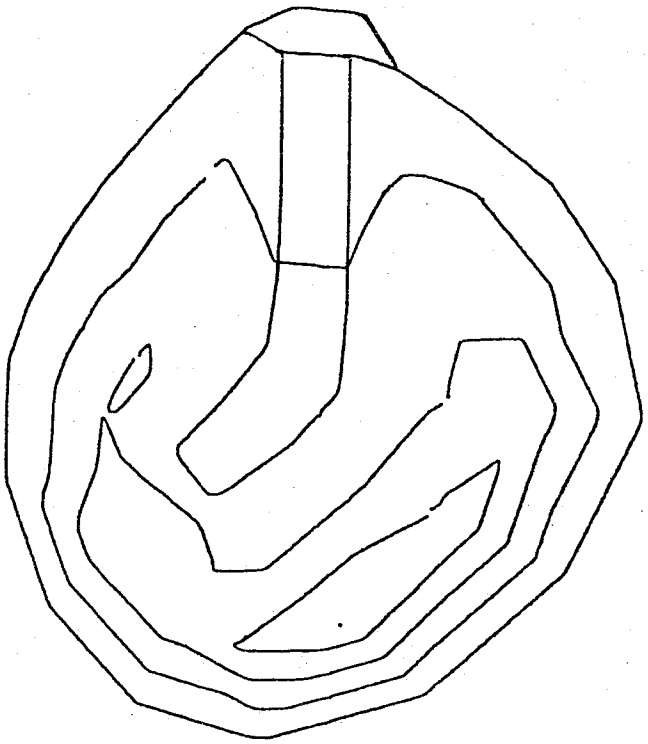

Fig. 12.3. Displacement contours for human shell model.

be taken as representative of lower-frequency displacements, because of post-mortem changes at the low frequencies. As values for comparison with the model, therefore, I shall take the figure of 0.19 μm for malleolar-tip displacement (at 996 Hz, 105 dB SPL; their Fig. 3), and the figure of 3.5 for the ratio $\frac{\text{peak}}{\text{tip}}$ (their Fig. 4). This corresponds to a peak drum displacement of 0.37 μm at 100 dB SPL.

By comparison, the results of Fig. 12.3 show a peak displacement of 0.47 μm and a ratio $\frac{\text{peak}}{\text{tip}}$ of 2.2.

As in the case of the cat, the experimental data here were obtained with closed middle-ear cavities while the model assumes them to be open. Here again, however, the human cavities are relatively large and thus have little effect, especially at low frequencies.

12.5 Variation of Drum Stiffness

The Young's modulus of 2×10^8 used here is based on an experimental result of Békésy, as discussed in Chapter 3. The figure is not necessarily exactly correct, but it is probably in the right range. I have therefore investigated variations of it only within a factor of two on either side. The results are presented in Fig. 12.4. The peak displacement decreases from 0.70 μm at 10^8 dyn cm^{-2}, to 0.25 μm at 4×10^8 dyn cm^{-2}. The ratio $\frac{\text{peak}}{\text{tip}}$ decreases from 2.6 to 2.3 over the same range.

12.6 Variation of Poisson's Ratio

As stated in Section 12.2 above, using a Poisson's ratio of 0.3 gave a peak displacement of 0.43 μm and a ratio $\frac{\text{peak}}{\text{tip}}$ of 2.4. Reducing Poisson's ratio to 0.0 changes the peak displacement to 0.44 μm, and the ratio to 2.2. A Poisson's ratio of 0.5 gives a peak displacement of 0.40 μm and a ratio of 2.5. It can thus be seen that the value adopted for Poisson's ratio is not critical: varying it from 0 to $\frac{1}{2}$ decreases the peak amplitude by about 10% and increases the ratio $\frac{\text{peak}}{\text{tip}}$ by about 14%.

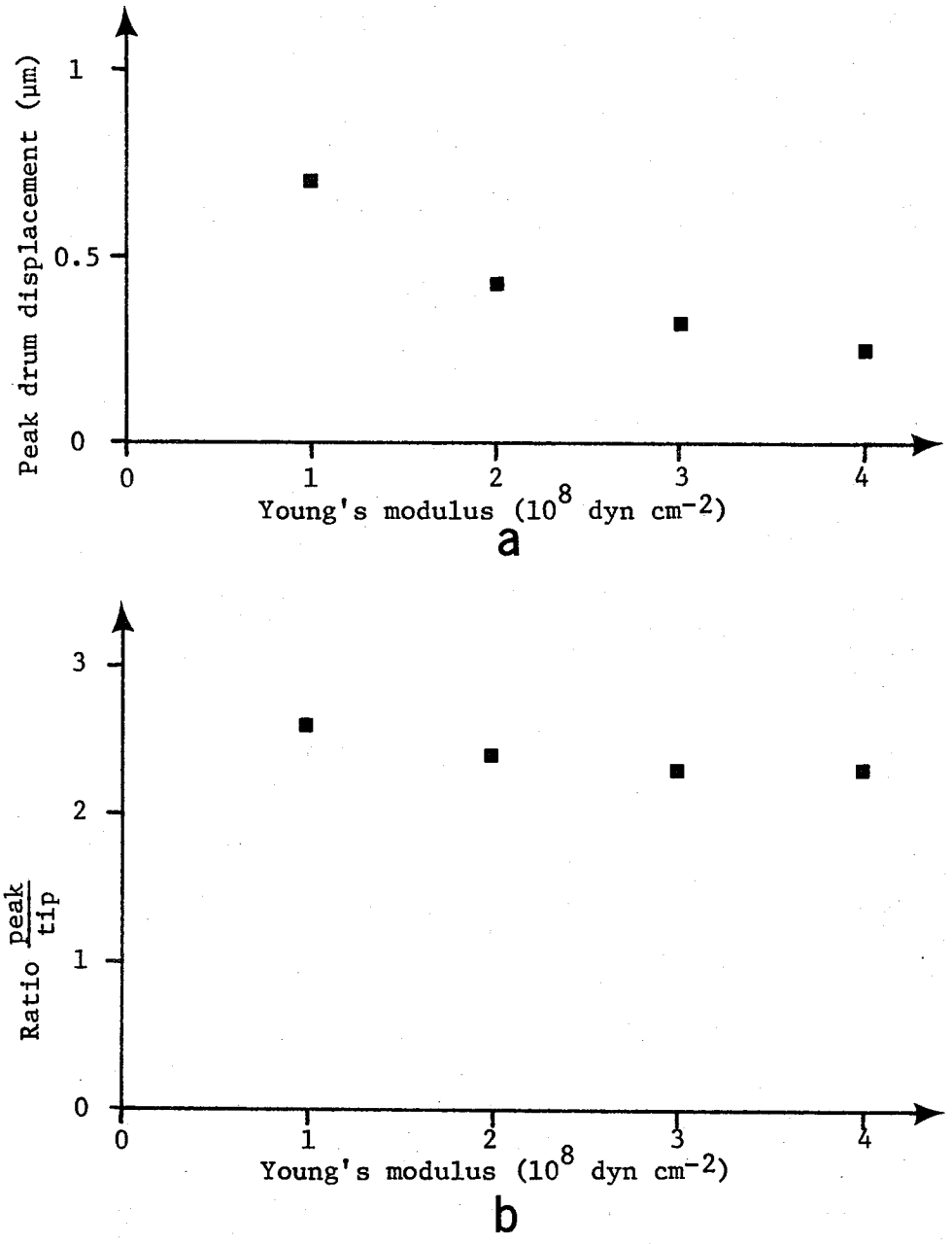

Fig. 12.4. Effects of variation of eardrum stiffness on peak drum displacement (*a*) and on the ratio $\frac{peak}{tip}$ (*b*).

12.7 Variation of Ossicular-Hinge Stiffness

Fig. 12.5 shows the effects of variations of the stiffness of the ossicular hinge. As expected, increasing the stiffness decreases the amplitude of the drum's displacements: most of the decrease occurs in the range 0 to 10^6, and above about 4×10^6 further increases have little effect since the manubrium's movements are by then too small to affect the rest of the drum much. The ratio $\frac{\text{peak}}{\text{tip}}$ is relatively unaffected by the hinge stiffness up to about 10^6, indicating that the shape of the vibration pattern is not changing much. Above that figure, the ratio starts to increase approximately in proportion to the stiffness, since the peak drum displacement is no longer changing significantly and the manubrial displacement is determined almost entirely by the stiffness of the ossicles.

Fig. 12.6 shows some examples of the vibration patterns for various values of hinge stiffness. The sequence shows how the manubrium moves less and less compared to the drum as the stiffness increases.

Note that at the highest values of hinge stiffness used here, the manubrium started to become bent because of the crude way in which the stiffness is introduced into the model (as discussed in Section 8.7). Fig. 12.7 shows the degree of distortion at two high stiffness values. The distortion was negligible at lower stiffnesses, and even that shown in the Figure is unlikely to cause very great errors in the vibration patterns. It does not matter that the distortion would become unacceptable at much higher values of hinge stiffness since such values would not be physiologically reasonable anyways, as evidenced by the fact that even in the range used here the ratio $\frac{\text{peak}}{\text{tip}}$ has already become larger than that observed experimentally. If one wished to simulate partially fixed ossicles one would have to do something about the method of introducing the hinge stiffness; fully fixed ossicles would be no problem since one could simply force all manubrial displacements to zero.

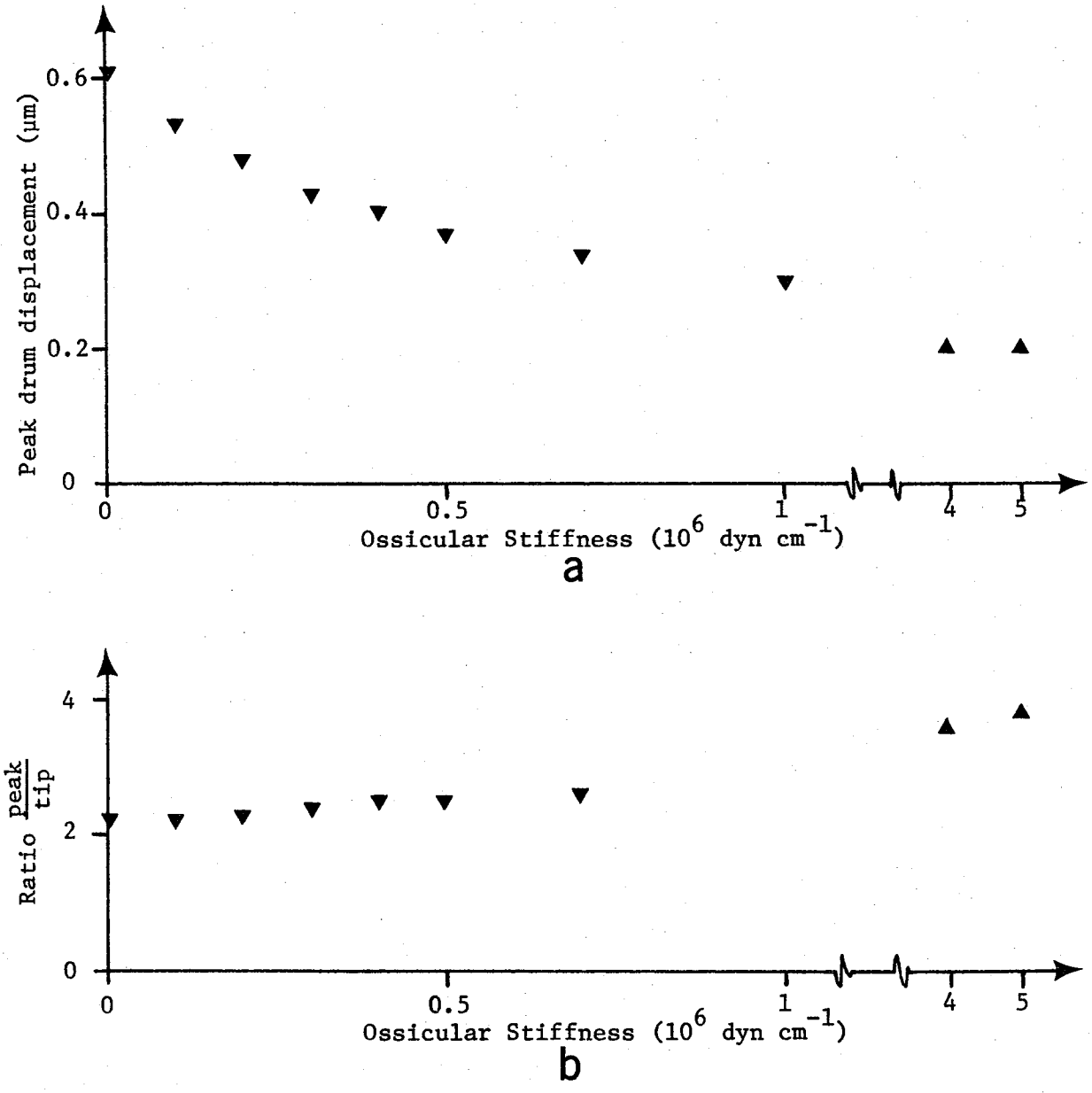

Fig. 12.5. Effects of variation of ossicular stiffness on peak drum displacement (*a*) and on the ratio $\frac{\text{peak}}{\text{tip}}$ (*b*).

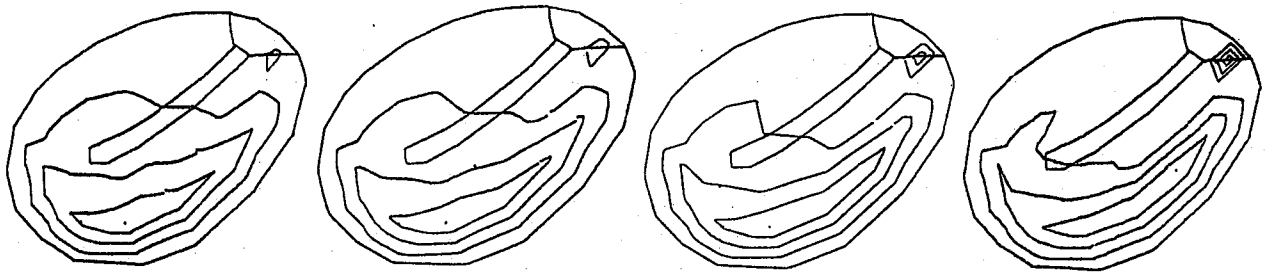

0 dyn cm^{-1} 0.3×10^6 dyn cm^{-1} 1×10^6 dyn cm^{-1} 4×10^6 dyn cm^{-1}

Fig. 12.6. Displacement contours for four values of ossicular stiffness.

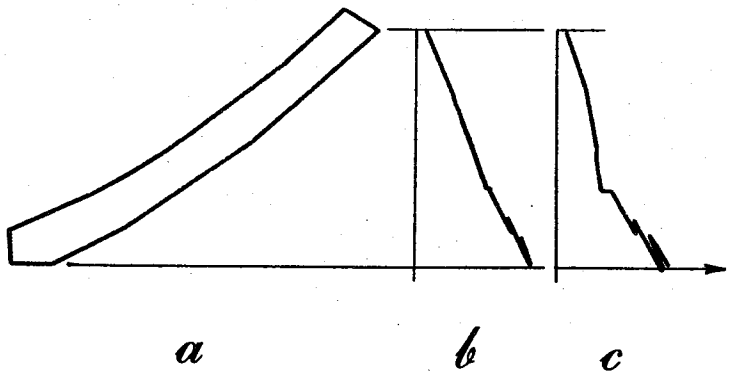

Fig. 12.7. Distortion of manubrium due to high ossicular stiffness. Part *a* is a plan view of the manubrium, for reference. Part *b* represents the displacement (normalized) of the manubrium, and indicates a slight distortion when the ossicular stiffness is 10^6 dyn cm^{-1}. Part *c* indicates greater distortion when the stiffness is 4×10^6 dyn cm^{-1}.

12.8 Variation of Curvature

Fig. 12.8 shows the effects of varying the curvature of the drum over a range of about 10:1. The lower end of the range of the curvature parameter c, namely 0.93, is the smallest value permitted (see Section 11.3). The largest value of c , namely 9.5, defines a condition of almost straight sides. Over this range the peak drum displacement varies from 0.43 μm to 0.59 μm, with a minimum of 0.35 μm. The total variation is less than a factor of two. It can thus be seen that the curvature is not a very critical parameter in determining drum displacements.

The increase of peak displacement with increasing radius of curvature is expected on the basis of normal shell behaviour: a nearly flat shell cannot use its in-plane stiffness to resist transverse loads, and its bending stiffness will be low if the shell is thin. The increase in peak displacement at the smallest radii of curvature may be due to the fact that the drum is then better able to apply a transverse force to the manubrium. This increase in coupling of the air pressure to the manubrium is reflected in the fact that the ratio $\frac{\text{peak}}{\text{tip}}$ decreases monotonically, and quite rapidly, with decreasing radius of curvature, as shown in Fig. 12.8b. Fig. 12.9 more clearly shows that the drum's ability to move the ossicles in response to air pressure decreases with increasing radius of curvature, that is, with decreasing curvature.

Fig. 12.10 shows a sequence of vibration patterns for various degrees of curvature. Note that as the radius of curvature increases, the relative displacement of the manubrium decreases, as pointed out above, and also the relative displacement of the anterior region increases until a separate peak is formed, as found in experimental results.

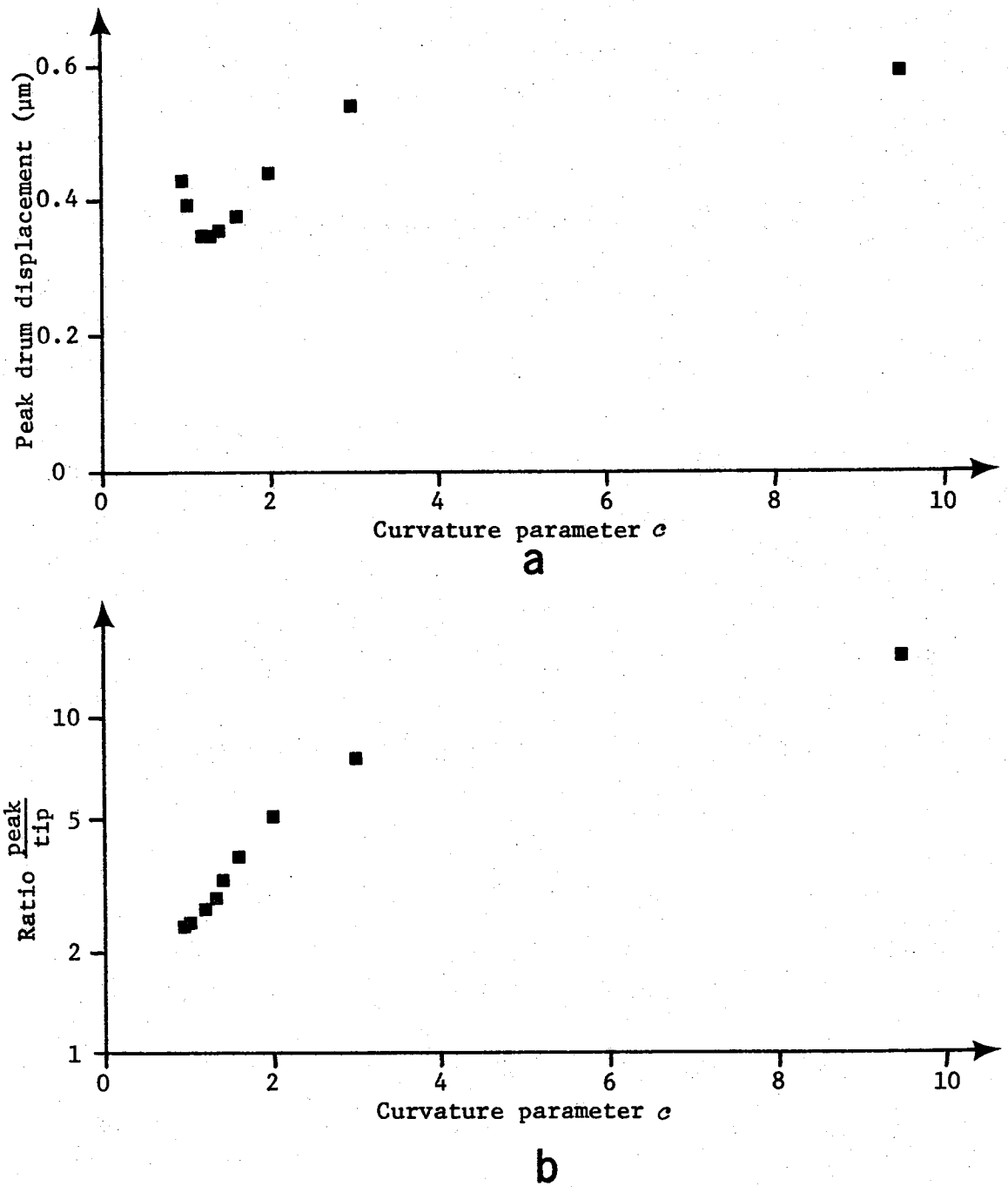

Fig. 12.8. Effects of variation of eardrum curvature on peak drum displacement (*a*) and on the ratio $\frac{\text{peak}}{\text{tip}}$ (*b*).

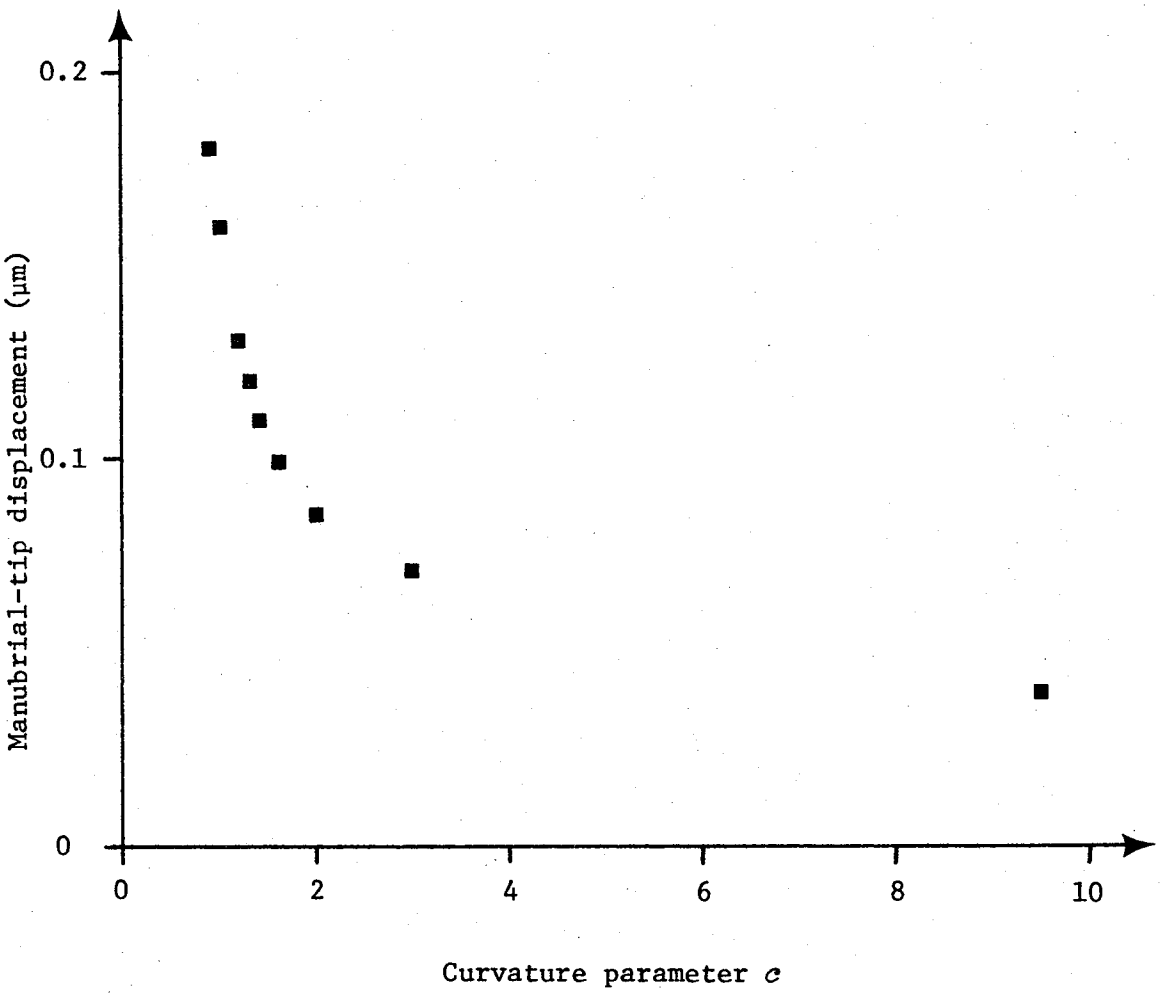

Fig. 12.9. Effect of variation of eardrum curvature on manubrial-tip displacement.

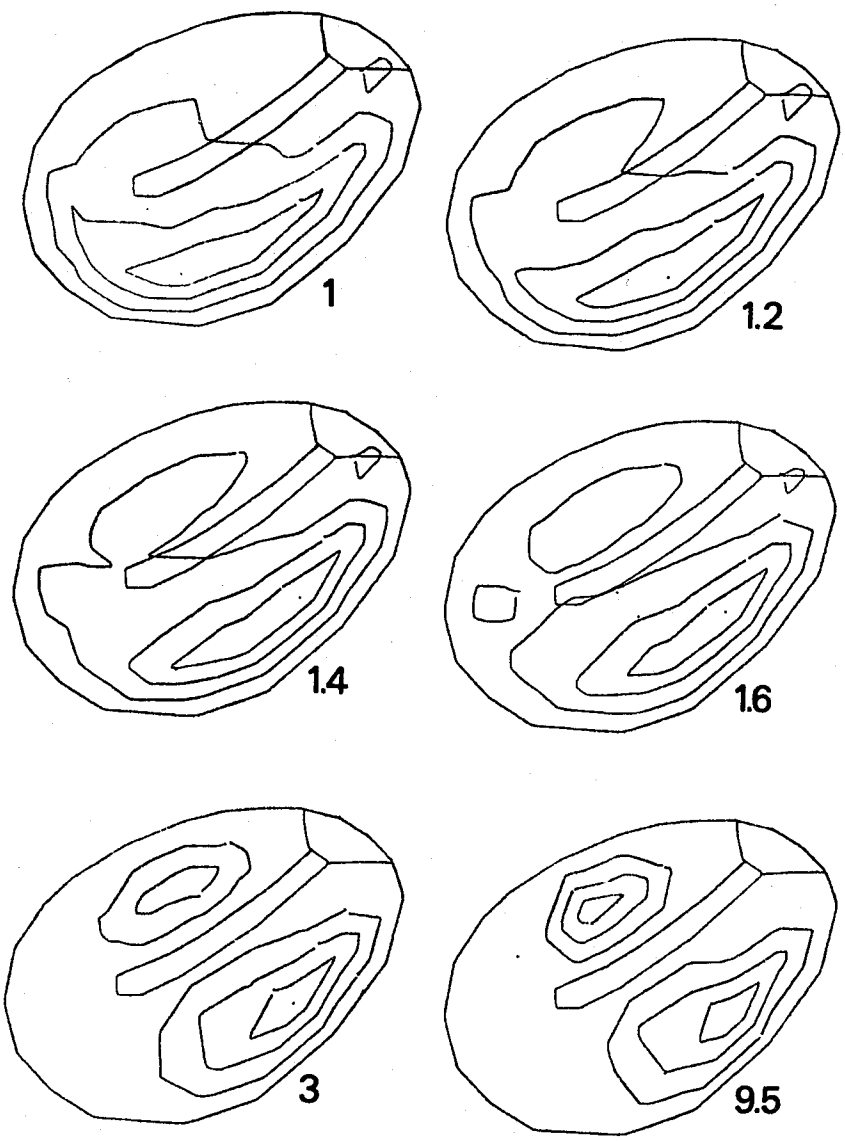

Fig. 12.10. Displacement contours for six values of eardrum curvature parameter c.

12.9 Variation of Depth of Cone

The previous section showed that the non-zero curvature of the sides of the cone formed by the eardrum could aid in transmitting sound to the ossicles. One might also wonder if the conical shape itself has some functional significance. Fig. 12.11 shows the effects on manubrial displacement of changing the depth of the cone. This was done by scaling the z-coordinates of each point in the model by a factor called the "relative depth". Note that the circular arcs formed by the radial fibres become elliptical under this operation.

The Figure shows both the case of large curvature ($c = 0.93$) and the case of practically no curvature ($c = 9.5$). In both situations, increasing the depth of the cone reduces the displacement of the manubrium, that is, reduces the ability of a given sound-pressure level to move the ossicles. This presumably is because the deeper conical shapes impart greater stiffness to the eardrum, just as argued (in favour of the conical shape) by Békésy in connection with his hinged-plate model (see Section 6.3 above).

It would thus appear that the conical shape is disadvantageous, assuming that the eardrum actually functions as modelled here. One might speculate, however, that the conical shape provides an "adequate" middle-ear sensitivity while permitting low eardrum mass, and thus good high-frequency response. If the drum were flat, or a very shallow cone, then a given degree of sensitivity would require a stiffer (and thus heavier) drum than if it were a deeper cone. As mentioned in Section 6.5 above, Gran (1968) found that a stiffness of 60 to 250 times the true value was required to get reasonable displacements with a plane-plate model.

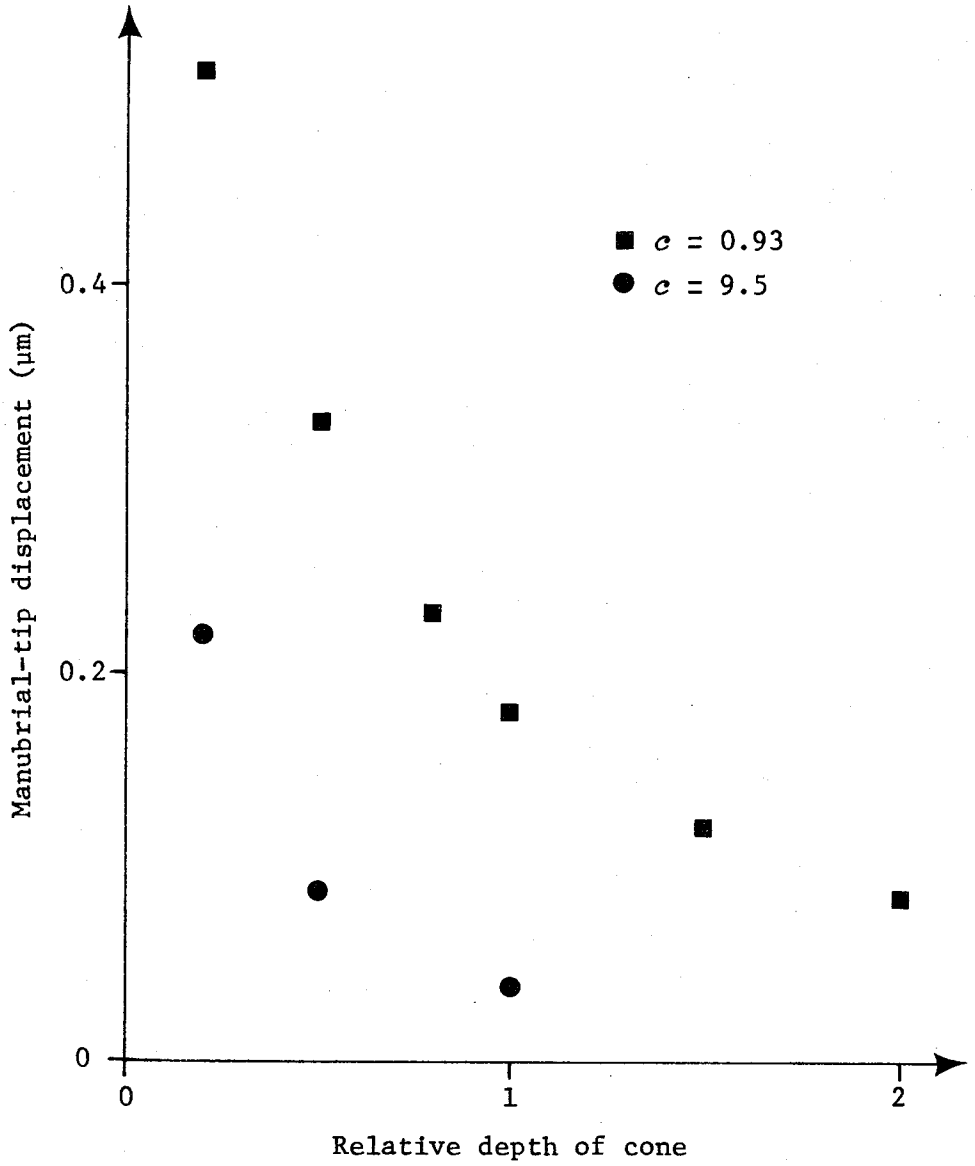

Fig. 12.11. Effects of variation of relative depth of cone formed by eardrum, for two values of the eardrum curvature parameter c.

12.10 Effect of Anisotropy

Since the model is quite successful using isotropic material properties, it has not been necessary to introduce anisotropy, and it does not seem worthwhile at the moment to do a detailed study of the effects of anisotropy in view of the number of experimental questions still unresolved concerning eardrum properties and behaviour. However, this section presents a single example of displacements calculated with an anisotropic model, to give an idea of what may be expected.

In line with the assumptions of Helmholtz and Esser (see Section 6.2), the radial fibres have been assumed to be much less extensible than the circular fibres. In particular, the Young's modulus in the radial direction (as defined by the element boundaries shown in Fig. 11.1) has been left at the value of 2×10^8 dyn cm^{-2} used before, while the Young's modulus in the perpendicular direction (in each element) has been reduced to 10^6 dyn cm^{-2}. The two Poisson's ratios, and the shear modulus, have been set to zero, equivalent to assuming that the radial fibres slide over one another without lateral interaction. This assumption is open to question, but there are no experimental data available to decide the issue.

The vibration pattern shown in Fig. 12.12 is basically the same as those calculated using isotropic material properties, but the peak drum displacement, 1.3 μm, is about three times higher (*cf.* 0.43 μm for Fig. 12.1). This is not surprising since the overall stiffness of the drum has been decreased. The ratio $\frac{\text{peak}}{\text{tip}}$ is about 2.7, almost the same as the value of 2.4 in Fig. 12.1; the manubrial-tip displacement, 0.49 μm, is more than 2.7 times the value calculated for isotropic properties. This indicates the drum would be more effective in transmitting vibrations to the ossicles if it were anisotropic in the way described here. This expectation, of course, was what prompted Helmholtz' original hypothesis that the circular fibres were much more extensible than the radial fibres: the latter are in an ideal position to transmit forces to the manubrium, while the former can only interfere with this action.

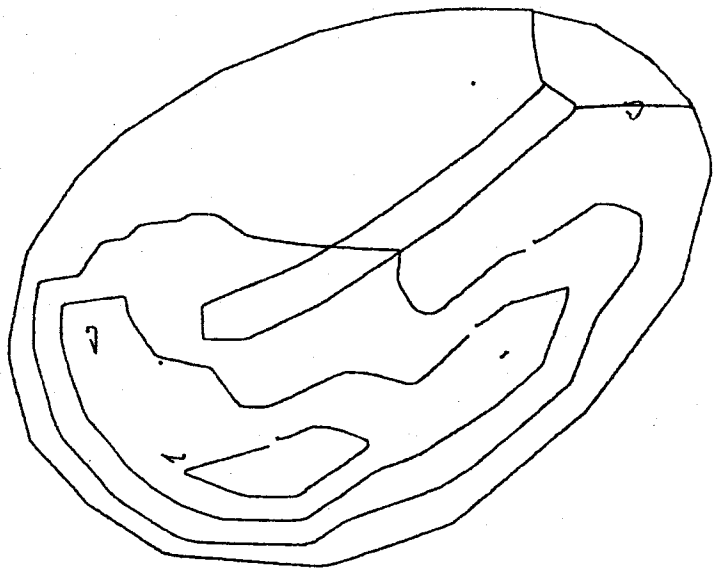

Fig. 12.12. Displacement contours calculated using anisotropic material properties.

12.11 Boundary Conditions around Ring

The model results presented so far have assumed that the drum is fully clamped around its periphery. To determine the importance of this assumption, I simulated a condition identical to that presented in Fig. 12.1 except that the boundary conditions around the tympanic ring were changed to the simply supported type. The resultant vibration pattern is almost the same as Fig. 12.1. The peak drum displacement becomes 0.45 μm instead of 0.43 μm, and the ratio $\frac{\text{peak}}{\text{tip}}$ remains the same at 2.4. Evidently it does not make much difference what type of boundary condition is assumed.

12.12 Boundary Conditions along Manubrium

The model also assumes that the drum is fully clamped to the manubrium. One cannot change this assumption simply by changing a boundary condition: one would have to insert a small flexible element between the drum and the manubrium in order to model a support of the simple type. It is not worth doing so, however. Especially considering the results of the previous section, it seems very unlikely that the change would make a significant difference in the calculated vibration pattern and amplitude.

12.13 Position of Axis

As implemented at the moment, the model is not suitable for any definition of the position of the ossicular axis other than through the upper end of the manubrium. It is well known, however, that the axis actually lies higher. The only reasonably straight-forward way of estimating the seriousness of this discrepancy with the present model is to remove the boundary condition which specifies that the upper end of the manubrium is fixed, and then to see where the axis falls naturally and how the displacements are affected. Fig. 12.13 shows the results for two different values

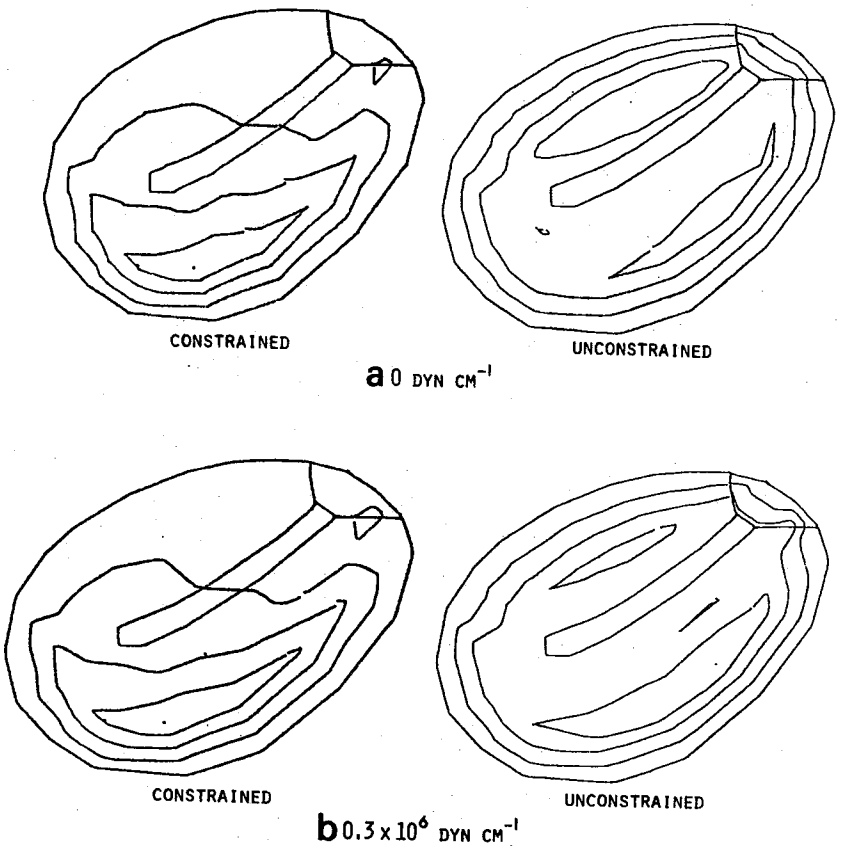

Fig. 12.13. Effects of removing the constraints on the axis of rotation for two values of ossicular stiffness: 0 (*a*) and 0.3×10^6 dyn cm^{-1} (*b*). In each case, the displacement contours on the left are for the axis constrained as usual, while those on the right are for no constraint on the axis. See text for discussion.

of hinge stiffness. The left-hand Figure in part *a* shows the vibration pattern with the axis defined normally, for zero hinge stiffness. The right-hand figure shows the pattern with the axis undefined. It can be seen that the pattern is considerably changed, although it still shows the basic feature of a posterior amplitude peak. (It also shows a smaller anterior peak similar to the one present in experimental data.) The displacement of the lower tip of the manubrium is actually slightly smaller than that of the upper end, indicating that the "axis" is a considerable distance *below* the drum, which is obviously not reasonable. In spite of these differences, however, the actual peak drum displacement is the same, 0.61 μm, in both cases. Part *b* of the figure shows a similar situation when the hinge stiffness is set to 0.3×10^6. Again, in spite of differences in the vibration pattern, the peak displacement is not drastically affected: in this case it is reduced from 0.43 μm to 0.34 μm. These results suggest that, although it would certainly be desirable to improve the representation of the axis, the displacement values calculated with the present model are probably not too far wrong.

12.14 Conclusions

Using physiologically reasonable parameter values, the shell models for all three species yielded results quite close to previous experimental findings. On this basis, one can conclude that presently available experimental evidence is consistent with the hypothesis that the eardrum is basically equivalent to an isotropic thin curved shell. It is not necessary at this time to postulate either resting tension in the drum, or anisotropy (that is, differences in properties between the radial and circular fibres).

CHAPTER 13

CONCLUSIONS AND FUTURE DEVELOPMENTS

13.1 Conclusions

13.1.1 Summary. The work reported here consists of a theoretical study of eardrum vibrations. No new experimental results are presented, but previously published results are reviewed critically and in some cases reinterpreted. Available data on the eardrum and eardrum vibrations are then used in modelling the system. Attention is restricted to mammalian eardrums specialized to receive air-conducted sounds.

13.1.2 Major original contributions. The following items constitute the major original contributions of this work:

(1) the first application of the finite-element method to study of the eardrum;

(2) the demonstration, on the basis of a review and reinterpretation of the literature, that the widely accepted observations of Békésy concerning eardrum vibrations were in fact anomalous;

(3) the first theoretical estimate of the effective moments of inertia of the ossicular chains of man, cat and guinea pig, based on simplified representations of their geometry;

(4) the demonstration that the observed vibration patterns of the eardrum do not necessarily involve any lever action on its part; and

(5) the presentation of a new hypothesis concerning eardrum function.

These points are discussed in more detail in the following sections.

13.1.3 Introduction of finite-element method. This work represents the first use of the finite-element method for the study of the eardrum. This application has involved the development of the procedures discussed in Sections 8.7 to 8.9 for the treatment of particular features of the eardrum, namely, the presence of a rigid hinged rod in the vibrating surface, the

existence of reactive forces on this rod, and the presence of closed air cavities behind the drum.

13.1.4 Review of structure and function. Perhaps the most important single result of the review in Chapters 2 to 5 is the recognition that the observation of a hinged-plate mode of eardrum vibration was unique to Békésy. However, the conflict with other observations has been tempered by my reinterpretation of his published contour plot (Section 5.2.5). The data of Dahmann have also been reinterpreted (Section 5.2.4).

A useful procedure is introduced in Section 4.5 for the estimation of ossicular moments of inertia on the basis of available data.

The most overwhelming impression produced by this review is that much more work is required to measure and describe eardrum properties and behaviour properly. Some suggestions for such work are presented in Section 13.2.1.

13.1.5 Simulation of simple models. The models presented in Chapters 9 to 12 do not embody the actual complexity of the eardrum, but they do show that the main features of observed eardrum vibrations can be easily explained. In particular, the plane-membrane model demonstrates quantitatively that the low-frequency vibration pattern of the eardrum (with smaller displacements at the manubrium than elsewhere) does not necessarily involve any lever action on the part of the eardrum.

13.1.6 Presentation of a new hypothesis. The success of the shell model presented in Chapters 11 and 12 indicates that the essential mechanical function of the eardrum requires neither resting tensions nor special anisotropies.

13.2 Future Developments

13.2.1 Experimental. More information is required on the anatomy of the eardrum. Specifically, more quantitative data are needed to describe eardrum thickness, and the distribution and paths of the fibres. Such research could

be a very useful application of interactive computerized image processing, particularly in tracing fibre paths over long distances and in large numbers.

More work is also required to define the dependence of eardrum mechanical properties on position, direction and frequency. Techniques should be used which can identify the linear ranges of the variables measured, and which can quantify the viscoelastic properties of the eardrum. Particular mention should be made of recent techniques for performing mechanical measurements on very small samples. Furukawa *et al.* (1974) examined individual wood fibres under an electron microscope; these fibres were 30 to 50 μm in diameter and a few mm long, and had stiffnesses and ultimate strengths similar to collagen fibres. With some loss of resolution light microscopy can be used (Page *et al.*, 1972). (Even 15 years ago, Morgan (1960) reported averaged stress-strain curves for collagen fibres with diameters in the range of 60 to 180 μm and lengths of 6 mm.) With these methods one might be able to characterize very small sections of the eardrum, perhaps even separating the radial and circular layers.

As mentioned in Section 2.2.4 above, Khanna & Tonndorf (1975) have started to apply moiré topography to measurements of the shape of the eardrum. Quantitative and comparative shape data will be important in modelling the eardrum. At the moment these measurements must be static in nature, since they require the use of a casting. With further developments of this method, one possibly could do dynamic measurements of the effects of slow air-pressure changes and of middle-ear-muscle contractions. Indeed, the recent development of such things as 4.5-mm endoscopes incorporating colour-television cameras (*Electronics* 48(1): 55, 1975) raises hopes of such measurements on waking patients. Note that computerized image processing could also be useful in interpreting the moiré contour lines.

Further developments are also possible for the holographic method of measuring vibration patterns, such as the addition of the ability to measure phase information (Khanna & Tonndorf, 1972b). It is also possible to adapt the method to measure amplitudes intermediate between those of conventional holography and those of moiré topography (Der *et al.*, 1974). Dragsten *et al.*

(1974) have described a technique that they call "optical heterodyne spectroscopy". It is extremely sensitive (down to 0.01 nm) and has a wide dynamic range (up to about 50 nm), and can automatically compensate for small body movements during measurements *in vivo*. Unfortunately it involves point displacement measurements rather than contour-line detection, but the laser beam can relatively easily be scanned across the structure under observation; it also requires an averaging time of a few seconds per point. The observation of vibration patterns in real time was discussed by Khanna *et al.* (1973), who used a modification of their laser holographic technique.

Apart from the development of new measurement methods, further work is needed to measure eardrum vibration patterns in different species, and after various interventions in the middle ear such as interruption or fixing of the ossicular chain. Such data would permit much more conclusive modelling of the eardrum and of the middle ear as a whole.

13.2.2 Modelling. Apart from improvements in the models based on new experimental data, there are also a number of improvements that can be made in the modelling procedures themselves. First of all, the shell-model programme can be made more efficient by incorporating some of the methods used in the membrane programme as discussed in Sections 8.5, 8.7 and 8.8. Furthermore, the shell programme should be extended to handle frequency effects and damping as is done in the membrane programme. It might also be worthwhile to add the effects of radiation impedance to the model, using extensions of the techniques of Hunt *et al.* (1974, 1975).

The actual elements used in the shell model could be improved. A number of curved-shell finite elements have been developed which would permit a more faithful representation of the shape of the eardrum than is possible using flat elements.

The shell elements may be refined by considering them as being composed of a number of laminae instead of a single uniform layer. One may also attempt to model the fact that the radial and circular layers are composed of arrays

of fibres embedded in ground substance; Chamis & Sendeckyj (1968) and Adams (1974b) have reviewed this topic. However, both of these areas for improvement require further experimental data before realizing their full worth.

As mentioned in Section 7.6.2, extension of the models to handle large displacements would permit the modelling of the effects of large static pressure changes and of middle-ear-muscle contractions. It would also permit the study of resting tonus of the muscles. This change would increase the computation times drastically, since iterative techniques would be required, but will become very desirable if experimental data become available concerning vibration patterns under these conditions.

Finally, it would be useful if a method could be found of calculating the frequency response of the model's acoustical impedance without having to invert the full system matrix at each frequency point. As mentioned in Section 8.10, one cannot use the usual eigenvalue method because of the frequency-dependent elements in the matrix. Gupta (1974) has shown an efficient way of including damping terms in the eigenvalue problem, but this does not overcome the difficulties introduced by the effects of the ossicular chain and of the air cavities.

13.2.3 Clinical applications. The immediate objectives of this work do not include the production of clinically useful information, since the models are not yet adequate. It should be kept in mind, however, that this work should lead to significant advances in two areas: interpretation of the results of impedance audiometry and tympanometry, and the evaluation of certain types of corrective middle-ear surgery.

Impedance audiometry and tympanometry have been found to be very useful for certain types of diagnosis. Bel *et al.* (1975), for example, have found that impedance measurements are "much more sensitive than pure-tone or speech audiometry" for the early detection of otosclerosis. On the other hand, the results are greatly affected by the condition of the eardrum, which may mask pathology elsewhere in the middle ear. This is particularly true at higher frequencies (Alberti & Jerger, 1974; Feldman, 1974), which is one reason why

clinical impedance audiometry has generally been restricted to frequencies of a few hundred Hertz. The fact that impedance measurements are strongly affected by even slight eardrum abnormalities also hinders its use for screening, since these abnormalities may be the results of completely healed disease processes, or even of congenital abnormalities, that have little or no effect on hearing. The ability to simulate eardrum behaviour reliably might make it possible to correct for these factors.

A second potential application of good eardrum models, and of a consequently good understanding of eardrum mechanics, is the evaluation of methods of eardrum repair. Recent work has suggested that the eardrum contributes actively to the effective lever ratio of the middle ear. If this is true, then it might be important to replace the functional elements involved when repairing the drum. In particular, it might be important to reproduce the peculiar arrangement of highly organized radial and circular fibres. Current methods of repairing drum perforations do not accomplish this, but if it were worthwhile recent methods of reconstituting collagen films (Chvapil *et al.*, 1973) might be developed to that extent. Admittedly the apparent contribution of the eardrum to the middle-ear lever action is small, but even hearing losses of only a few decibels can affect early learning (Brooks, 1973) and speech discrimination.

Appendix 1

ANALYSIS OF SLIT BEHAVIOUR IN A TENSE EARDRUM

In this Appendix I shall present some very rough calculations intended to give some idea of how much spreading can be expected in a slit of the type used by Kirikae (1960), as discussed in Section 3.6 above. The fundamental assumption is that the resting tension in the eardrum is of the same order as *could* be supplied by the tensor tympani.

Fig. A1.1 is a schematic cross-section of the eardrum. A force f_t exerted by the tensor tympani will be equivalent to a force f_u at the umbo. The ratio of f_u to f_t will be taken to be r. This force must be balanced by the tension acting around the circumference c, which has a vertical component of $T \sin \Theta$. Thus,

$$f_u = r\, f_t = T\, c \sin \Theta \ ,$$

or

$$T = \frac{r\, f_t}{c \sin \Theta} \ .$$

The radial fibres have length ℓ and stiffness E, and the thickness of the drum is t. Thus the tension T imposes a total stretch on the radial fibres equal to

$$s = \text{strain} \cdot \text{length} = \frac{\text{stress}}{E}\, \ell$$

$$= \frac{T}{E\, t}\ell = \frac{r\, \ell}{E\, t\, c \sin \Theta}\, f_t \ .$$

If we take, for example, $f_t = 10$ gm $= 10^4$ dyn; $r = \frac{1}{2}$; $\ell = 0.4$ cm; $E = 2\times10^8$ dyn cm^{-2}; $t = 50$ μm; $c = 2.6$ cm; and $\Theta = 20^{\circ}$; then the stretch, which will be released by the slit, is

$$s = 22.5 \text{ μm}.$$

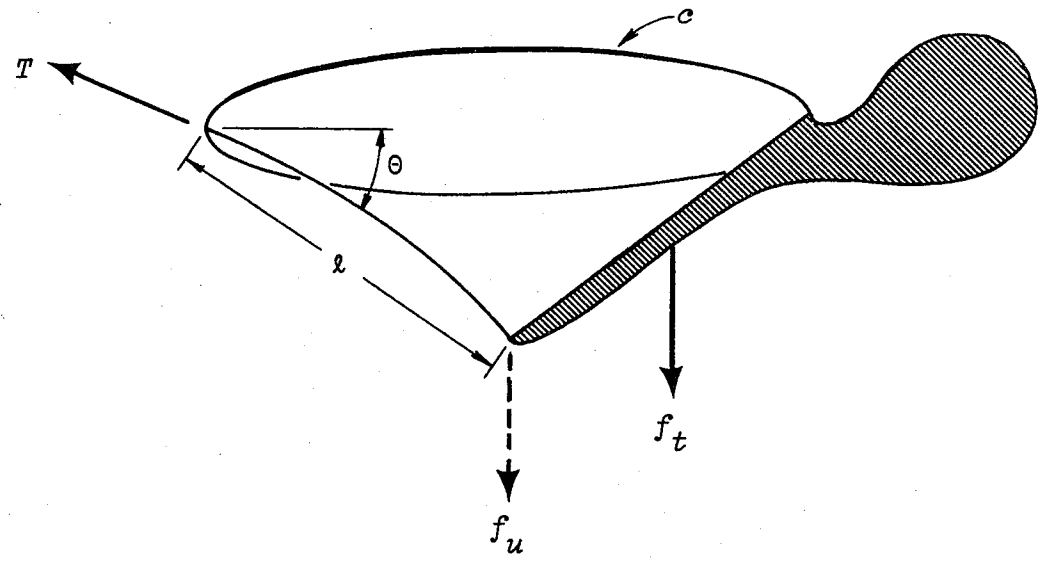

Fig. A1.1. Schematic cross-section of eardrum, defining notation used in analyzing slit behaviour.

Appendix 2

INTERPRETATION OF DAHMANN'S DEFLECTION DATA

This Appendix discusses a method for estimating the eardrum displacement profile corresponding to the mirror-deflection data of Dahmann (1929, 1930) shown in Fig. 5.2. The basic procedure is to assume that the shape of the profile can be expressed in terms of two cubic polynomials. The profile on the left-hand side is represented by

$$y = y_1(x) = a_1x + a_2x^2 + a_3x^3 ,$$

and that on the right by

$$y = y_2(x) = a_4(w-x) + a_5(w-x)^2 + a_6(w-x)^3 ,$$

where w is the width of the drum, as shown in Fig. A2.1. Note that each polynomial is equal to zero at its respective drum boundary.

The slopes of these polynomials are specified at four points by the measured mirror deflections, the slopes being taken as equal to the lengths of the streaks in Dahmann's Figure. I have used the following values for the positions and slopes of the mirrors:

Mirror 7	x = 0.15 mm	s = 1.7 mm
6	1.7	±0.6
2	4.4	±1.0
3	6.15	-2.1

These data represent four constraints on the values of the six constants a_i. A fifth constraint is the fact that the displacements of the two edges of the manubrium must be equal; that is, $y_1(x_{m1}) = y_2(x_{m2})$, where x_{m1} and x_{m2}, representing the edges of the manubrium, have the values 2.35 mm and 3.0 mm, respectively.

A sixth constraint is obtained by deciding to reduce the left-hand polynomial to a quadratic, that is, by setting $a_3 = 0$. This can be justified by the fact that the left-hand side is narrower than the right.

The combination of these constraints leads to a system of six linear algebraic equations in the a_i. The solutions for various combinations of the signs of s_6 and s_2 are shown in Fig. 5.2.

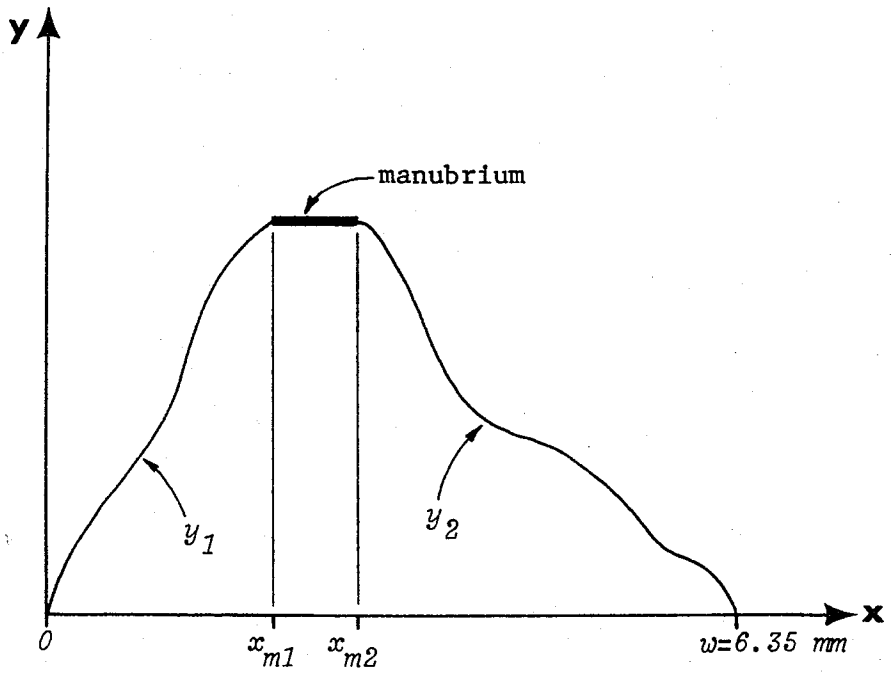

Fig. A2.1. Definition of notation for analysis of Dahmann's data. The abscissa represents distance from one edge of the eardrum to the other, along a horizontal line through the umbo; w is the width of the drum. The ordinate represents eardrum displacement.

References

Adams, D.F. (1974a): Elastoplastic crack propagation in a transversely loaded unidirectional composite. *J.Composite Mat.* 8(1): 38-54

Adams, D.F. (1974b): Practical problems associated with the application of the finite element method to composite material micromechanical analyses. *Fibre Sci.&Technol.* 7(2): 111-122

Adams, W.B. (1972): Mechanical tuning of the acoustic receptor of *Prodenia eridania* (Cramer)(Noctuidae). *J.Exp.Biol.* 57(2): 297-304

Aitkin, L.M., & B.M. Johnstone (1972): Middle-ear function in a monotreme: the echidna (*Tachyglossus aculeatus*). *J.Exp.Zool.* 180(2): 245-250

Alberti, P.W. (1963): *Patterns of epithelial migration of the tympanic membrane.* Ph.D. thesis, Washington Univ., 156 pp.

Alberti, P.W. (1964): Epithelial migration on the tympanic membrane. *J.Laryngol.* 78: 808-830

Alberti, P.W. (1974): Probe-tone frequency and the diagnostic value of tympanometry. *Arch.Otolaryngol.* 99(3): 206-210

Baker, M.A., R.A. Stocking & J.P. Meehan (1972): Thermal relationship between tympanic membrane and hypothalamus in conscious cat and monkey. *J.Appl. Physiol.* 32(6): 739-742

Békésy, G.v. (1933): On clicks and the theory of hearing. *Physik.Zeitschr.* 34: 577-582 (in German)

Békésy, G.v. (1936): On the physics of the middle ear and on hearing with a missing eardrum. *Akust.Zeitschr.* 1: 13-23 (in German)

Békésy, G.v. (1941): On the measurement of the amplitude of vibration of the ossicles with a capacitive probe. *Akust.Zeitschr.* 6: 1-16 (in German)

Békésy, G.v. (1949): The structure of the middle ear and the hearing of one's own voice by bone conduction. *J.Acoust.Soc.Am.* 21: 217-232

Békésy, G.v. (1960): *Experiments in Hearing.* McGraw-Hill, Toronto, x+745 pp.

Bel, J., J. Causse & P. Michaux (1975): Paradoxical compliances in otosclerosis. *Audiology* 14: 118-129

Beranek, L.L. (1954): *Acoustics.* McGraw-Hill, Toronto, x+481 pp.

Borg, E. (1972): On the change in the acoustic impedance of the ear as a measure of middle ear muscle reflex activity. *Acta Otolaryngol.* 74(3): 163-171

Brebbia, C.A., & J.J. Connor (1974): *Fundamentals of Finite Element Techniques for Structural Engineers.* Wiley, New York, 269 pp.

Brockhaus, F.A. (1966): *Der Sprach-Brockhaus. Deutsches Bildwörterbuch für jedermann.* Brockhaus, Wiesbaden, 800 pp.

Brooks, D. (1973): presentation to 2nd Int.Symp.Impedance Measurement, Houston, September; brief summary by J. Jerger in *Audiology* 13(3): 273, 1974

Carton, R.W., J. Dainauskas & J.W. Clark (1962): Elastic properties of single elastic fibers. *J.Appl.Physiol.* 17(3): 547-551

Chamis, C.C., & G.P. Sendeckyj (1968): Critique on theories predicting thermo-elastic properties of fibrous composites. *J.Composite Materials* 2: 332; cited by Adams (1974a)

Chvapil, M., R.L. Kronenthal & W.v. Winkle, Jr. (1973): Medical and surgical applications of collagen. *Int.Rev.Conn.Tiss.Res.* 6: 1-61

Csendes, Z., & P. Silvester (1972): FINPLT: A finite-element field-plotting program. *IEEE Trans.* MTT-20: 294-295

Dahmann, H. (1929): On the physiology of hearing: experimental studies on the mechanics of the ossicular chain, as well as on the behaviours of tones and air pressure I. *Zeitschr.f.Hals.Nas.Ohrenhlk.* 24:462-498 (in German)

Dahmann, H. (1930): On the physiology of hearing: experimental studies on the mechanics of the ossicular chain, as well as on the behaviours of tones and air pressure II-IV. *Zeitschr.f.Hals.Nas.Ohrenhlk.* 27: 329-368; see also discussion, pp. 398-402 (in German)

Dayhoff, M.O. (1972): *Atlas of Protein Sequence and Structure Vol. 5.* Nat. Biomed.Res.Found., Washington, D.C., xxx+124+418 pp.

Der, V.K., D.C. Holloway & W.L. Fourney (1974): A technique for reducing the fringe frequency in large-displacement holography. *Exp.Mech.*14(7): 286-289

Desai, C.S., & J.F. Abel (1972): *Introduction to the Finite Element Method. A numerical method for engineering analysis.* van Nostrand Reinhold, New York, xvii+477 pp.

Dragsten, P.R., W.W. Webb, J.A. Paton & R.R. Capranica (1974): Auditory membrane vibrations: measurements at sub-Ångstrom levels by optical heterodyne spectroscopy. *Science* 185(4145): 55-57

Elpern, B.S., O. Greisen & H.C. Andersen (1965): Experimental studies on sound transmission in the human ear. VI. Clinical and experimental observations on non-otosclerotic ossicle fixation. *Acta Otolaryngol.* 60: 223-230

Esser, M.H.M. (1947): The mechanism of the middle ear: II. The drum. *Bull.Math. Biophys.* 9(2): 75-91

Feldman, A.S. (1974): Eardrum abnormality and the measurement of middle ear function. *Arch.Otolaryngol.* 99(3): 211-217

Filogamo, G. (1943): On the morphogenesis and architecture of the tympanic membrane. *Zeitschr.f.Zellforsch.&Mikroskop.Anat.* A33(1): 14-39 (in Italian)

Filogamo, G. (1949): Recherches sur la structure de la membrane du tympan chez les différents vertébrés. *Acta Anat.* 7: 248-272

Forsythe, G.E., & W.R. Wasow (1960): *Finite-Difference Methods for Partial Differential Equations.* Wiley, New York; cited by Silvester (1969)

Frank, O. (1923): Sound conduction in the ear. *Sitzungsber.math.-physikal.Klass. Bayerischen Akad.Wiss.München* 1923: 11-77 (in German)

Fumagalli, Z. (1949): Morphological research on the sound-transmission apparatus. *Arch.Ital.Otol.Rinol.e Laringol.* 60 Suppl. 1: ix+323 pp. (in Italian; Figure captions and Chapter 7 in English also)

Funnell, W.R.J. (1972): *The acoustical impedance of the guinea-pig middle ear and the effects of the middle-ear muscles.* M.Eng.thesis, McGill Univ., Montréal, vi+93 pp.

Funnell, W.R.J. (1975): *Computer programmes and model definitions for study of eardrum vibrations using the finite-element method.* Rept.no. BMEU 1975-2, BioMed.Eng.Unit, McGill Univ., Montréal

Funnell, W.R.J., & C.A. Laszlo (1972): The acoustical impedance of the guinea-pig middle ear and the effects of the middle-ear muscles. *J.Acoust.Soc.Am.* 52(1): 129 (A)

Furukawa, I., H. Saiki & H. Harada (1974): A micro tensile-testing method for single wood fibre in a scanning electron microscope. *J.Electron Micros.* 23(2): 89-97

Galante, J.O. (1967): Tensile properties of the human lumbar annulus fibrosus. *Acta Orthopaed.Scand.* S100: 91 pp.

Gates, G.R., J.C. Saunders, G.R. Bock, L.M. Aitkin & M.A. Elliott (1974): Peripheral auditory function in the platypus, *Ornithorhynchus anatinus.* *J.Acoust. Soc.Am.* 56(1): 152-156

Gaudin, E.P. (1968): On the middle ear of birds. *Acta Otolaryngol.* 65: 316-326

George, J.A. (1971): *Computer implementation of the finite element method.* Ph.D. thesis, Stanford Univ., 227 pp.

Grahame, R. (1970): A method for measuring human skin elasticity *in vivo* with observations on the effects of age, sex and pregnancy. *Clin.Sci.* 39(2): 223-238

Gran, S. (1968): *The analytical basis of middle-ear mechanics. A contribution to the application of the acoustical impedance of the ear.* Dissertation, Univ.Oslo, iv+63 pp. (in German)

Gruber, J. (1867): Contributions to the anatomy of the eardrum. *Wochenblatt. d.k.k.Gesellschaft d.Aerzte Wien* 7: 1-3, 169-173 (in German)

Gupta, K.K. (1974): Eigenproblem solution of damped structural systems. *Int. J.Num.Meth.Eng.* 8(4): 877-911

Harkness, R.D. (1961): Biological functions of collagen. *Biol.Rev.Cambridge Phil.Soc.* 36(4): 399-463 + 1 plate

Hartman, W.F. (1971): An error in Helmholtz's calculation of the displacement of the tympanic membrane. *J.Acoust.Soc.Am.* 49(4): 1317

Haut, R.C., & R.W. Little (1969): The rheological properties of canine anterior cruciate ligaments. *J.Biomech.* 2: 289-298

Hearmon, R.F.S. (1961): *An Introduction to Applied Anisotropic Elasticity.* Oxford Univ.Press, London, ix+136 pp.

Helmholtz, H.L.F. (1869): The mechanism of the middle-ear ossicles and of the eardrum. *Pflügers Archiv.f.Physiol.(Bonn)* 1: 1-60 (in German; transl. by A.H. Buck & N. Smith {W.Wood & Co., New York, 69 pp., 1873} and by J. Hinton {*Pub.New Sydenham Soc.(London)* 62: 97-155, 1874})

Hoeft, L.O., E. Ackerman & A. Anthony (1964): Measurement of the displacements and nonlinearities of the guinea-pig tympanum. *J.Acoust.Soc.Am.* 36(10): 1836-1844

Hunt, J.T., M.R. Knittel & D. Barach (1974): Finite element approach to acoustic radiation from elastic structures. *J.Acoust.Soc.Am.* 55(2): 269-280

Hunt, J.T., M.R. Knittel, C.S. Nichols & D. Barach (1975): Finite-element approach to acoustic scattering from elastic structures. *J.Acoust.Soc.Am.* 57(2): 287-299

Johnson, F.R., R.M.H. McMinn & G.N. Atfield (1968): Ultrastructural and biochemical observations on the tympanic membrane. *J.Anat.* 103(2): 297-310

Johnstone, B.M., & K.J. Taylor (1971): Physiology of the middle ear transmission system. *J.Oto-laryngol.Soc.Australia* 3: 226-228

Keith, A. (1923): *Human Embryology and Morphology*, Chapter 16. E.Arnold, London, viii+491 pp.

Kessel, J. (1874): On the influence of the middle-ear muscles on the displacements and vibrations of the eardrum in the cadaver ear. *Arch.Ohrenhlk.* 8(1-2): 80-92 (in German)

Khanna, S.M. (1970): *A holographic study of tympanic membrane vibrations in cats.* Ph.D. thesis, City Univ.New York, 214 pp.

Khanna, S.M., & J. Tonndorf (1972a): Tympanic membrane vibrations in cats studied by time-averaged holography. *J.Acoust.Soc.Am.* 51(6): 1904-1920

Khanna, S.M., & J. Tonndorf (1972b): Real-time observation of submicroscopic vibration by stroboscopic holography. 84th Mtg.Acoust.Soc.Am., Miami Beach, November

Khanna, S.M., & J. Tonndorf (1975): Tympanic membrane shape determined by moiré topography. 89th Mtg.Acoust.Soc.Am., Austin, April

Khanna, S.M., J. Tonndorf & I. Janecka (1973): Vibratory patterns examined by real-time and time-averaged holography. *J.Acoust.Soc.Am.* 54(6): 1686-1693

Kinsler, L.E., & A.R. Frey (1962): *Fundamentals of Acoustics*, 2nd ed. Wiley, New York, ix+524 pp.

Kirikae, I. (1960): *The Structure and Function of the Middle Ear.* Univ.Tokyo Press, Tokyo, vi+157 pp.

Kobrak, H.G. (1941): A cinematographic study of the conduction of sound in the human ear. *J.Acoust.Soc.Am.* 13(2): 179-181

Kobrak, H.G. (1943): Direct observations of the acoustic oscillations of the human ear. *J.Acoust.Soc.Am.* 15(1): 54-56

Kobrak, H.G. (1959): *The Middle Ear.* Univ.Chicago Press, Chicago, xvi+254 pp. + 6 plates (ed.& contributor)

Köhler, W. (1910): Acoustical studies I. *Zeitschr.f.Psychol.* 54: 241-289 + 3 plates

Kojo, Y. (1954): Morphological studies of the human tympanic membrane. *J.O.-R.-L. Soc.Japan* 57(2): 115-126 (in Japanese)

Konrad, A., & P. Silvester (1971): Scalar finite-element program package for two-dimensional field problems. *IEEE Trans.* MTT-19: 952-954

Lay, D.M. (1972): The anatomy, physiology, functional significance and evolution of specialized hearing organs of gerbilline rodents. *J.Morph.* 138(1): 41-120

Lim, D.J. (1968a): Tympanic membrane. Electron microscopic observation. Part I. Pars tensa. *Acta Otolaryngol.* 66: 181-198

Lim, D.J. (1968b): Tympanic membrane. Part II. Pars flaccida. *Acta Otolaryngol.* 66: 515-532

Lim, D.J. (1970): Human tympanic membrane. An ultrastructural observation. *Acta Otolaryngol.* 70: 176-186

Litton, W.B. (1968): Epidermal migration in the ear: the location and characteristics of the generation centre revealed by utilizing a radioactive desoxyribose nucleic acid precursor. *Acta Otolaryngol.* Suppl.240: 39 pp.

Lucae, A. (1900a): Vibratory massage in the treatment of progressive deafness, with especial consideration of my elastic pressure probe. *Laryngoscope* 9(3): 157-168

Lucae, A. (1900b): Critical review and new results concerning vibration massage of the ear. *Archiv.f.Ohrenhlk.* 51(1): 1-18 (in German)

Lucae, A. (1901): The otostroboscope and its physiological diagnostic significance. *Arch.f.Ohrenhlk.* 53: 39-51 (in German)

Mach, E., & J. Kessel (1874): Studies on the topography and mechanics of the middle ear. *SitzBer.Math.-Naturw.Cl.Kaiser.Akad.Wiss.(Wien)* Abt.3. 69(4): 221-243 + 1 plate (in German)

Mader, L. (1900): Microphonic studies of the sound-conducting apparatus of the human ear. *SitzBer.Math.-Naturw.Cl.Kaiser.Akad.Wiss.(Wien)* Abt.3. 109(2): 37-75 (in German; abstract in *Laryngoscope* 9(5): 371, 1900)

Magnoni, A. (1938): Migration of epithelium of tympanic membrane. *Valsalva* 14(5): 234-240

Manley, G.A., & B.M. Johnstone (1974): Middle-ear function in the guinea pig. *J.Acoust.Soc.Am.* 56(2): 571-576

Marquet, J., K.J.v. Camp, W.L. Creten, W.F. Decraemer, H.B. Wolff & P. Schepens (1973): Topics in physics and middle ear surgery. *Acta O.-R.-L.Belg.* 27: 137-320

Martin, H.C., & G.F. Carey (1973): *Introduction to Finite Element Analysis. Theory and application.* McGraw-Hill, xiii+386 pp.

McArdle, F.E., & J. Tonndorf (1968): Perforations of the tympanic membrane and their effects upon middle-ear transmission. *Arch.klin.exp.Ohr.Nas. Kehlkopfhlk.* 192: 145-162

Mehrotra, B.L. (1969): *Matrix analysis of welded tubular joints.* Ph.D. thesis, McGill Univ., Montréal, x+156 pp.

Mehrotra, B.L., A.A. Mufti & R.G. Redwood (1969): Analysis of three-dimensional thin-walled structures. *J.Struct.Div.ASCE* 95(ST12): 2863-2872

Michelsen, A. (1971): The physiology of the locust ear. *Zeitschr.vergl.Physiol.* 71(1): 49-128

Michelsen, A. (1973): The mechanics of the locust ear: an invertebrate frequency analyzer. Pp. 911-934 in *Basic Mechanisms in Hearing*, A.R. Møller (ed.), Academic Press, New York, xi+941 pp.

Morgan, F.R. (1960): The mechanical properties of collagen fiber: stress-strain curves. *Soc.Leather Trades' Chem.J.* 44(4): 170-182

Mufti, A.A. (1969): *Matrix analysis of thin shells using finite elements.* Ph.D. thesis, McGill Univ., Montréal, xi+141 pp.

Mufti, A.A., & P.J. Harris (1969): Matrix analysis of shells using finite elements. *Trans.EIC* 12(A-9): 8 pp.

Mundie, J.R. (1962): The impedance of the ear — a variable quantity. Middle ear function seminar, May. Publ.in U.S.Army Med.Res.Lab. report no. 576, pp. 63-85, 1963; abstract in *J.Acoust.Soc.Am.* 34: 721, 1962

Mundie, J.R. (1971): personal communication

Norrie, D.H., & G. de Vries (1973): *The Finite Element Method. Fundamentals and applications.* Academic Press, New York, xiii+322 pp.

Nuttall, A.L. (1972): *Tympanic muscle effects on middle-ear transfer characteristic.* Ph.D. thesis, Univ.Michigan, 209 pp.

Oden, J.T. (1972): *Finite Elements of Nonlinear Continua.* McGraw-Hill, New York, xv+432 pp.

Onchi, Y. (1961): Mechanism of the middle ear. *J.Acoust.Soc.Am.* 33: 794-805

Owada, I. (1959): Fibrous structure of the tympanic membrane in vertebrates. *J. Otorhinolaryngol.Soc.Japan* 62(1): 28-43 + 3 plates (in Japanese)

Page, D.H., F. El-Hosseiny, K. Winkler & R. Bain (1972): The mechanical properties of single wood-pulp fibres. Part I: A new approach. *Pulp Paper Mag.Can.* 73(8): 72-77

Patten, B.M. (1953): *Human Embryology*, 2nd ed. Blakiston, New York, xvii+798 pp.

Payne, M.C.,Jr., & F.J. Githler (1951): Effects of perforations of the tympanic membrane on cochlear potentials. *A.M.A.Arch.Otolaryngol.* 54(6): 666-674

Peake, W.T., & J.J. Guinan, Jr. (1967): A circuit model for the cat's middle ear. *M.I.T.Lab.Electron.Q.Prog.Report* 84: 320-326

Pearson, A.A., A.D. Jacobson, R.J.v. Calcar & R.W. Sauter (1967): *The Development of the Ear.* Univ.Oregon Med.School, iii+32 pp.

Perlman, H.B. (1945): Stroboscopic examination of the ear. *Ann.O.R.L.* 54(3): 483-494

Politzer, A. (1889): *The anatomical and histological dissection of the human ear in the normal and diseased condition.* Enke, Stuttgart, x+245 pp. (in German; transl. by G. Stone {Baillière, Tindall & Cox, Strand, xv+272 pp., 1892})

Rayleigh, Lord [J.W. Strutt] (1877): *The Theory of Sound.* 2nd ed., 1894; reprinted, Dover, New York, xlii+504 pp.

Reijnen, C.J.H., & W. Kuijpers (1971): The healing pattern of the drum membrane. *Acta Otolaryngol.* Suppl. 287, 74 pp.

Ruttin, E. (1921): External and internal ligaments of the tympanic membrane. *Anat.Anz.* 54(20-21): 433-435 (in German)

Seely, F.B., & J.O. Smith (1956): *Resistance of Materials.* Wiley, New York,xvi+459 pp

Shimada, T., & D.J. Lim (1971): The fiber arrangement of the human tympanic membrane: a scanning electron microscopic observation. *Ann.O.R.L.* 80(2): 210-217

Silvester, P. (1969): High-order polynomial triangular finite elements for potential problems. *Int.J.Engng.Sci.* 7: 849-861

Silvester, P. (1973): Finite element analysis of planar microwave networks. *IEEE Trans.* MTT-21(2): 104-108

Snowdon, J.C. (1968): *Vibration and Shock in Damped Mechanical Systems.* Wiley, New York, xiv+486 pp.

Stakgold, I. (1968): *Boundary Value Problems of Mathematical Physics, Vol. II.* Macmillan, New York, viii+408 pp.

Stenzel, K.H., T. Miyata & A.L. Rubin (1974): Collagen as a biomaterial. *Ann. Rev.Biophys.Bioeng.* 3: 231-253

Stuhlman, O.,Jr. (1937): The nonlinear transmission characteristics of the auditory ossicles. *J.Acoust.Soc.Am.* 9(2): 119-128

Stuhlman, O.,Jr. (1943): *An Introduction to Biophysics*. Wiley, New York, vii+375 pp.

Sudderth, M.E. (1974): Tympanoplasty in blast-induced perforation. *Arch. Otolaryngol.* 99(3): 157-159

Tonndorf, J., & S.M. Khanna (1970): The role of the tympanic membrane in middle ear transmission. *Ann.O.R.L.* 79(4): 743-753

Tonndorf, J., & S.M. Khanna (1971a): The tympanic membrane as a part of the middle ear transformer. *Acta Otolaryngol.* 71: 177-180

Tonndorf, J., & S.M. Khanna (1971b): Validation of holographic observations on the displacement of the tympanic membrane in cats. 81st Mtg.Acoust.Soc. Am., Washington, D.C.

Tonndorf, J., & S.M. Khanna (1972): Tympanic-membrane vibrations in human cadaver ears studied by time-averaged holography. *J.Acoust.Soc.Am.* 52(4): 1221-1233

Tonndorf, J., S.M. Khanna & E.C. Greenfield (1971): The function of reconstructed tympanic membranes in cats. *Ann.O.R.L.* 80(6): 861-870

Tonndorf, J., S.M. Khanna & E.C. Greenfield (1972): Total myringoplasty: functional aspects. *Acta Otolaryngol.* 73(2-3): 87-93

Ural, O. (1973): *Finite Element Method. Basic concepts and applications*. Intext Educational Pub., New York, xiii+272 pp.

Vayo, H.W. (1971): Wave propagation in bone media. *Bull.Math.Biophysics* 33(3): 463-479

Viidik, A. (1973): Functional properties of collagenous tissues. *Int.Rev.Conn. Tiss.Res.* 6: 127-215

Wada, Y. (1924): Contribution to the comparative physiology of the ear. *Pflügers Arch.f.d.ges.Physiol.* 202: 46-69 (in German)

Webster, D.B. (1962): A function of the enlarged middle-ear cavities of the kangaroo rat, *Dipodomys*. *Physiol.Zool.* 35: 248-255

Wever, E.G., & M. Lawrence (1954): *Physiological Acoustics*. Princeton Univ. Press, Princeton, xii+454 pp.

Wilkes, G.L., I.A. Brown & R.H. Wildnauer (1973): The biomechanical properties of skin. *CRC Crit.Rev.Bioeng.* 1(4): 453-495

Witnauer, L.P., & W.E. Palm (1961): Preliminary studies of dynamic mechanical properties of leather. *Am.Leather Chemists' Ass.J.* 56(2): 58-67

Zanzucchi, G. (1938): Modification of the elastic fibres of the tympanic membrane at various ages. *Arch.Ital.Otol.* 50: 203-221 (in Italian)

Zienkiewicz, O.C., & Y.K. Cheung (1967): *The Finite Element Method in Structural and Continuum Mechanics.* McGraw-Hill

Zienkiewicz, O.C. (1971): *The Finite Element Method in Engineering Science.* McGraw-Hill, London, xiv+521 pp.

Zwislocki, J. (1962): Analysis of the middle ear function. Part I. Input impedance. *J.Acoust.Soc.Am.* 34(9): 1514-1523

Zwislocki, J. (1963): Analysis of the middle ear function. Part II. Guinea-pig ear. *J.Acoust.Soc.Am.* 35: 1034-1040